University of Cape Town

Antibody engineering to evaluate binding, internalisation, and intracellular routing of tumour-targeting fusion proteins

Master of Science (Medicine) Dissertation

Maryam Karaan

Supervisor: Prof. Dr. Dr. Stefan Barth

Medical Biotechnology and Immunotherapy Research Unit
Department of Integrative Biomedical Sciences
Faculty of Health Sciences

This dissertation is submitted to the Faculty of Health Sciences, University of Cape Town, in fulfilment of the requirements for the degree of Master of Science.

March 2023

Contents

Declaration

I declare that the work contained in this dissertation is my own unaided work, both in concept and execution and that apart from the normal guidance from my supervisor, I have received no assistance.

Neither the substance nor any part of this dissertation has been (in the past), is currently being, or is to be submitted for a degree at this University, or any other university other than this Master of Science at the University of Cape Town.

The Cancer Immunology, Immunotherapy referencing style has been applied as the convention for in-text citations and referencing. Each significant contribution to, and quotation in, this thesis from the work(s) of other authors and collaborators has been attributed, cited, and referenced.

This dissertation has been submitted to the Turnitin module (or equivalent similarity and originality checking software) and I confirm that my supervisor has seen my report and that any concerns revealed by such have been resolved with my supervisor.

I grant the University of Cape Town free licence to reproduce the content of this dissertation, in whole or in part, for the purpose of research.

Signature: Signed by candidate

Date: 31 March 2023

For my father,

who encouraged me to explore the wonders of this world through science.

May we meet again in the next.

Acknowledgements

Firstly, I need to thank my family who carried me throughout this harrowing yet enlightening journey. The past few years have been incredibly challenging, and without their unwavering love and support, I would certainly not have reached this point.

To my supervisor and mentor, Prof. Dr. Dr. Stefan Barth, I am forever happy to have been your student. Your absolute love for science and steadfast leadership has been inspiring. Thank you for your patience, encouragement, and confidence during my most difficult experiences. I am exceptionally fortunate to have had your guidance, support, and mentorship at this stage of my scientific career.

To my found family at the MB&I, it has been a privilege to embark on this journey with you. I have thoroughly enjoyed all our conversations (many of which were rants) and camaraderie. Neelakshi, Trishana, Grace, Sanele, Sandra, Marc, Chardae, Siya, and Akiko (to name but a few) – I appreciate you all more than I can express.

My co-supervisor and friend, Dr. Dharanidharan Ramamurthy, deserves special thanks for his mentorship and guidance. Today, I am a better scientist because of your invaluable insight, encouragement, and candour.

I would also like to extend my sincere thanks to Prof. Dirk Lang, Dr. Viantha Naidoo, and Carla van Niekerk for their assistance and training at the UCT Confocal Microscopy Unit.

I am grateful to the Blackburn, Sturrock and Katz labs for their steady technical support. You have been lovely neighbours.

My gratitude is also extended to the National Research Foundation (NRF) and South African Research Chair Initiative (SARChI) for Cancer Biotechnology for funding this study.

List of abbreviations

ADC	Antibody-drug conjugate
ADCC	Antibody-dependent cellular cytotoxicity
ADCP	Antibody-dependent cellular phagocytosis
AGT	O6-alkylguanine-DNA alkyltransferase
Amp	Ampicillin
AURIF	Monomethyl auristatin F
BG	Benzyl guanine
BG	O6-benzylguanine
BiTE	Bispecific T cell engager
BRCA	Breast cancer gene
BSA	Bovine serum albumin
BV	Bivalent (scFv) fusion protein
CDC	Complement-dependent cytotoxicity
CDR	Complementarity-determining region
CFS	Cell-free supernatant
CMV	Cytomegalovirus
CSPG4	Chondroitin sulphate proteoglycan 4
CV	Column volume
DAR	Drug-to-antibody ratio
DMEM	Dulbecco's Modified Eagle Medium
DTT	Dithiothreitol
ECM	Extracellular matrix
EGFR	Epidermal growth factor receptor
EpCAM	Epithelial cell adhesion molecule
ER	Estrogen receptor
ERK 1/2	Extracellular signal-regulated kinase 1 and 2

Fab	Antigen-binding fragment
FBS	Foetal bovine serum albumin
Fc	Crystallizable fragment
FcRn	Neonatal Fc receptor
FP	Fusion protein
GFP	Green fluorescent protein
HEK293T	Human embryonic kidney cells
HER2	Human epidermal growth factor receptor 2
His	Histidine
HRP	Horseradish peroxidase
IEC	Ion-exchange chromatography
Ig	Immunoglobulin
IgG	Immunoglobulin G
IHC	Immunohistochemistry
IMAC	Immobilised metal affinity chromatography
LB	Luria-Bertani
mAb	Monoclonal antibody
MAPK	Mitogen-activated protein kinase
MB&I	Medical Biotechnology and Immunotherapy Research Unit
MRI	Magnetic resonance imaging
MV	Monovalent (scFv) fusion protein
MWCO	Molecular weight cut off
NEB	New England Biolabs
ORF	Open reading frame
PBS	Phosphate-buffered saline
PD-1	Programmed death 1
PD-L1	Programmed death ligand 1

PD-L2	Programmed death ligand 2
PI3K	Phosphoinositide 3- kinase
PKC	Protein Kinase C
PR	Progesterone receptor
PVDF	Polyvinylidene difluoride
rcf	Relative centrifugal force
RNA	Ribonucleic acid
RO	Reverse osmosis
RPMI	Roswell Park Memorial Institute (Medium)
scFv	Single chain variable fragment
SDS	Sodium dodecyl sulphate
SDS-PAGE	Sodium dodecyl sulphate polyacrylamide gel electrophoresis
SEC	Size exclusion chromatography
SOC	Super Optimal Broth with Catabolite repression
TAA	Tumour-associated antigen
TAE	Tris-acetate-EDTA
TBS-T	Tris-buffered saline - Tween
TCR	T cell receptor
tGN	Trans-Golgi network
TNBC	Triple-negative breast cancer
VEGF	Vascular endothelial growth factor
VH	Variable heavy chain
VL	Variable light chain

Abstract

Breast cancer is a major global health crisis, particularly affecting women, and triple-negative breast cancer (TNBC) is an aggressive subtype with limited treatment options. TNBC is challenging to treat due to the lack of specific therapeutic markers such as estrogen receptor (ER), progesterone receptor (PR), and human epidermal growth factor receptor 2 (HER2). Current treatments primarily involve chemotherapy, radiotherapy, and surgery, as targeted therapies are limited. TNBC also exhibits significant heterogeneity among patients, emphasizing the need for precise diagnostic and therapeutic approaches.

Immunotherapy, the manipulation of the immune system to target diseases, holds promise for precision medicine. Antibody-drug conjugates (ADCs) use antibodies to deliver drugs selectively. This study focused on a novel recombinant fusion protein format for ADCs using a single chain variable fragment (scFv) specific to chondroitin sulphate proteoglycan 4 (CSPG4), a tumour-associated antigen often overexpressed in TNBC. The scFv antibody derivative was genetically fused to a SNAP-tag, enabling stable and site-specific conjugation of the scFv to diagnostic and therapeutic substrates.

To enhance antigen binding, internalisation, and therapeutic efficacy, a bivalent scFv fusion protein was created in tandem with the standard monovalent fusion protein. *In vitro* experiments using fluorophores and the cytotoxin, monomethyl auristatin F (AURIF), demonstrated that the bivalent fusion protein exhibited improved binding, faster uptake, and efficient release of the conjugate within target cells. Colocalization analysis revealed that the fusion proteins were routed to the lysosomal degradation pathway which is essential for the functionality of ADCs. The cell viability assays revealed that the enhanced binding and uptake of the bivalent fusion protein resulted in a more potent cytotoxic effect on antigen-positive TNBC cells.

This study successfully compared mono- and bivalent αCSPG4-SNAP fusion proteins, revealing the superiority of the bivalent format in antigen binding and targeted drug delivery. It also, for the first time, explored the intracellular routing of scFv SNAP-tag fusion proteins upon uptake. The findings may influence the design of future scFv-based immunotherapeutics, possibly resulting in the incorporation of multiple scFv domains for increased efficacy. Furthermore, the diagnostic potential of

these fusion proteins, aiding in prognosis prediction and patient responsiveness to targeted therapies have been highlighted. The versatility of SNAP-tag technology makes it relatively easy to transform immunodiagnostic fusion proteins into immunotherapeutic tools, potentially advancing TNBC management.

In summary, this study contributes to the development of precision medicine tools for TNBC, addressing its complex nature and limited treatment options. The bivalent fusion protein format shows promise for improved TNBC therapy, offering a new avenue for research and potential clinical applications.

1. Chapter 1: Literature review

1.1. Breast cancer

The breast cancer disease burden is considerably high since it is the most prevalent female cancer and the leading cause of cancer-related death in women globally [1]. In 2020, breast cancer accounted for 30.3% of all diagnosed cancer cases in females and resulted in an estimated 685,000 deaths [2]. The most common breast cancers occur in the lining of the lobules and ducts of the breast, resulting in lobular and ductal carcinomas, respectively [3] (**Figure 1**).

Decades of research have discerned that cancer is a highly complex and multifactorial disease arising from various acquired biological capabilities, known as the hallmarks of cancer [4]. For cancer to develop, cells should have the ability to escape the body's intrinsic regulatory and defence mechanisms [5]. They should, therefore, be able to (i) evade growth suppressors, (ii) sustain proliferative signalling, (iii) resist cell death, (iv) enable replicative immortality, (v) induce angiogenesis, (vi) activate invasion and metastasis, (vii) reprogramme energy metabolism, and (viii) evade immune destruction [4]. The first step to acquiring these capabilities is through genetic mutations that result in carcinogenesis [6].

Determining the risk factors involved in the development of breast cancer has been an epidemiological challenge, however, the consensus is that genetic and environmental factors play important roles [3]. A family history of breast cancer is a strong risk factor since 5-10% of all breast cancer incidences result from inherited gene mutations [7]. Environmental risk factors generally result from exposure to carcinogens that damage cell proliferation genes or enhance tumour cell growth [5]. Studies have found that breast cancer development is correlated with high or prolonged exposure to female hormones (estrogen and progesterone), whether intrinsic or extrinsic [8]. This includes the use of hormone replacement therapy or hormonal contraceptives, delayed menopause, early onset of menstruation, and no history of pregnancy or childbirth [9].

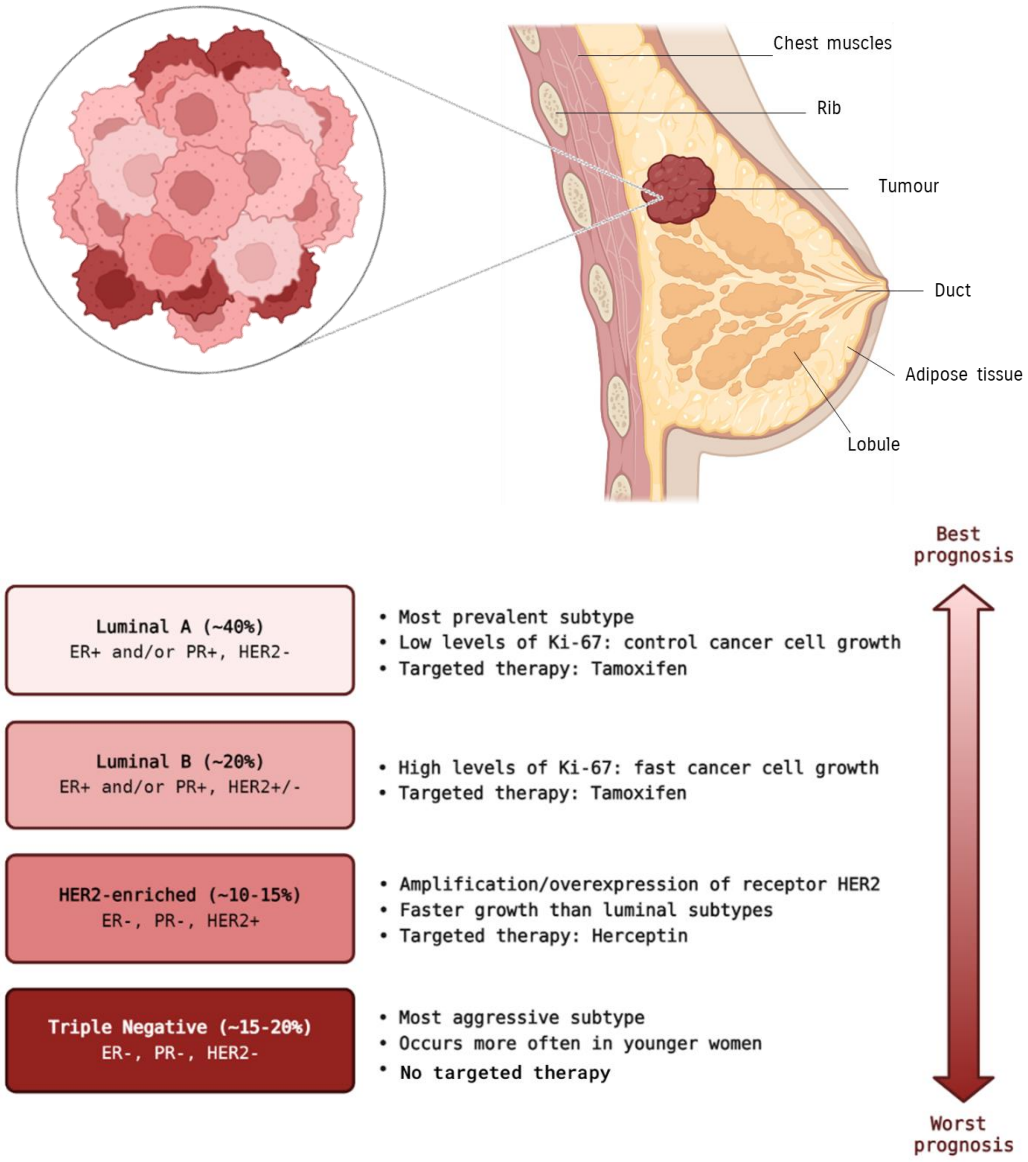

Figure 1. Breast cancer anatomy and molecular subtypes. (A) The anatomy of a female breast is made up of fatty tissue, ducts, and lobules. Breast tumours are typically located in the lobules and ducts. (B) Breast cancer subtypes can be characterised based on the expression of certain biomarkers. These include hormone receptors, namely estrogen receptor (ER) and progesterone receptor (PR), cellular proliferation markers such as Ki-67, and the receptor tyrosine kinase, human epidermal growth factor receptor 2 (HER2). Once the expression of these biomarkers is confirmed on tumours, therapies that target ER (Tamoxifen) and/or HER2 (Herceptin) can be used to treat these breast cancers. Tumours that do not express these biomarkers (referred to as triple-negative) solely rely on standard therapies. The prognosis varies depending on the subtype of breast cancer. Information adapted from Dai *et al.* 2015. Created with BioRender.

The prognosis and survival of breast cancer patients are significantly improved by an early and accurate diagnosis [10]. Initial breast screenings typically involve a physical examination followed by imaging with x-ray mammography, breast ultrasound, or magnetic resonance imaging (MRI) [3]. Once detected, the tumour can be characterised according to different systems that consider various factors. In clinical settings, TNM staging is used, where the size of the tumour (T), presence of nodal metastasis (N) and distant metastasis (M) are assessed [11]. If the initial screening reveals the presence of a potential tumour, a biopsy followed by histological analysis is employed to determine the histological grading of the tumour based on its morphological characteristics [12]. Immunohistochemistry (IHC) analysis is also performed at this point to determine the presence or absence of IHC biomarkers [13]. The latest methods of tumour classification involve DNA microarray platforms that provide insight into the molecular complexity of the carcinoma [14].

Using high-throughput genetic analysis, four molecular (intrinsic) breast cancer subtypes were identified based on the expression of cellular components involved in signalling pathways (**Figure 1**) [15]. These subtypes are based on the presence or absence of estrogen receptor (ER), progesterone receptor (PR), and the normal or reduced expression of human epidermal growth factor receptor 2 (HER2). ER is an intracellular receptor that plays a complex role in breast cancer progression through the promotion of cell proliferation and metastasis [16]. Tumours expressing ER can be targeted with Tamoxifen, a selective ER modulator [17]. PR is also an intracellular hormone receptor that plays a role in breast tissue development along with ER, however, its exact role in breast cancer progression is not well understood [18]. HER2 is a transmembrane tyrosine kinase receptor which can activate multiple cell proliferation pathways including the MAPK (mitogen-activated protein kinase), PKC (Protein kinase C), and PI3K (phosphoinositide 3- kinase) pathways [19]. The expression of HER2 on breast cancer cells is associated with higher-grade tumours and disease recurrence [20]. Trastuzumab (Herceptin) is an antibody-based treatment designed to target HER2-positive tumours [21]. ER, PR and HER2 are the classical IHC markers that are assessed to diagnose and characterise breast cancers into intrinsic subtypes [15]. The nuclear antigen, Ki67, is a proliferation marker that is commonly used to

predict the breast cancer subtype and prognosis [22, 23]. The most aggressive breast cancer subtype is the basal-like subtype, wherein the majority of cases are categorised as “triple-negative” [24].

1.2. Triple-negative breast cancer

Triple-negative breast cancer (TNBC) is a heterogeneous and aggressive breast cancer subtype, characterised by the absent or low expression of hormone receptors (ER and PR) and HER2 (Perou et al., 2000). The triple-negative phenotype accounts for 15-20% of all diagnosed breast cancer cases [25]. Various studies have reported that women of premenopausal age (< 40 years) with African ancestry are known to be highly predisposed to TNBC [24, 26]. An important risk factor for TNBC is a positive breast cancer gene (BRCA) mutation status – up to 20% of patients with TNBC carry a BRCA mutation [27, 28]. The BRCA1/2 genes play important roles in DNA damage repair and maintaining DNA stability [29]. Mutations in these genes commonly result in hereditary breast cancer [29]. On a histological and transcriptional level, TNBCs share many similarities with BRCA1-associated breast cancers, signifying a connection between this mutation status and the disease [30]. Currently, the BRCA mutation status is the only biomarker that has been clinically validated for the implementation of personalised medicine in breast cancer patients [31].

TNBC tumours are larger with more lymph node involvement and are typically diagnosed at a higher grade compared to other breast cancer cases [32]. Furthermore, the survival of patients after metastatic relapse is considerably lower compared to other breast cancer subtypes [24, 26, 33]. The TNBC subtype is clinically associated with a poor prognosis due to its aggressive progression, the increased risk of relapse in comparison with other subtypes and the presence of cancer stem cell populations within tumours [30, 34, 35]. The great heterogeneity of the disease in addition to its aggressive nature has led to challenges in its management and treatment.

Extensive genomic and biological analysis have led to the categorisation of TNBC into six subtypes as described in Table 1. The gene expression analysis revealed which genes were impacted in these subtypes, along with the signalling pathways affected by the expression of these genes, and ultimately

the tumour responsiveness to chemotherapy [32]. Based on this information, potential therapeutic options could be predicted.

Table 1. Characterisation of triple-negative breast cancer subtypes. Based on gene expression analysis across 21 different breast cancer data sets, these subtypes were identified and characterised according to gene expression profiles, implicated signalling pathways, and chemosensitivity [32].

TNBC subtype	Signalling pathways affected	Chemosensitivity
Basal-like 1 (BL1)	DNA damage, cell proliferation, and cell cycle pathways	Very good
Basal-like 2 (BL2)	Cell proliferation, growth factor signalling, glycolysis, gluconeogenesis	Very poor
Immunomodulatory (IM)	Immune cell signalling processes	Medium
Mesenchymal (M)	Epithelial-mesenchymal transition (EMT), cell proliferation, differentiation, motility	Medium
Mesenchymal stem-like (MSL)	Growth factor signalling, differentiation, cell motility, angiogenesis, EMT	Medium
Luminal androgen receptor (LAR)	Androgen/estrogen metabolism, steroid synthesis, porphyrin metabolism	Poor

1.2.1. Current standard diagnosis and treatment

TNBC is initially diagnosed by the absence of ER, PR, and HER2, which is typically determined by IHC or microarray for gene expression analysis of tumour biopsies [36]. This should ideally be followed by genetic testing to determine the BRCA mutation status of the patient [27]. Unlike other subtypes, TNBC tumours are not typically detected by routine screenings using mammography and ultrasound – presumably because these tumours grow rapidly and often develop during the intervals between screenings [37]. This is exacerbated by the fact that women under the age of 40 are more susceptible to TNBC, however, routine screenings are only recommended for women after they have reached 40 years [10]. As such, clinical examinations have been the best method of detecting and diagnosing TNBC, however, the diagnosis is often made at a later stage of tumour progression [38]. This presents a problem since early diagnosis is crucial for the survival of the patient and the prognosis is significantly reduced once the disease reaches a metastatic stage [38, 39].

TNBC has also been characterised by a lack of available targeted therapies due to the absence of therapeutic targets, namely ER and HER2. As such, cytotoxic chemotherapy remains the primary systemic therapy for TNBC and is often used in combination with surgical resection [34]. However, despite the higher rates of initial clinical response to adjuvant (presurgical) chemotherapy, the risk of distal recurrence is high and the prognosis after metastatic relapse is exceedingly reduced [36, 40]. Generally, less than 30% of metastatic TNBC patients survive after five years, and the vast majority of these patients ultimately succumb to the disease [41].

The lack of effective targeted treatment for TNBC and poor disease prognosis often results in intensive social and economic burden [24]. This may be attributed to the elevated risk of relapse, the need for frequent and high therapeutic doses, as well as post-therapy care for systemic side effects in patients undergoing treatment [24, 42]. Furthermore, in many developing countries, the low rates of survival following chemotherapeutic treatment are exacerbated by poverty and limited healthcare facilities [43]. Thus, there is a demanding need for novel detection methods that ideally lead to targeted TNBC therapies.

1.3. Immunotherapy

1.3.1. The significance of immunotherapy for TNBC

Immunotherapy has been considered for improving the outcomes of TNBC patients by exploring novel targeted treatments [44]. An immunotherapeutic approach aims to exploit components of the human immune system to selectively target diseased cells without damaging healthy cells and has the potential for improved potency in therapy-resistant cancers [45]. Immunotherapy may improve the survival rates and prognosis of TNBC patients due to its high specificity and immune memory [46]. Furthermore, the reduced systemic toxicity significantly contributes to a better quality of life for patients undergoing treatment for aggressive cancers such as TNBC [34]. Studies on immunotherapy for TNBC patients involving immune checkpoint inhibitors, monoclonal antibodies (mAbs), T-cell activation and immune vaccines have been conducted [45, 46]. While many of these studies are still at the elementary research

stage and require further exploration and clinical validation, some clinical trials show immense promise [44–48].

In a phase 3 study, the immunotherapeutic drug, pembrolizumab (Keytruda) was used in combination with chemotherapy to treat advanced TNBC. The study demonstrated that, when compared to chemotherapy alone, this combination treatment significantly improved progression-free survival in patients with TNBC tumours expressing programmed death ligand 1 (PD-L1) [49]. Pembrolizumab is a therapeutic mAb that targets the programmed death 1 (PD-1) receptor on T cells, thereby preventing it from binding to its ligands, PD-L1 and PD-L2, on the surface of tumour cells [50]. These ligands are generally found on healthy cells to prevent their destruction by activated T-cells. Cancer cells mimic this to evade the immune system, therefore, by hindering this interaction, the T-cells remain active against tumour cells expressing PD-L1 and PD-L2 [50]. This form of immunotherapy is known as immune checkpoint inhibition and pembrolizumab is now approved for combination therapy in patients with advanced TNBC and high PD-L1 expression in tumours [49].

Another immunotherapeutic strategy that shows promise involves a targeted method of drug delivery using antibodies or antibody derivatives recognising differentially upregulated tumour-associated antigens (TAAs). It is possible to conjugate these antibodies or their derivatives to a toxic moiety or cytolytic effector to produce immunotherapeutic antibody-drug conjugates (ADCs) [51]. The therapeutic potential of ADCs targeting TAAs in TNBC is exemplified by Sacituzumab govitecan (Trodelvy). This is an ADC that was recently approved for the treatment of unresectable, locally advanced or metastatic TNBC [52]. The antibody targets human trophoblast cell-surface antigen 2 (Trop-2), a transmembrane TAA that is highly expressed in multiple tumour types, including TNBC [53]. The drug conjugated with the antibody is SN-38, a topoisomerase I inhibitor [52]. In the phase 3 clinical trial, this ADC significantly improved the progression-free and overall survival of patients with metastatic TNBC compared to chemotherapy [52, 54]. These findings are promising for the development of TAA-targeting ADCs.

Several membrane-bound proteins have been identified for targeted therapy by high-throughput gene expression profiling and other technologies [55]. Considering the difficulty in targeting TNBC via endocrine receptors and HER2, these provide promising alternative targets for immunotherapy. While TAAs are not exclusively expressed in tumours, their expression is comparatively lower and negligible in healthy tissue and cells [56, 57]. It is, therefore, important to select TAAs depending on their differential expression, as well as the binding and internalisation potential. It is also preferable for TAAs to be cell-bound since antigens secreted by target cells, or otherwise abundant in the extracellular matrix, would isolate antibodies extracellularly with minimal or no effect on the tumour [58, 59]. Furthermore, the identification of TAAs as biomarkers can be used to diagnose and characterise tumours and directly inform potential treatment strategies.

1.3.2. A target for TNBC: chondroitin sulphate proteoglycan 4

A highly appealing target for TNBC is chondroitin sulphate proteoglycan 4 (CSPG4) – (**Figure 2**) [60]. CSPG4 is heterogeneously expressed in adult progenitor cells and has been implicated in maintaining and differentiating progenitor cells into various adult tissues [61, 62]. Since the expression of CSPG4 is downregulated during terminal differentiation, its expression on normal adult tissue is comparatively low [61, 62]. While its physiological functions are yet to be fully understood, various studies have reported its role in cellular differentiation, migration, angiogenesis, vascularization, and the development of multiple tissues [63–65]. In terms of its structure (**Figure 3**), CPSG4 is a transmembrane cell surface proteoglycan consisting of an N-linked 280 kDa glycoprotein and a 450 kDa chondroitin sulphate proteoglycan [66]. The extracellular region is comprised of three distinct domains (D1, D2, D3) that play structural and functional roles, including maintaining stability and enabling the binding of growth factors and ligands [67]. The intracellular region contains a proline- and threonine-rich motif, which serves as extracellular regulated signal kinase (ERK) phosphorylation sites (**Figure 3**) [67]. Threonine phosphorylation results in the downstream activation of mitogenic pathways and transcription that promote survival, proliferation, and migration [62, 68].

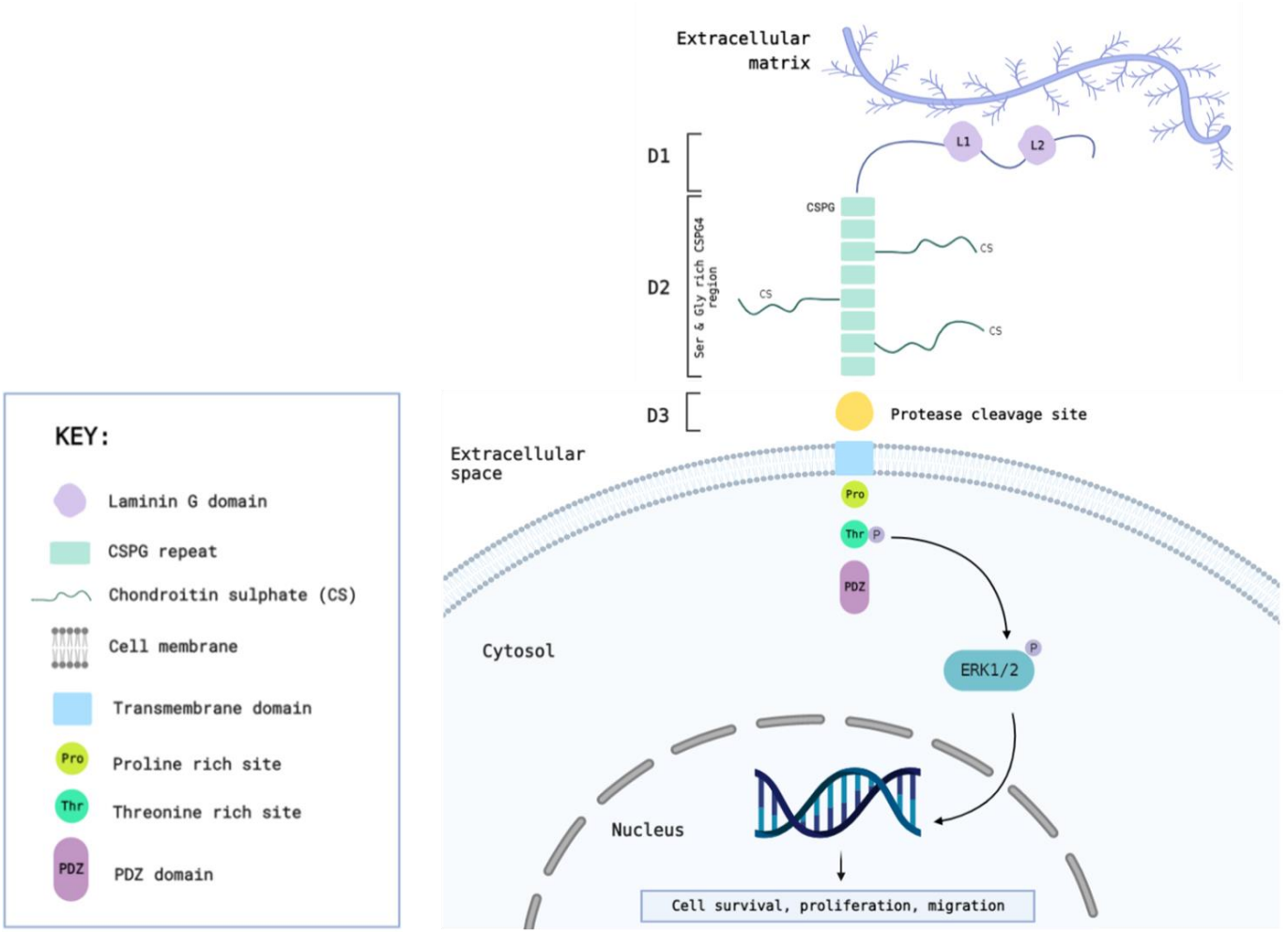

Figure 2: Schematic representation of chondroitin sulphate proteoglycan 4 (CSPG4) proposed structure and function. CSPG4 is comprised of three extracellular domains: D1, D2 and D3. The two laminin G-like domains (L1 and L2) of D1 are thought to interact with the extracellular matrix (ECM). The CSPG repeats of D2 contain chondroitin sulphate (CS) chains that interact with integrins and ECM proteins, along with binding and presenting growth factors to receptor tyrosine kinases. D3 is composed of a protease cleavage site. The cytoplasmic region contains a phosphorylation site for the extracellular signal-regulated kinase 1/2 (ERK1/2). CSPG4 is therefore implicated in cellular signalling pathways through ERK1/2. These pathways promote survival, proliferation and migration, and may advance the motility, invasiveness, and angiogenesis of cancer. Adapted from Price *et al.* 2011. Created using BioRender.

CSPG4 was originally discovered in melanoma cells and has since been identified on the cell surfaces of differentiated malignant cells and progenitor cells in various cancer types, particularly those associated with aggressive progression [69, 70]. A study reported that CSPG4 was overexpressed in 72.7% of primary tissues of TNBC, including TNBC cell lines and tumour cells in the pleural effusion from metastatic TNBC patients [60]. In cancer cells, CSPG4 is known to play important roles in growth, migration and metastasis [69]. Interestingly, CSPG4 is also expressed in cancer stem cells, which are known to be particularly resistant to various cytotoxic therapies and signify a leading cause of relapse through the re-establishment of local or distal tumours after conventional therapy [60, 69]. This, along with its role in cell survival, migration and metastasis, distinguishes CSPG4 as a favourable prognostic marker and therapeutic target.

The majority of the proteoglycan is extracellular, where it interacts with various activating ligands, prompting the recruitment of multiple receptors and clathrin-mediated endocytosis [58]. This, in conjunction with the abundance of proteoglycan on tumour cells, emphasises that CSPG4 may be a suitable target for ADCs, which require internalisation for the release and activation of their toxin [65]. Additionally, its association with several hallmarks of cancer, along with its comparatively low expression in normal breast epithelium, represents a favourable target for immunotherapy [69]. This is exemplified in studies which have successfully targeted CSPG4 with mAbs and ADCs to inhibit cell proliferation, adhesion and migration in addition to inducing tumour-specific cytotoxicity in multiple TNBC tumour models [60, 63, 71, 72].

1.3.3. Antibody variants and derivatives

Immunoglobulins (Ig) or antibodies are multifunctional components of the immune system that are responsible for facilitating various cellular and humoral responses [73]. Antibodies have been used to selectively target diseases, especially since the discovery of hybridoma technology in 1975, which involves engineering and producing highly specific monoclonal antibodies (mAbs) in murine hosts [74]. The term “monoclonal” is an indication that these antibodies have identical protein sequences and, therefore, the same antigen recognition site, affinity, biological interactions, and biological effects [74].

Most mAbs belong to the immunoglobulin G (IgG) isotype and are widely used in cancer therapy once they are selected for their interaction with target surface antigens [75]. mAbs exert their anti-tumour function by preventing downstream signalling for growth and proliferation or by activating the immune system through complement-dependent cytotoxicity (CDC), antibody-dependent cellular cytotoxicity (ADCC), and antibody-dependent cellular phagocytosis (ADCP) [75, 76]. To date, more than 100 mAbs have been approved as designated drugs since 1985, and new additions are regularly approved for the treatment of cancer and immunological diseases [77, 78].

Full-length IgG molecules are Y-shaped heterodimeric proteins of ~150 kDa (**Figure 3**). The antibody is comprised of two heavy chains (~50 kDa) and two light chains (~25 kDa) [79]. The heavy chains are connected by disulphide bonds and each heavy chain interacts with one of the light chains – giving rise to the Y-shaped structure [73]. The antibody is further separated into two antigen-binding fragments (Fab) and a crystallizable fragment (Fc). The two Fab regions are identical, producing two antigen-binding domains on one antibody. Each full-length IgG can, therefore, bind to two identical antigens through the hypervariable or complementarity-determining region (CDR) on their variable light and heavy chains (**Figure 3**) [73]. The Fc region is responsible for immune effector functions and is capable of interacting with various cell surface receptors [80].

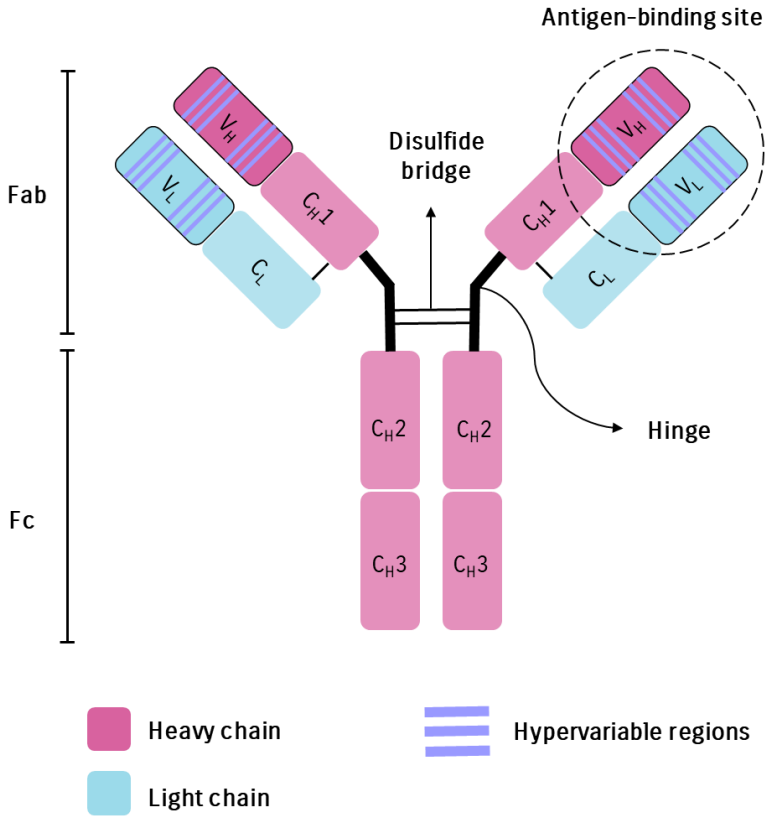

Figure 3. Schematic diagram of an IgG antibody. Antibody-binding fragment (Fab) and Fc regions are depicted, along with the antigen binding site. The heavy chain and light chains are distinguished by colour, as well as the hypervariable regions (purple). An IgG antibody is comprised of two identical heavy chains and light chains that are connected by disulphide bonds. Furthermore, each heavy and light chain is comprised of variable (VH and VL) and constant domains (CH and CL). Each IgG molecule contains two antigen-binding domains (Fab) that is connected to the fragment crystallizable (Fc) domain through the flexible hinge. The Fc domain is responsible for immune effector functions.

The use of conventional full-length mAbs in immunotherapy was initially limited in its clinical efficacy due to the immunogenicity of mouse antibodies in human patients [81]. Furthermore, the inadequate and disproportionate tumour penetration due to their relatively large sizes represented a challenge [57]. This motivated the development of chimeric or fully humanised antibodies to circumvent the immunological response to non-human antibodies using molecular and genetic engineering techniques [75]. The problems arising from the large size of the full-length mAbs inspired the generation of smaller antibody derivatives that retain that ability to bind antigens (**Figure 4**). Various recombinant antibody

formats have since been engineered with variable molecular weights and derivatives capable of binding different antigens (bispecific) were also developed [82].

Single-chain variable fragments (scFvs) are antibody derivates (~28 kDa) comprised of the variable heavy (VH) and variable light (VL) chains of an antibody, linked via a synthetic peptide (spacer) of 10-20 amino acids [83]. These antibody derivatives are either engineered from mAbs or the genetic sequences of high affinity and specific VH and VL chains are selected from phage-antibody libraries [84, 85]. It has been demonstrated that scFvs and other small antibody derivatives (**Figure 4**) can penetrate tumours more rapidly and achieve a more dispersed distribution within tumours compared to full-length mAbs [83, 86, 87]. scFvs are also known for their relatively low immunogenicity, rapid renal clearance, and highly specific tumour localisation [84, 88]. While the scFv format has been shown to be effective at targeting tumours, its retention is short-lived since it is rapidly cleared from circulation, which may limit its therapeutic efficacy in patients [89–91]. This is postulated to be due to the absence of a functional Fc region which can prolong the serum half-life by interacting with the neonatal Fc receptor (FcRn) [76]. Research has accordingly been dedicated to balancing the favourable properties of scFvs with the limitation resulting from its decreased bioavailability.

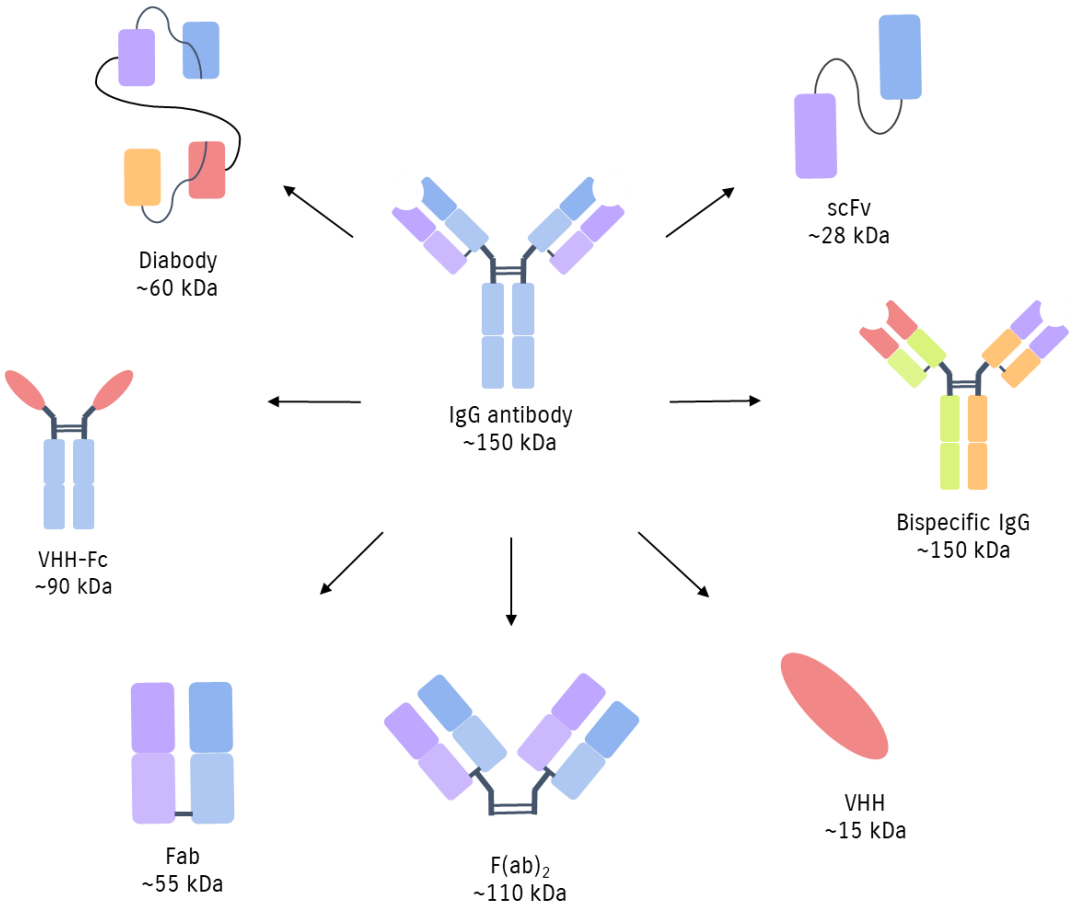

Figure 4. Antibody derivatives and variants resulting from recombinant antibody technology molecular engineering. The different antibody derivatives vary in size, antigen affinity, and specificity. The Fab (antigen-binding fragment) and $F(ab)_2$ are cleaved from full-length IgG at different, where the $F(ab)_2$ retains the highly flexible hinge and bivalent nature (bind two identical antigens). The scFv (single chain variable fragment) consists of one variable heavy (VH) and one variable light (VL) chain linked by a synthetic peptide and can bind one antigen. The diabody is comprised of two linked scFvs that are bispecific in their ability to bind two different antigens (identical scFvs can also be linked to produce a monospecific bivalent diabody). The bispecific IgG is composed of two different heavy chains and two different light chains and is therefore capable of binding different antigens. The VHH (nanobody) is the antigen-binding fragment of single domain antibodies which are comprised of only the heavy chain, known as camelid antibodies (VHH-Fc). Adapted from Hendriks *et al*. 2017.

1.3.4. SNAP-tag technology for antibody-drug conjugation

Full-length mAbs and derivatives (**Figure 4**) can be linked to small effector molecules such as fluorophores and toxins to generate antibody-based diagnostic and therapeutic agents, respectively [92]. The linker between an antibody and its conjugate is an important factor to consider when generating ADCs [82, 93]. Most linking methods involve the direct functionalisation of lysine side chains or the reduction of disulphide bonds [94]. While these methods are commonly employed, they are known to result in heterogeneous ADC products with inconsistent functional and safety profiles [94]. With the large quantities of lysine and cysteine side chains in antibodies, utilising the aforementioned techniques commonly results in many conjugation variants [57]. This shortcoming prompted the development of several site-specific conjugation methods that rely on the chemical attachment of the desired effector molecules to the antibody at a designated site in the molecule [95]. These methods allow for the consistent production of homogeneously labelled antibodies.

The human DNA repair enzyme, O^6-alkylguanine-DNA alkyltransferase (AGT), was engineered to produce SNAP-tag [96]. In cells, wild-type AGT plays a role in maintaining DNA integrity by removing alkyl residues from damaged DNA [96]. AGT and SNAP-tag can, therefore, irreversibly react with O^6-benzylguanine (BG) through the transfer of an alkyl group to a cysteine residue (**Figure 5A**). SNAP-tag (~19.4 kDa) was engineered to have increased catalytic reactivity to BG-modified substrates, reduced binding to DNA, fewer amino acid residues and improved folding under oxidative conditions [91]. This functionality is used to conjugate or label proteins of interest with BG-modified substrates in a rapid, site-directed, and autocatalytic reaction under physiological conditions with a 1:1 stoichiometry (**Figure 5A**) [91]. The SNAP-tag was also further developed to produce SNAPf, a rapid-labelling variant of the SNAP-tag, which exhibits a significant increase in catalytic reactivity towards BG-modified substrates [97]

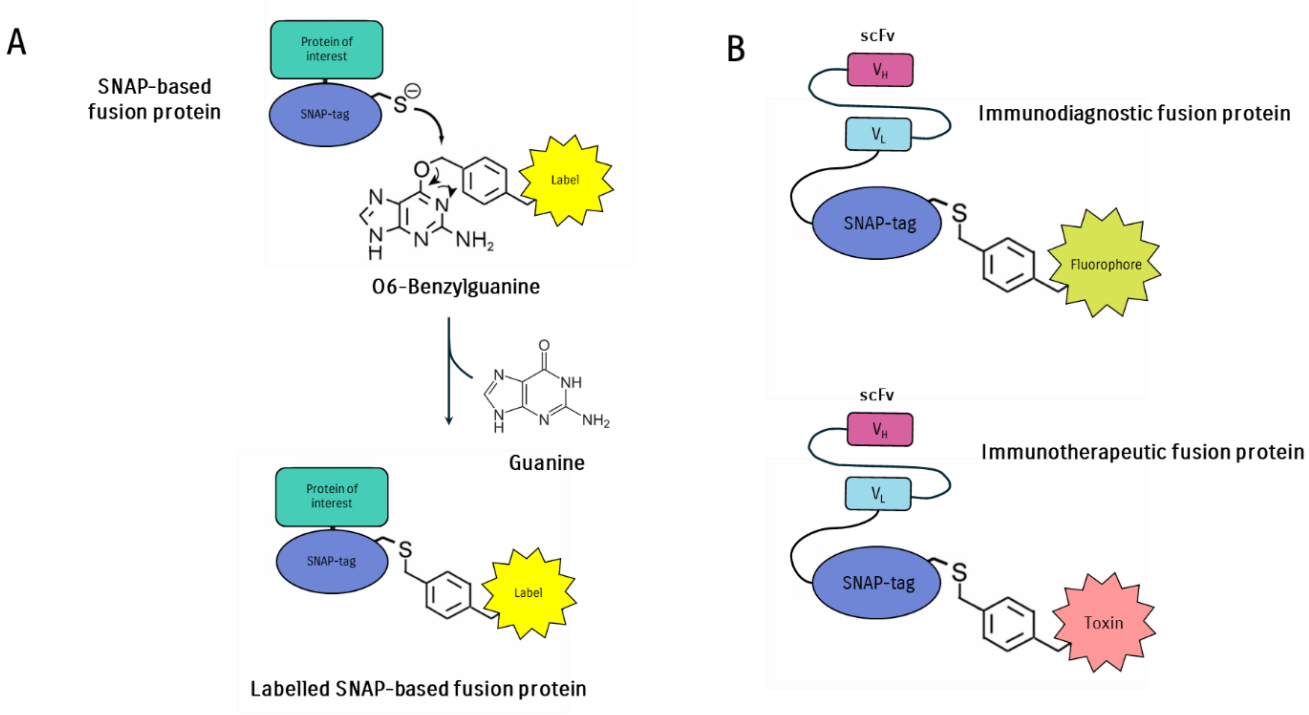

Figure 5. Schematic of SNAP-tag fusion proteins conjugated to O^6-benzylguanine (BG) modified substrates. (A) SNAP-tag is recombinantly fused to a protein of interest. In the labelling (conjugation) reaction, the benzyl group reacts with a cysteine residue in the SNAP-tag active site, releasing the guanine group and resulting in a covalent bond between the SNAP-tag and the label. (B) The protein of interest is a single-chain variable fragment (scFv) recombinantly fused to SNAP-tag and conjugated to either a fluorophore (top) or a toxin (bottom) to product immunodiagnostic and immunotherapeutic fusion proteins, respectively.

There are various advantages to using SNAP-tag technology – (i) the reduced risk of immunogenicity since it is derived from a human enzyme, (ii) convenience due to the simplistic nature of the reaction, (iii) selective and site-specific conjugation as SNAP-tag only reacts with BG-modified substrates at a well-defined site, and (iv) the variety of BG-modified substrates available [92]. SNAP-tag is, therefore, a highly versatile tool that has been applied in various biomedical applications, including *in vitro* and *in vivo* animal imaging, protein isolation, the evaluation of protein functions and interactions, and the production of ADCs [92]. Studies have shown that SNAP-tag genetically fused to antibody derivatives such as scFvs can be produced in mammalian protein expression systems [91, 98, 99]. These fusion proteins (FPs) retain their specific antigen-binding properties and can undergo conjugation reactions with BG-modified substrates such as fluorescent dyes and small molecule toxins to produce

immunodiagnostic and immunotherapeutic FPs, respectively (**Figure 5B**). The FPs are relatively small compared to full-length mAb-based ADCs and *in vivo* studies demonstrated their ability to accumulate at tumour sites and their rapid clearance from circulation [100–103].

1.4. Targeted drug delivery

As previously stated, ADCs are primarily used in cancer therapy for the targeted delivery of the attached drug. ADCs have been researched for many years and there are currently 14 ADCs approved for therapeutic application [104, 105]. Generating an effective ADC is challenging since various factors need to be considered and optimised. ADCs are generally composed of three components: (i) a TAA-targeting antibody or antibody derivative, (ii) a cytotoxic payload that is highly potent once released in the tumour cell, and (iii) the linker between the aforementioned components [106]. Research efforts are, therefore, directed at selecting suitable components and optimising each to produce highly effective ADCs.

1.4.1. Targeting and binding the antigen

Once an ADC is administered (usually intravenously) it needs to travel through the patient's circulation to reach the target site [107]. The antibody or antibody derivative used in the ADC is responsible for identifying and binding to cell surface antigens on the target (tumour) cells [81]. Smaller molecules, such as antibody derivatives, generally display improved diffusion through the bloodstream to reach the tumour site, where they need to penetrate and disperse through the tumour [108]. However, these smaller antibody derivatives also tend to have shorter serum half-lives due to rapid clearance from circulation by renal filtration and degradation [88]. Full-length IgG mAbs can have therapeutic half-lives of multiple days to a month, whereas the half-life of an scFv is generally ~30 min [109]. This may impact the ability of the ADC to reach its target and should also be taken into consideration when designing ADCs [84]. To mitigate this, strategies can be employed to sufficiently extend the half-life of the ADC. These include increasing the size of the ADC through the addition of multiple binding fragments or incorporating an active Fc region in derivatives that lack one [81, 88].

Once the ADC diffuses into the tumour site, the antibody must have sufficient antigen specificity and binding affinity to facilitate effective uptake of the ADC by the tumour cells [81, 84]. The interaction between an antibody and antigen occurs between the paratope of the antigen and the epitope of the antibody [73]. The binding is a reversible, non-covalent reaction that consists of electrostatic and hydrophobic interactions, hydrogen bonds as well as van Der Waal's forces [73]. Binding affinity refers to the strength between a single antigen-binding site and the antigen and is one of the primary parameters used to assess and select mAbs for tumour targeting and drug delivery [110]. The antigen specificity and affinity of an antibody are determined by the amino acid sequences of the CDR and can, therefore be manipulated with site-directed mutagenesis [84]. Alternatively, additional antibody-binding regions can be included to increase the total strength of interaction (referred to as avidity) between multiple antigenic epitopes [111, 112].

1.4.2. Receptor-mediated endocytosis

Once an ADC has successfully reached and bound its target on the surface of tumour cells, it must be internalised by the cell. This is typically achieved through clathrin-mediated endocytosis (also referred to as receptor-mediated endocytosis), which is characterised by the formation of the clathrin-coated pit (**Figure 7**) [113]. The binding of the antibody to the antigen initiates the signal for clathrin-mediated endocytosis and the strength of this signal is thought to be dependent on the binding affinity and avidity of the antibody, where a stronger affinity leads to more efficient uptake of the antibody-antigen ligand (**Figure 6**) [114]. The ability of bivalent antibodies or antibody derivatives to bind to two identical antigens is known to increase the binding avidity (total strength of the reaction) [73, 111]. Various studies have shown that increasing the affinity and valency of mAbs results in enhanced tumour uptake [86, 111, 115–118]. Furthermore, bivalent mAbs with high affinities can induce greater *in vitro* potency compared to lower avidity mAbs that recognise an identical epitope [86, 117]. This was also illustrated in several studies using bivalent immunotoxins that displayed increased efficacy and potency both *in vitro* and *in vivo* [119–123].

This phenomenon is hypothesised to be attributed to the formation of antibody-antigen homodimers – multivalent antibodies with more than one antigen-binding site interacting with multiple antigens on the surface of the target cell, thereby increasing the stability of the interaction [111, 114, 124]. The activation of multiple receptors that are clustered together into one clathrin-coated pit results in the improved uptake of these receptor-ligand complexes [114]. In contrast, monovalent antibody derivatives can bind one antigen at a given time, thereby inducing a reduced signal for internalisation which may be less efficient than multivalent antibodies [88, 125]. Therefore, to produce sufficient clustering to initiate clathrin-mediated endocytosis, higher concentrations of the monovalent ADCs may be required. This was clearly illustrated in a study using a biparatropic ADC targeting two epitopes on HER2, which induced receptor clustering and improved internalisation [116].

While selecting the highest affinity antibodies may seem ideal, there are also disadvantages for translational therapy and two primary hypotheses that may explain them. The binding site barrier effect, which mainly occurs in solid tumours, postulates that high-affinity antibodies display restricted binding to receptors on the tumour surface and therefore low penetration into the tumour mass [126, 127]. The second phenomenon is known as target-mediated drug disposition, which refers to antibody uptake by antigen-expressing non-target tissues as well as the rapid uptake, catabolism, and efflux of the antibody within the target tissue [128]. This leads to an overall reduction in tumour exposure and accelerated clearance of the antibody [128]. These phenomena were illustrated in different studies indicating that they are important to consider when designing high-affinity mAbs and ADCs [110, 125, 129].

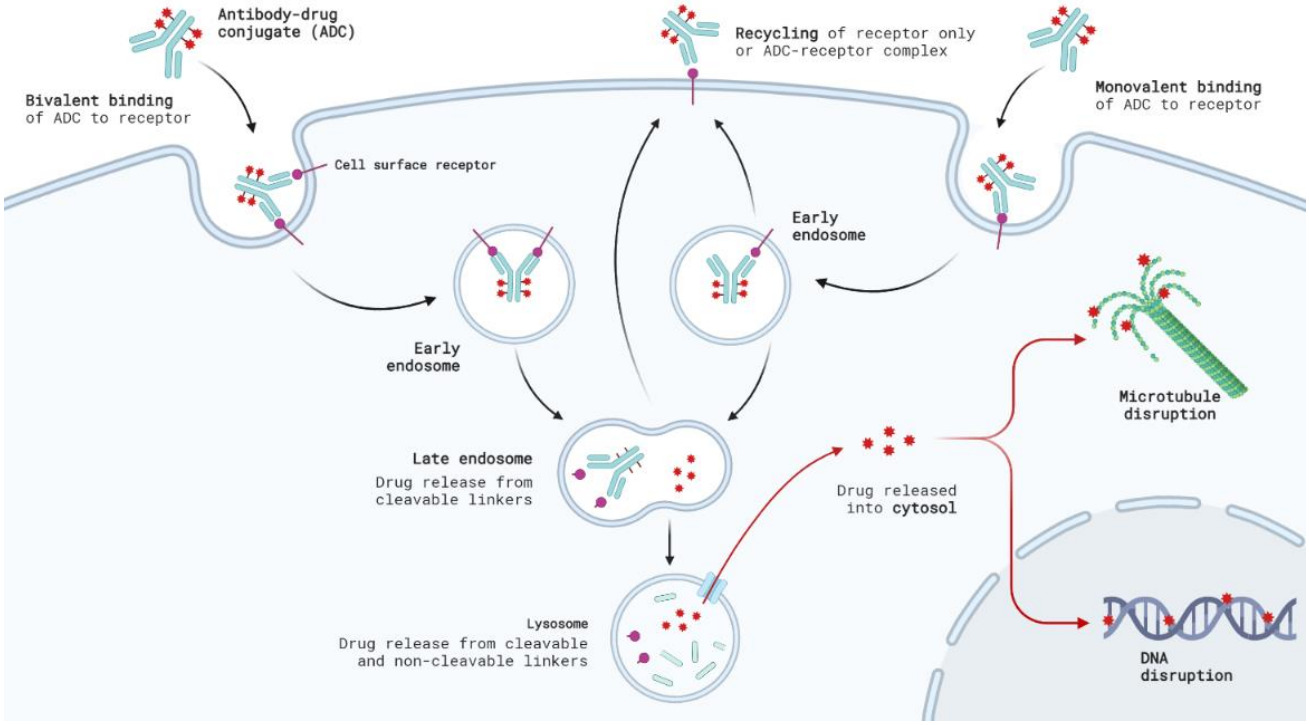

Figure 6. The general mechanism of action of antibody-drug conjugates (ADCs). The binding of the antibody to the cell surface receptor initiates the signal for receptor-mediated internalisation. Multivalent antibodies can interact with multiple antigens and can therefore form clusters or homodimers of antibody-antigen complexes (1). The formation of these homodimers enhances the signal for clathrin-mediated endocytosis, resulting in more efficient uptake of the complex by the cell. Alternatively, a monovalent antibody can interact with one antigen at a given time resulting in reduced cluster formation (2). Receptor-mediated endocytosis for this form of antigen-antibody complex is less robust. Once endocytosed, the complex is shuttled to early endosomes, where they can either be recycled back to the cell surface or mature into the late endosome where its intracellular pathway is determined. The recycling process can also be initiated from the late endosomal stage. Receptor-mediated endocytosis resulting from monovalent ligands is hypothesised to frequently be subjected to receptor recycling. Depending on the class of cytotoxic drug attached to the antibody, once the drug is released into the cytosol, it can initiate cell death through microtubule or DNA disruption. Created using BioRender.

1.4.3. Intracellular routing and release of therapeutic agent

Following the internalisation of receptor-ligand complexes (cargo) by clathrin-mediated endocytosis they are enclosed in endocytic vesicles and await their intracellular fate (**Figure 7**). There are generally three intracellular routes that the internalised cargo may be subjected to which are determined by various factors such as the cell type, receptor, and ligand among others [113, 130]. The first intracellular route or pathway is termed receptor recycling, where the cargo is either recycled back to the plasma membrane or the receptor and ligand separate and only the receptor is carried back to the cell membrane [131]. This mechanism is often utilised by the cell to replenish and maintain the robustness of the plasma membranes and is often mediated by the Fc region interacting with the FcRn [131, 132]. The cargo can also be driven to the degradation pathway, which involves the progression of the endosomes to lysosomes, where the cargo is degraded by the acidic environment of the lysosomes or by the myriad of proteases present in the lysosomes [113, 130]. The degradation products are then released into the cytosol. From the endosomal stage, the cargo may also be subjected to retrograde transport, where it is trafficked to the trans-Golgi network (tGN) for further synthesis and translocation into the cytosol or secretion [133].

Each pathway is driven by cellular mechanisms that are crucial for a multitude of physiological and biochemical processes [113]. ADCs generally rely on lysosomal degradation, where the antibody (ligand) can be separated from its payload which is then released into the cytosol to exert its cytotoxic effect [57]. A bivalent interaction between an ADC and a TAA may also promote its uptake and lysosomal degradation of the cargo. This was clearly illustrated in a study using a biparatropic ADC targeting two epitopes on HER2, which induced receptor clustering and improved internalisation with increased lysosomal trafficking as opposed to receptor recycling [116]. Similar results were illustrated in studies using a combination of mAbs targeting different epitopes on a receptor that was prone to recycling rather than degrading [134, 135]. These studies synergistically downregulated the activity of receptor tyrosine kinases through improved receptor degradation [134, 135]. This provides further support for the consideration of multivalent ADCs to improve their therapeutic efficacy. Alternately, when the cytotoxic payload is a cytolytic protein (commonly used in immunotoxins), retrograde

transport is preferred and can be enhanced using endoplasmic retention signal peptides such as KDEL (lysine-aspartic-acid-glutamic acid-leucine) [136]. The desired routing of ADCs is therefore largely dependent on its cytotoxic payload and can be manipulated to an extent to ensure its efficacy.

The most common cytotoxic drugs used to generate ADCs fall into two categories – microtubule inhibitors or DNA damaging agents [93]. A popular anti-tubulin agent used in ADCs is monomethyl auristatin F (commonly referred to as auristatin F). Auristatin F (AURIF) has shown considerably higher potency than the chemotherapeutic drug, doxorubicin, and high efficacy against multi-drug resistant tumours [137]. It induces cell cycle arrest and apoptosis by inhibiting the polymerisation of tubulin (microtubule assembly). In order to be effective, AURIF requires access to the microtubules in the cytosol, and should therefore be released into the cytosol following its release from the antibody carrying it into the cell [95]. As described above, this release is achieved through lysosomal degradation. The released drugs may also cross the cell membrane and enter neighbouring cells to exert their cytotoxic effect – known as the bystander effect [114].

Current literature suggests that various factors are involved in the development of TAA-targeting ADCs, including size, pharmacokinetics, tumour uptake and penetration, as well as accumulation in tumour lesions [138]. The challenge to achieving the ultimate efficacy of these ADCs is finding the balance between these various factors as well as considering the type of cancer involved. Effectively diagnosing and characterising different types of cancers is also critical to this process.

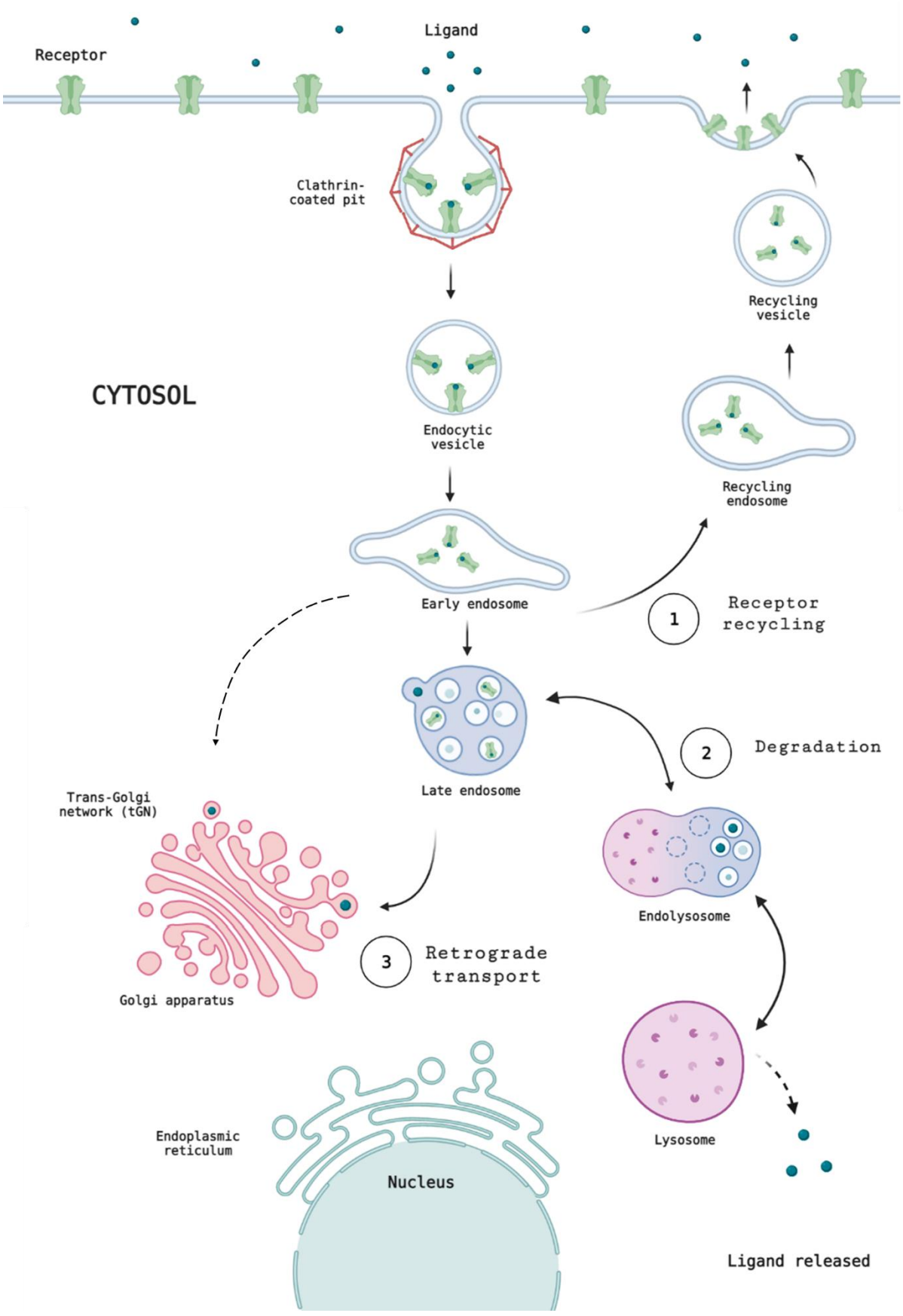
Receptor
Ligand
Clathrin-coated pit
Recycling vesicle
CYTOSOL
Endocytic vesicle
Recycling endosome
Early endosome
1
Receptor recycling
Late endosome
2
Degradation
Trans-Golgi network (tGN)
Endolysosome
3
Retrograde transport
Golgi apparatus
Endoplasmic reticulum
Nucleus
Lysosome
Ligand released

Figure 7. Clathrin-mediated endocytosis and potential intracellular pathways of the cargo. Upon internalisation by clathrin-mediated endocytosis, there are generally three intracellular pathways the receptor-ligand complex can follow once it reaches the endosomal stage. Firstly, the complex can be recycled back to the plasma membrane or secreted via exosomes (1). Secondly, the cargo can be tagged for degradation in the lysosomes, where the endosomes develop into the endo-lysosome, and finally the lysosome (2). The degradation products can then be released into the cytosol. Thirdly, the cargo can be trafficked from the endosomes to the trans-Golgi network (tGN) for processing and secretion – termed retrograde transport (3). The fate of the internalised cargo is determined by various complex cellular processes. Created using BioRender.

1.5. Study rationale, aims and objectives

The lack of targeted therapy for TNBC, which is associated with aggressive progression and poor prognosis prompted investigations into novel therapeutic methods. There is a particular need for diagnostic methods that can reliably translate into therapeutic strategies. In the African context, the burden of this heterogenous and aggressive breast cancer subtype is relatively high compared to other populations [139].

Due to the lack of therapeutic targets, cytotoxic chemotherapy remains the primary systemic therapy [34], however, the risk of recurrence and disease progression among patients treated with chemotherapy is comparably high [40]. This leads to a severe socio-economic burden attributable to the increased need for high therapeutic doses and frequent relapse. Furthermore, in African countries, the low rates of survival following chemotherapeutic treatment are exacerbated by poverty and limited healthcare facilities [43].

An immunotherapeutic approach aims to utilise the human immune system to selectively target diseased cells and has the potential for improved potency in therapy-resistant cancers [45]. Immunotherapy may improve the survival rates and prognosis of TNBC patients due to its high specificity and immune memory [46]. Furthermore, the reduced systemic toxicity significantly contributes to a better quality of life for patients undergoing treatment for aggressive cancers such as TNBC [34]. The use of ADCs to treat cancer with confirmed antigens expressed on the surfaces of tumour cells is a promising immunotherapeutic strategy.

Based on the evidence from previously established research, this study sought to improve the design of ADCs by introducing bivalency and studying the intracellular pathways after their internalisation. **The major aim of this study was to evaluate valency-dependent differences of CSPG4-targeting ADCs in terms of binding affinity (avidity), internalisation, intracellular routing, and cytotoxic effect**. The objectives employed to achieve this aim are described below in **Figure 8**.

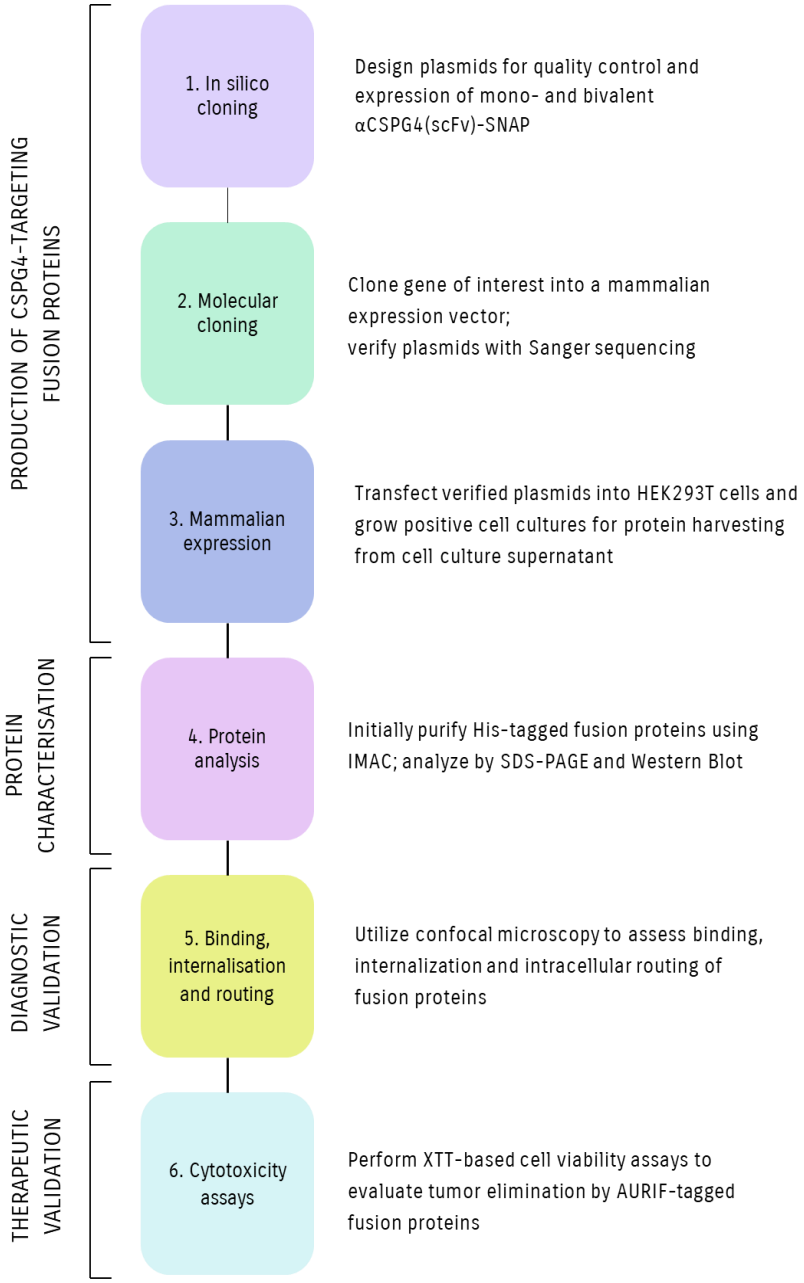

Figure 8: Study workflow and objectives. Abbreviations included: Chondroitin sulphate proteoglycan 4 (CSPG4); single chain variable fragment (scFv); histidine (His); immobilised metal affinity chromatography (IMAC); sodium dodecyl sulphate polyacrylamide gel electrophoresis (SDS-PAGE); auristatin F (AURIF).

Since full-length IgG molecules are relatively large, resulting in low penetration of tumour masses, ADCs using the scFv antibody format were opted for, which is known for its small size, increased tumour penetration, low immunogenicity and rapid clearance from circulation [140]. The target, CSPG4, is a transmembrane cell surface proteoglycan that is overexpressed in tumour cells of many aggressive cancer types without established targeted therapies, including TNBC [69]. Due to the versatility, simplicity, and robust nature of SNAP-tag technology, the gene encoding SNAP-tag was genetically attached to the scFv-encoding DNA to produce scFv-SNAP FPs [92]. The findings of previous studies suggest that increasing the valency of ADCs can enhance their efficacy due to improved antigen binding and cellular uptake. The literature also emphasizes that lysosomal degradation is crucial for the mechanism of action of ADCs [57]. Based on this information, monovalent and bivalent versions of the FPs were designed, generated, and evaluated. Briefly, valency-dependent differences were analysed as follows:

- Fluorophore-conjugated FPs were generated to compare the effect that valency would have on the binding efficiency and internalisation of the FPs in CSPG4-positive cells using confocal microscopy. Furthermore, colocalization analysis was used for the first time to identify the intracellular pathway of the internalised scFv-SNAP FPs.
- AURIF-conjugated FPs were generated to compare valency-dependent differences in cytotoxic potency against CSPG4-positive TNBC cells using cell viability assays.

The results of this study may have implications for the use of scFv-SNAP FPs as (i) diagnostic tools for the characterisation of tumours by identifying biomarkers as potential targets and (ii) as ADCs for the targeted treatment of tumours with relevant cell surface biomarkers. It will also provide insight into the mechanism of action of these FPs once they bind to their target antigen (CSPG4) and are internalised into tumour cells.

2. Chapter 2: Materials and Methods

This chapter provides information on the materials and devices used to develop and establish methods, protocols, and standard operating procedures at the Medical Biotechnology and Immunotherapy Research Unit (MB&I). The methodology described is used by members of the MB&I and is thus representative of MB&I background and know-how as documented by standard operating procedures, student theses, and original publications.

2.1. Cloning

2.1.1. *In silico* plasmid design

The open reading frames (ORFs) encoding the bivalent αCSPG4-SNAPf FPs were designed using SnapGene (v4.1.9) software. ORFs were designed to be cloned into the pCB expression vector (**Figure 8**), which was generated previously. The scFv sequence of the CSPG4-specific mAb 9.2.27 was based on VDJ and VJ gene sequences of the mouse immunoglobulin (Ig) heavy and light chains, respectively [141–143]. The domain between the variable heavy (VH) and light (VL) chains of the scFv contained a $(G_4S)_3$ sequence (5'-GGTGGCGGTGGATCC-3') encoding a flexible and biochemically inert linker. The first CSPG4 (scFv) gene was flanked by single SfiI and NotI restriction sites at the 5' and 3' end respectively. The second CSPG4 (scFv) gene was flanked by an EcoRI restriction site at the 3' end. The sequence encoding the SNAPf gene was situated between the first and second CSPG4 (scFv) genes. Cleavage of these restriction sites with the restriction endonucleases produced long overhangs thereby allowing for ligation in the correct orientation. The amino acid sequence of the ORFs was used to calculate the approximate molecular weights and isoelectric points (pI) of the FPs using the ExPaSy Compute pI/MW tool [144]. The designed ORF was synthesised by GenScript (New Jersey, USA) and received in a pUC57 vector.

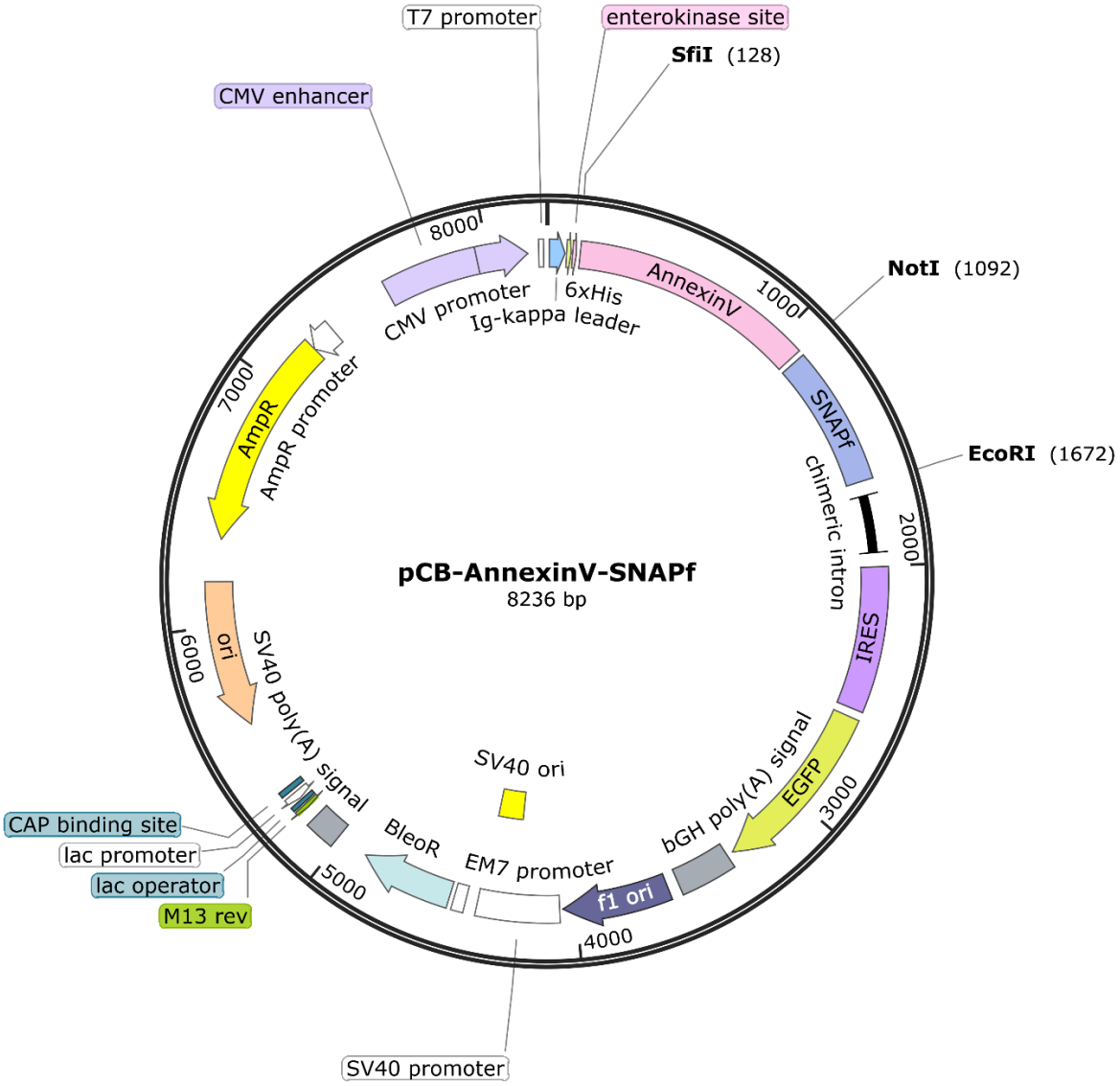

Figure 9. Plasmid map depicting pCB mammalian expression vector backbone. Different elements of the construct are labelled, and their functions are described in **Table 2**. The important endonuclease restriction sites and their corresponding positions are included (in bold). Plasmid map generated with SnapGene.

Table 2. Elements of the pCB mammalian expression vector are depicted in Figure 8 and their functions.

Element	**Function**
Cytomegalovirus (CMV) promotor	Induces the expression of the downstream ORF in the construct [145]
T7 promoter	Regulates gene expression of recombinant proteins [146]
Ig-kappa leader	Allows for the translated FP to be secreted into the supernatant [147]

N-terminal poly-histidine tag (6x His)	Used for protein enrichment with immobilised metal affinity chromatography [148] and to detect the protein of interest with immunoblot analysis
Enterokinase cleavage site	Allows for the isolation of the FP from the 6x His tag [149]
Annexin V	A phospholipid-binding protein, commonly used to detect apoptotic cells [150]. This sequence is used as a placeholder for the scFv sequence.
SNAPf	A variant of SNAP-tag known for its increased reactivity to BG-modified substrates [151]
Chimeric intron	Increases the expression of the downstream ORF by enhancing mRNA processing [152]
Internal ribosome entry site (IRES)	Mediates the translation of the EGFP gene [153]
Enhanced green fluorescent protein (EGFP)	A reporter protein which indicates successful transfection and expression in mammalian cells [153]
Bovine growth hormone polyadenylation (bGH poly(A)) signal	Allows for efficient termination and polyadenylation of the transcribed mRNA for EGFP [154]
f1 bacteriophage origin of replication (f1 ori)	Rescue of (+) single-stranded DNA [155]
Simian virus 40 (SV40) promoter	Improves transgene expression in eukaryotic host cells [156]
SV40 ori	Simian virus 40 origin of replication [156]
EM7 promoter	Synthetic bacterial promoter derived from the T7 promoter [157]
BleoR	Expresses an antibiotic-resistant protein which confers resistance to bleomycin, phleomycin and Zeocin thereby allowing for the selection of successfully transfected cells [158]
SV40 poly(A) signal	Allows for efficient termination and polyadenylation of the transcribed mRNA for BleoR [159]
Lac operator	In the absence of lactose, this sequence interacts with the lac repressor to inhibit the transcription of lac genes [160]
Lac promoter	Controls the transcription of the lac operon [160]
Catabolite activator protein (CAP) binding site	The binding of CAP to this sequence activates the transcription of various genes involved in sugar metabolism in the presence of cyclic AMP (cAMP) [161]
Ampicillin resistance gene (AmpR)	Confers resistance to ampicillin thereby allowing for the selection of plasmid-carrying cells [162]

2.1.2. Molecular cloning

2.1.2.1. Liquid transformation of competent cells

The lyophilised pUC57 plasmid DNA containing the designed ORF was dissolved in nuclease-free water (QIAGEN) to a final concentration of 100 ng/µL as per the manufacturer's instruction. The plasmid DNA was then introduced into chemically competent DH5α *E. coli* cells (New England Biolabs). One vial of chemically competent cells was thawed on ice for 5 min. 50 ng of plasmid DNA was mixed with 25 µL of competent cells and incubated on ice for 30 min. The cells were then subjected to heat shock at 42°C for 60 sec and subsequently placed on ice for 5 min. 50 mL of Luria-Bertani (LB) broth was prepared with 200 ng/µL ampicillin in a sterile glass flask. 500 µL of Super Optimal Broth with Catabolite repression (SOC) media (NEB) was added to the competent cell mixture to ensure maximal transformation efficiency and added to the LB broth supplemented with 100 µg/mL ampicillin. The flask was then incubated overnight at 37°C on a shaker.

Previously prepared DH5α cells containing a laboratory pCB plasmid were retrieved from glycerol stocks stored at -80°C. A vial was carefully thawed on ice and inoculated with 50mL LB broth supplemented with ampicillin (200 ng/µL). This was incubated overnight at 37°C on a shaker.

2.1.2.2. DNA extraction

Plasmid DNA was extracted from the overnight DH5α cultures using a laboratory-optimised phenol-chloroform isolation method. Glycerol stocks of the cultures were first prepared in a 1:1 ratio with 50% glycerol and subsequently stored at -80°C. The bacterial cells in the culture were collected by centrifugation at 4000 rcf for 10 min (4°C). The supernatant was carefully discarded, and the pellet was resuspended in 1 mL Lysis Solution I (**Table A1**) which is used to lyse the cells. The DNA was then denatured with the addition of 2 mL Lysis Solution II (**Table A1**) and incubated on ice for 5 min. The circular DNA was then renatured after adding 1.5 mL of Lysis Solution III (**Table A1**). The mixture was centrifuged at 15 000 rcf for 10 min to separate the supernatant containing the plasmid DNA from the pellet containing the cellular debris and denatured DNA. The supernatant was isolated, and 1 mg/mL RNase A was added and incubated at 42°C for 30 min to eliminate RNA contaminants. The plasmid

DNA was precipitated by the addition of 30% (v/v) isopropanol and incubated for 10 min at room temperature. To separate the protein from the DNA, 300 mM sodium acetate and 700 µL phenol-chloroform (1:1; v/v) were added and vortexed. The sample was then centrifuged at 15 000 rcf for 10 min, and the aqueous phase (top layer) containing the DNA was isolated. 300 µL of chloroform: isoamyl alcohol (24:1; v/v) was then added to the recovered DNA and mixed by inversion, followed by centrifugation at 15 000 rcf for 10 min. The aqueous phase was once again recovered, and the DNA was allowed to precipitate at -20°C for 30 min after the addition of 100% ethanol. The plasmid DNA was pelleted by centrifugation at 15 000 rcf for 30 min and rinsed with 70% cold ethanol. The pellet was allowed to dry at room temperature before its resuspension in nuclease-free water. The DNA was quantified by the DS-11 spectrophotometer (DeNovix).

2.1.2.3. Restriction endonuclease reactions

Restriction digest reactions with appropriate restriction endonuclease enzymes from NEB were performed to isolate the ORFs from the pUC57 vector and the backbone from the laboratory pCB vector. The enzymes SfiI and NotI were used to generate the monovalent construct and the bivalent construct was generated using SfI and EcoRI. **Table 3** below describes the reaction setup.

Table 3. Reaction parameters for restriction endonuclease reactions.

Component	**Amount**
DNA	2 ug
10x CutSmart Buffer	1x
SfiI	20 units
NotI / EcoRI	20 units
Nuclease-free H_2O	Adjusted to 20 µL

The reactions were initially prepared with SfiI only and incubated at 50°C for 3 hours, followed by the addition of either NotI or EcoRI and incubated at 37°C overnight. Undigested and single-digest controls were included to determine the efficacy of the enzymes. The products of the restriction digest reactions were then visualised on agarose gels.

2.1.2.4. Agarose gel electrophoresis and gel DNA extraction

Agarose gel electrophoresis was used to resolve the fragments of DNA after endonuclease digestion. 1.2% (w/v) agarose gels were prepared in 1x TAE buffer (**Table A1**) and supplemented with a 1:10 000 dilution of SYBR Safe nucleic acid marker (ThermoFisher Scientific). As a reference, 5 µL of Quick-Load 1 kb DNA marker (NEB) was used. The digested DNA samples and controls were mixed with 2 µL of 6x Purple Gel Loading Dye (NEB) and electrophoresed at 100V for 60 min. The gels were visualised using a Gel Doc XR+ imaging device (BioRad) and Image Lab (v6.1.0) software.

After visualisation, the desired mono- and bivalent insert fragments as well as the pCB backbone fragments were excised from the gel. The DNA from these fragments were purified using the QIAquick Gel Extraction Kit (QIAGEN) according to the manufacturer's instructions. The DNA was eluted with nuclease-free water and quantified using the DeNovix spectrophotometer.

2.1.2.5. Ligation and transformation

Ligation of the insert fragments and pCB backbone DNA was achieved using T4 DNA ligase (**Table 4**) and incubated at 16°C overnight according to the manufacturer's instructions. Vector-to-insert ratios of 1:3 and 1:5 were used and vector-only (no insert) controls were included to determine vector self-ligation. The amounts that were used for these ratios were dependent on the fragment sizes and calculated accordingly. After the overnight incubation, the T4 DNA ligase was then inactivated at 65°C for 10 min and then chilled on ice.

Table 4. Reaction parameters for DNA ligation reactions.

Component	**Amount**
T4 DNA Ligase Buffer	1x
Vector DNA	50 ng
Insert DNA	Variable
T4 DNA Ligase	400 units
Nuclease-free H_2O	Adjusted to 20 µL

The preparation of competent DH5α was described in section **2.1.2.1.** Here, 50 µL of competent cells were transformed with 5 µL of the ligation product. After the addition of SOC, the cells were incubated at 37°C for 60 min and 100 µL of the mixture was spread on LB agar plates supplemented with 200 ng/µL ampicillin. The plates were incubated at 37°C overnight to allow for the growth of bacterial colonies and the transformation efficiencies were determined. To determine which colonies carried the desired recombinant plasmids, colonies were selected from the plates and screened using restriction mapping analysis.

2.1.3. Restriction mapping analysis

Single colonies were selected from the plates and inoculated in 2 mL of LB broth supplemented with 200 ng/µL ampicillin and incubated at 37°C overnight on a shaker. Plasmid DNA was isolated from 1.5 mL of the cultures using the Zyppy Plasmid Miniprep kit (Zymo Research) according to the manufacturer's instructions. The plasmid DNA was resuspended in nuclease-free water and quantified using the DeNovix spectrophotometer.

DNA from the selected clones and pCB backbone was digested with HindIII and BamHI at 37°C for 1 hour. Digestion products were separated on a 1.2% agarose gel for 1 hour at 100 V. The gel was visualised using a Gel Doc XR+ imager and the fragment profile was qualitatively compared to a simulated digest profile generated by SnapGene software to evaluate ligation and ORF integration.

2.1.4. Sequencing analysis

The remaining 0.5 mL of culture from the identified positive colonies was inoculated in 50 mL LB broth supplemented with 200 ng/µL ampicillin and incubated at 37°C overnight on a shaker. DNA was extracted from these cultures using the phenol-chloroform method described in section **2.1.2.2.** The DNA was subjected to Sanger sequencing at Inqaba Biotec (South Africa) with the primers described in **Table 5**. Sequencing data were analysed using SnapGene and aligned to the designed ORF as the reference sequence.

Table 5. Primers used for the Sanger sequencing of cloned expression constructs.

Primer Name	Primer sequence (5'-3')
CMV-For	CGCAAATGGGCGGTAGGCGTG
SNAPf-For	CAAGGACTGCGAGATGAAGAGAACCACCC
pCB-Rev	CAGCTGGCCCTCGCAGACAG
SNAPf-Rev	CCTCGCCGAACTTCACCACCTTC

2.2. Recombinant protein expression

2.2.1. Transfection of HEK293T cells

Human embryonic kidney (HEK293T; ATCC: CRL-3216) cells were used as the mammalian expression system. The mammalian expression plasmid (**Figure 9**) was specifically designed for this expression system. HEK293T cells were cultured in RPMI-1640 media (Gibco) supplemented with 10% foetal bovine serum (FBS; Gibco), 100 U/mL penicillin and 100 ug/mL streptomycin (Gibco) and incubated at 37°C and 95% humidity with 5% CO_2. HEK293T cells are semi-adherent and were sub-cultured by physical aspiration.

After establishing a stable culture, cells were transiently transfected with the DNA of verified plasmids encoding the recombinant FPs using the X-tremeGENE HP DNA Transfection Reagent (Roche). Cells were seeded in a 35 mm round cell culture dish and allowed to grow until 50-70% confluency. A mixture containing 3 µg DNA and 9 µL transfection reagent in RPMI-1640 media was incubated for 15 min. The transfection mixture was then added in a dropwise manner to the cells and incubated at 37°C and 5% CO_2. A dish containing the transfection reagent without DNA was included as a negative control. After 72-96 hours, the media was replaced and the GFP expression was monitored visually using a ZOE fluorescent cell imager (BioRad).

2.2.2. Fusion protein expression in HEK293T cells

The cells were treated with 100-300 µg/µL Zeocin (ThermoFisher Scientific) for 3 months after transfection in T25 flasks to select and enrich for positively transfected cells and improve GFP

expression. Once the cultures were more than 80% positive for GFP expression, they were expanded into T75 and eventually T175 flasks. The cell cultures were maintained in T175 flasks and cell-free supernatant (CFS) was collected on a biweekly basis, clarified by centrifugation at 4000 rcf for 15 min, and stored at 4°C weeks-months. The protein expressing HEK293T cells were maintained at high confluency (>80%) and sub-cultured fortnightly.

2.3. Protein purification and characterisation

2.3.1. Immobilised metal affinity chromatography

Enrichment of the His-tagged recombinant FPs was achieved with IMAC using the ÄKTA Avant system (GE Healthcare). The buffers were prepared with ultrapure water, pH balanced, degassed, and filtered using a 0.45 µm polyvinylidene difluoride (PVDF) membrane. The CFS was applied to a HisTrap Excel column (GE Healthcare) containing a 5mL Ni^{2+} Sepharose Excel affinity resin at a flow rate of 5 mL/min. The equilibration buffer was used as the mobile phase and the resin was the stationary phase. After the column wash, the proteins that bound to the resin were eluted firstly using a gradient from 0-150 mM imidazole followed by a step elution at 500 mM imidazole.

Table 6. Steps of the immobilised metal affinity chromatography (IMAC) process and corresponding column volume (CV) and flow rate.

IMAC steps	**CV, flow rate**
Column equilibration	5 CV, 7 mL/min
Sample application	5 mL/min
Column wash	20 CV, 5 mL/min
Gradient elution (0-150 mM imidazole)	20 CV, 5 mL/min
Step elution (500 mM imidazole)	10 CV, 5 mL/min

2.3.2. SDS-PAGE analysis

Sodium dodecyl sulphate polyacrylamide gel electrophoresis (SDS-PAGE) was used to detect the presence and determine the integrity of the proteins after IMAC enrichment. Protein samples were mixed with 4x Laemmli Sample Buffer (Bio-Rad) according to the manufacturer's directions, denatured at 95°C for 10 min and loaded onto 10% polyacrylamide gel. Electrophoresis was set at 140 V for 90-120 min after which the gels were stained using AcquaStain (Bulldog Bio) overnight and de-stained in RO water for 2 hours. The gels were then visualised on a Gel Doc XR+ system (Bio-Rad).

2.3.2.1. Concentration and size exclusion

The individual IMAC fractions (15 µL) were analysed using SDS-PAGE to identify the fractions that contained the FPs. This was also used to determine which fractions should be pooled together in the subsequent concentration of fractions. Amicon Ultra-15 centrifugal filters (Merck) with a 10K MWCO were used to desalt, concentrate, and further enrich the eluted IMAC fractions for the recombinant FPs. The selected fractions were loaded onto the filter device and centrifuged at 4000 rcf for 10 min at 4°C. This was repeated until all the selected fractions had been concentrated into smaller samples. In order to preserve the integrity of the protein, 1 mM of the reducing agent, dithiothreitol (DTT), was added to the concentrated samples before the protein was quantified using the DeNovix spectrophotometer [92]. The samples were divided into 50 µL aliquots and stored at -20°C.

2.3.2.2. Quantification of purified protein

The enriched protein samples contained contaminants and cleaved or degraded protein products which could not be removed by size exclusion at that point. The concentration of full-length protein was, therefore, determined using serial dilutions of bovine serum albumin (BSA) and subsequent densitometry analysis on ImageJ software (v1.52). The BSA standards along with the concentrated protein samples were electrophoresed on a 10% polyacrylamide gel under reducing conditions as described above. After the gel image was captured, ImageJ was used to measure the relative intensity

of the bands. The data was then exported to Excel (Microsoft) and used to construct a standard curve, which was then used to calculate the concentration of the full-length recombinant FP in the samples.

2.3.3. Immunoblot analysis

Immunoblot analysis was used to determine the integrity of the recombinant FPs at the N-terminal, where the 6x His tag is situated (**Figure 9**). It was also used to identify which of the additional bands present on the SDS polyacrylamide gels were cleaved or degraded FP. Protein samples (20 µg) were prepared for SDS-PAGE which was performed in duplicate. One gel was intended for the immunoblot and the other was to be stained with AcquaStain to make an accurate comparison between the immunoblot and the denaturing polyacrylamide gel. The gel electrophoresis was performed as described above. The PVDF membrane (Roche) was activated with methanol and subsequently rinsed in transfer buffer (**Table A1**), along with the Whatman gel blotting paper (Merck). The transfer "sandwich" consisting of the layers of blotting paper, SDS polyacrylamide and PVDF membrane was assembled. The proteins were then transferred from the gel onto the membrane using the TransBlot Turbo transfer system (Bio-Rad) for 10 min at 25 V under semi-dry conditions. Once the transfer was complete, the sandwich was carefully disassembled, and the membrane was submerged in TBS-T and rinsed for 5 min. The membrane was blocked with fat-free milk for one hour and subsequently incubated with rabbit anti-His primary antibody (Cell Signaling Technology, #2365) diluted in fat-free milk (1:1000) at 4°C overnight. The following morning, the membrane was rinsed thrice with TBS-T for 5 min intervals. The membrane with incubated with the goat anti-rabbit horseradish peroxidase (HRP)-conjugated secondary antibody (Bio-Rad) dissolved in fat-free milk (1:5000) for 60 min at room temperature, and then washed thrice with TBS-T. To detect the HRP-bound proteins colourimetrically, the 1-Step Ultra TMB-Blotting Solution (ThermoFisher Scientific) was used according to the manufacturer's instructions and visualised using the Gel Doc XR+ imager.

2.3.4. Conjugation analysis

Owing to the covalent nature of the interaction between SNAP-tag and BG-modified substrates, once the FPs are conjugated to BG-modified substrates they can be subjected to denaturation without

affecting the bond [96]. Conjugated proteins could, therefore, be subjected to SDS-PAGE analysis. This was useful to determine the optimal ratio of the FP to BG-modified substrate to use for these FPs.

2.3.4.1. Conjugation to BG-modified fluorophores

The recombinant FPs were conjugated to BG-modified fluorophores for downstream imaging experiments. Since the SNAP protein is located at the C-terminal of the FP, the functionality of SNAP and thereby the integrity of the C-terminal was initially determined. The FP was incubated with a 2-fold molar excess of BG-modified Alexa Fluor 488 (NEB) for 1 hour at 37°C under dark conditions. The reaction (**Table 7**) was then mixed with 4x Laemmli Sample Buffer, resolved on a 10% SDS polyacrylamide gel which was carried out under dark conditions and visualised using the GelDoc XR+ imager. The gel was then stained with AcquaStain and visualised according to the methodology outlined in section **2.3.2.** This allowed for a parallel comparison of the FP.

Table 7. Reaction parameters for labelling SNAP-FP with BG-Alexa 488

Component	**[Final]**
DTT	1 mM
BG-Alexa 488	10 µM
SNAP-FP	5 µM
1x PBS	Adjusted to 20 µL

The two-fold molar excess of BG-Alexa 488 to SNAP-FP is recommended by the manufacturer and reported in the literature [92]. However, in order to be economical and further characterise the FPs, conjugation reactions at varying ratios of SNAP FP to BG-modified fluorophores were carried out. Initially, four single conjugations to either BG-Alexa 488 or BG-Alexa 647 (NEB) at 4:1, 2:1, 1:1 and 1:2 ratios of SNAP FP to fluorophore were conducted (**Table 8**), visualised on 10% resolving SDS polyacrylamide gels and compared for labelling efficiency. Thereafter, as described in **Table 9**, dual conjugations were conducted with varying concentrations of BG-Alexa 488 while the concentration of BG-Alexa 647 remained constant. The reaction was initially incubated without BG-Alexa 647 at 37°C for 1 hour in the dark. Thereafter, BG-Alexa 647 was added and incubated for an additional hour at

37°C. The reaction was resolved on an SDS polyacrylamide gel in the dark and visualised for both 488 and 647 fluorescence using the iBright FL1500 imager (Thermo Fisher Scientific). This allowed for the determination of SNAP-tag saturation at these different ratios. Furthermore, band intensities were compared using ImageJ software.

Table 8. Reaction for the single conjugation parameters of scFv-SNAP with BG-Alexa 488 or 647

Component	**[Final]**
DTT	1 mM
BG-Alexa 488 or 647	1.25; 2.5; 5; 10 µM
SNAP-FP	5 µM
1x PBS	Adjusted to 20 µL

Table 9. Dual conjugation reaction parameters of scFv-SNAP with BG-Alexa 488 and 647

Component	**[Final]**
DTT	1 mM
BG-Alexa 488	1.25; 2.5; 5; 10 µM
BG-Alexa 647	2.5 µM
SNAP-FP	5 µM
1x PBS	Adjusted to 20 µL

2.3.4.2. Conjugation to BG-modified auristatin F

Monomethyl auristatin F (BrightGene Bio-Medical Technology), was modified to contain benzyl guanine by Allan Huysamen (MSc, Department of Chemistry, University of Cape Town). Once again, to determine the most optimal ratio of SNAP FP to BG-AURIF, varying concentrations of BG-AURIF were used in the initial conjugation reactions (**Table 10**). The reaction was first incubated without the fluorophore at room temperature for 4 hours. BG-Alexa 488 was then added and incubated at 4°C overnight. The reaction product was separated and visualised on an SDS polyacrylamide gel.

Table 10. Dual conjugation reaction parameters of scFv-SNAP with BG-AURIF and BG-Alexa 488

Component	[Final]
DTT	1 mM
BG-AURIF	5; 10; 15 µM
BG-Alexa 488	5 µM
SNAP-FP	5 µM
1x PBS	Adjusted to 20 µL

2.4. *In vitro* functional assays

2.4.1. Tumour cell culture

The tumour cell lines, Hs578T (ATCC: HTB-126) and MCF-7 (ATCC: HTB-22) were selected as antigen-positive and antigen-negative breast cancer cell lines, respectively. Hs578T was cultured in Dulbecco's Modified Eagle Medium (DMEM; Gibco) and MCF-7 was cultured in RPMI-1640 supplemented with 10% FBS, 100 U/mL penicillin and 100 µg/mL streptomycin and incubated at 37°C and 95% humidity with 5% CO_2. The tumour cells were passaged at 90% confluency and the media was changed on a biweekly basis. Tumour cells are adherent and require trypsinization to subculture. This was achieved by removing all traces of FBS-supplemented media from the cell culture flasks by rinsing the cells twice with 1x PBS. 1x Trypsin-EDTA (Sigma) was added to the flasks until the cells were morphologically round and had nearly lifted. The Trypsin-EDTA was removed and inactivated with the addition of FBS-supplemented media, and the cells were resuspended by aspiration. The cultures were passaged by retaining 5% of the cells in fresh media.

2.4.2. Confocal microscopy

2.4.2.1. Preparation of tumour cells and fluorophore-conjugated fusion proteins

Live cell imaging was conducted on tumour cell lines to assess and compare the binding and internalisation profiles between the monovalent and bivalent FPs. 2 x 10^4 Hs578T and 4 x 10^4 MCF-7

cells were seeded in each quadrant of 35 mm live cell viewing dishes. The tumour cells were incubated overnight at 37°C and 95% humidity with 5% CO_2 in supplemented media.

The monovalent (MV) and bivalent (BV) SNAP FPs were conjugated to BG-Alexa 488 as per the conditions in **Table 11**. 200 µL reactions were prepared for each quadrant and allowed to conjugate under dark conditions for 60 min. These reactions were either stored at -20°C if they were to be used to next day or kept at room temperature if used the same day. The conjugated FPs were first sterilised using 0.22-micron syringe filters and mixed thoroughly with 200 µL unsupplemented medium under sterile conditions.

Table 11. Labelling reaction parameters of immunodiagnostic FPs for imaging experiments

Component	**[Final]**
DTT	1 mM
BG-Alexa 488	5 µM
SNAP-FP	5 µM
1x PBS	Adjusted to 200 µL

2.4.2.2. Binding, internalisation, and intracellular routing analysis

Once the cells were ready for staining, the media was removed, and the cells were washed with sterile 1x PBS. The conjugated FP and media mixtures were then added to the respective quadrants and allowed to incubate for 30 min at 37°C. Plain unsupplemented media was added to the designated Hoechst only and unstained quadrants. The cells were then washed thrice with 1x PBS and 200 µL Hoechst (1:5000) was added and incubated at room temperature for 10 min. 1x PBS was once again used to wash the cells and remove the excess dye, and fresh supplemented media was added to the quadrants. The cells were then visualised with a 63x oil objective on the Zeiss LSM 880 confocal microscope using the appropriate laser wavelengths and images captured for further analysis using the Zeiss ZEN lite software (v3.6).

Colocalization imaging experiments were conducted to determine the intracellular pathway of the FPs after internalisation. LysoTracker Red and ER-Tracker Red (Molecular Probes; Thermo Fisher Scientific) were used to stain the lysosomes and endoplasmic reticulum, respectively.

The SNAP FPs and cells were prepared as described in section **2.4.2.1** and the cells were first incubated with these for 30 min at 37°C. The FP was then removed and 50 ng of LysoTracker or 1 µM of endoplasmic reticulum (ER) tracker was added and incubated for 30 min at 37°C. Lastly, the nuclear stain, Hoechst (1:5000), was added and allowed to incubate at room temperature for 10 min. The cells were washed thrice with 1x PBS in between all the incubation steps, and plain supplemented media was added as the last step before visualisation on the Zeiss LSM 880 confocal microscope (37°C, 5% CO_2). Before visualisation, cells were maintained in sterile conditions at room temperature.

2.4.3. Cytotoxicity assays

The SNAP FPs were conjugated to BG-AURIF according to the conditions in **Table 12** for 2 hours at 37°C and then overnight at 4°C. Unbound BG-AURIF and DMSO were removed using buffer exchange with 1x PBS. To determine the concentration of full-length conjugated protein, densitometry analysis was conducted. Furthermore, the saturation of the SNAP-tag was determined by conjugation analysis with BG-Alexa 488 which was separated and visualised using SDS-PAGE analysis.

Table 12. Labelling reaction parameters of immunotherapeutic fusion proteins for cytotoxicity experiments

Component	**[Final]**
DTT	1 mM
BG-AURIF	20 µM
SNAP-FP	10 µM
1x PBS	Adjusted to 1000 µL

The same tumour cells used in the imaging experiments were used in the cytotoxicity analysis. 2 x 10^3 Hs578T and 4 x 10^3 MCF-7 cells were seeded in 96-well plates in their respective complete (supplemented) media and allowed to adhere and grow overnight under standard tissue culture conditions. The following day, the cells were treated with 1:5 serially diluted FP conjugated to BG-

AURIF, where the highest concentration was 1 µM. Additional controls included 1 µM BG-AURIF only, 1 µM unconjugated FP, 100 µg/mL Zeocin (positive control; 0% viability) and 1x PBS (negative control; 100% viability).

The XTT cell viability assay (Cell Proliferation Kit II; Roche) was used to assess the cytotoxic effect of the FPs conjugated to the drug, AURIF. This assay uses the tetrazolium salt, XTT, which is cleaved in the presence of phenazine (electron coupling agent), thereby producing a soluble formazan salt by metabolically active cells. This reduction results in a colourimetric change from yellow to orange which can be detected spectrophotometrically at 450 nm. At 44 hours post-treatment, micrographs were captured of cells to visually assess signs of apoptosis induced by the treatment. The cells were then treated with the XTT reagent according to the manufacturer's specifications and incubated for an additional 4 hours under dark conditions. The colourimetric change was detected spectrophotometrically at 450 nm and 650 nm (reference filter) using the iMark Microplate Absorbance Reader (Bio-Rad). These experiments were conducted in triplicate (n= 3) and included 3 technical repeats. The absorbance values were normalised using the PBS and Zeocin controls as the highest and lowest readings, respectively. The cytotoxic effect was accordingly calculated and presented as a percentage of cell viability. The IC_{50} value, which is defined as the concentration needed to reduce the cell viability by 50% was also determined. GraphPad Prism v5 software was used for all data analysis and calculations.

3. Chapter 3: Results

The role of CSPG4 in tumorigenesis, angiogenesis resistance and metastasis, along with its upregulation in TNBC tumours highlights it as a suitable target for antibody-based diagnostic and therapeutic strategies [67]. The aggressive and heterogeneous nature of this disease in addition to the lack of available targeted therapies means that novel diagnostic and therapeutic options are desperately needed. This study set out to build upon previous studies targeting CSPG4 in TNBC by utilising scFv FPs and SNAP-tag technology. A novel bivalent αCSPG4$(scFv)_2$-SNAP FP was generated to evaluate its potential in targeting antigen-positive TNBC cells and delivering diagnostic or therapeutic probes. Furthermore, these parameters were compared to a monovalent αCSPG4(scFv)-SNAP FP to determine notable valency-dependent differences. This chapter, therefore, describes the design and generation of these FPs, their functional characterisation and *in vitro* assessment.

3.1. Design and production of SNAP fusion proteins

3.1.1. *In silico* cloning

The designed ORFs were designed to include all the necessary components for downstream cloning, expression, and purification experiments (**Figure 10**). The amino acid sequences allowed for the determination of the pI and molecular weights (MW) of the resultant FPs using the ExPaSy Compute pI/MW tool [144]. This information is important for downstream protein identification and characterisation experiments. While the difference in pI is negligible, the monovalent is ~30 kDa lighter than the bivalent FP, owing to the addition of the scFv (~28 kDa). This allows for the differentiation between the two FPs on SDS polyacrylamide gels. The difference in size may also have implications for the transient expression and purification experiments.

In silico cloning techniques (SnapGene) using the pCB backbone (**Figure 8**) and the ORFs were utilized to visualise and assess the resultant plasmids for any errors that would lead to problems during the expression and purification process (**Figure 10**).

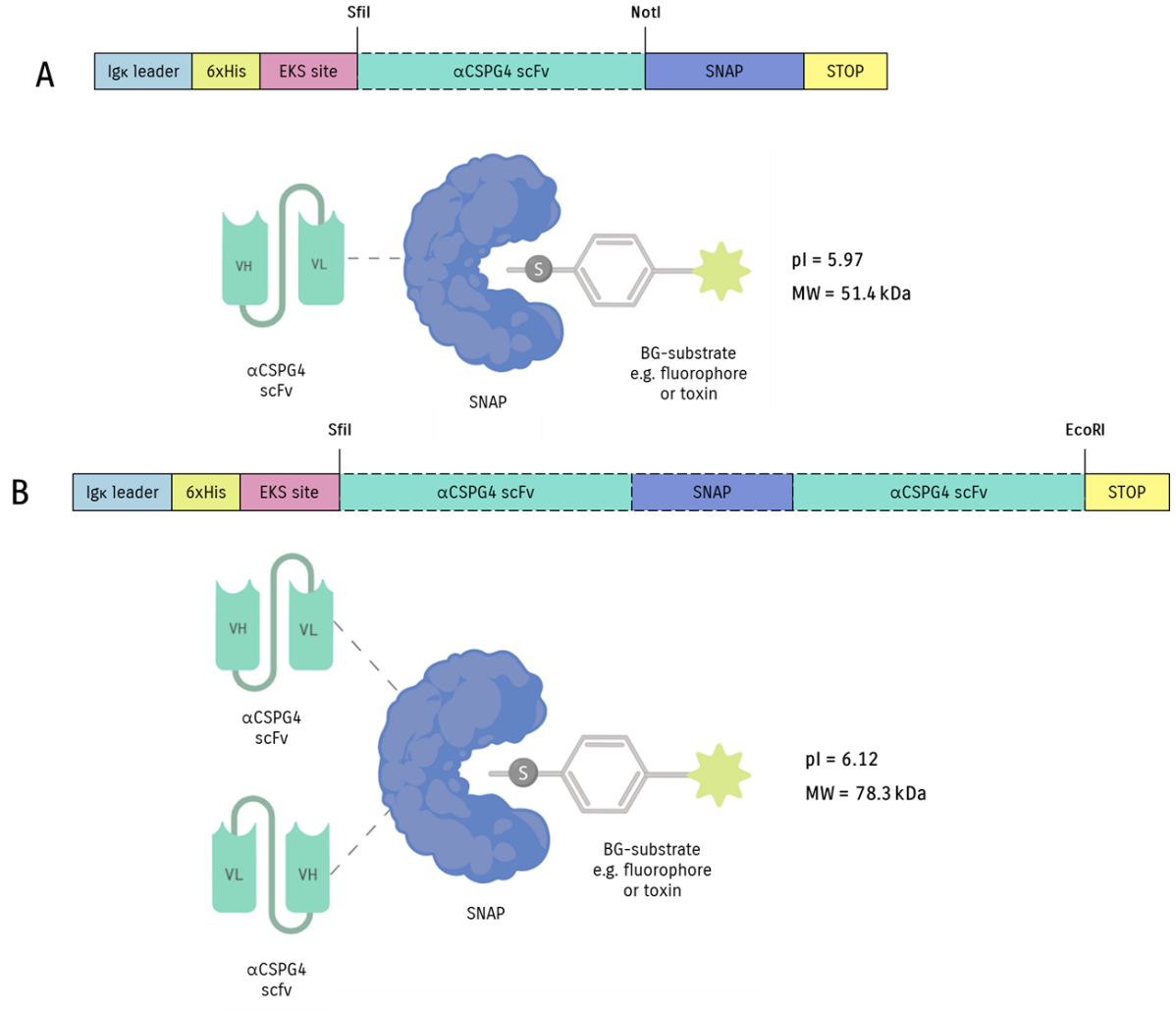

Figure 10. The *in silico* design of the αCSPG4-SNAP fusion proteins. (A) The designed open reading frame (ORF) and schematic diagram of the monovalent αCSPG4(scFv)-SNAP fusion protein. The NotI and SfiI endonuclease sites which were used during the molecular cloning process into the mammalian expression vector are indicated, along with the αCSPG4 scFv and other important components of the construct. The amino acid sequence of the ORF was used to determine the pI (isoelectric point) and molecular weight of the resulting protein. (B) The ORF and schematic diagram of the bivalent αCSPG4$(scFv)_2$-SNAP fusion protein. The SfiI and EcoRI restriction sites which were used during the molecular cloning process into the mammalian expression vector are indicated, along with the αCSPG4 scFv's and other important components of the construct. The amino acid sequence of the ORF was used to determine the pI (isoelectric point) and molecular weight of the resulting protein. Created using BioRender.

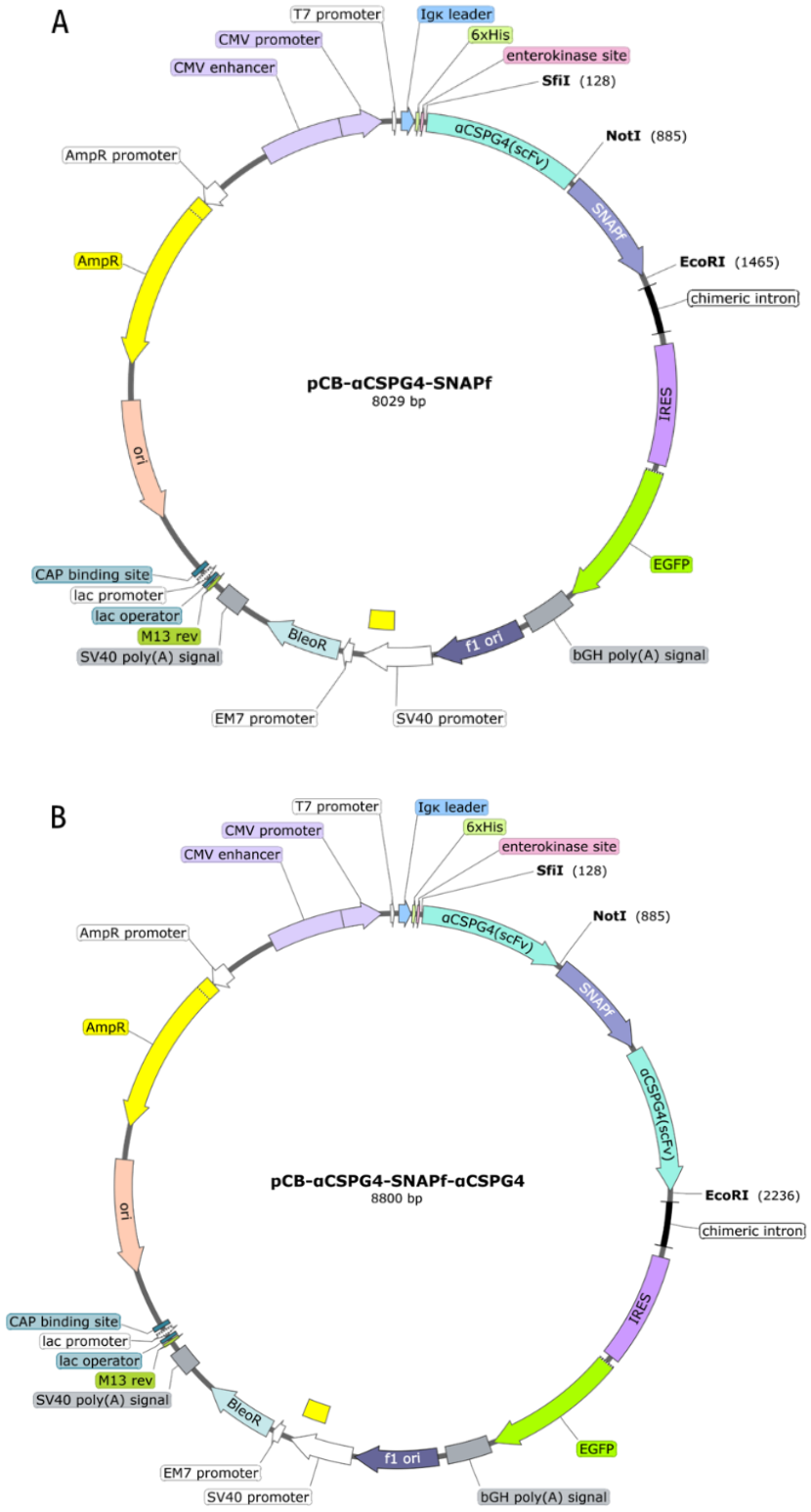

Figure 11. Mammalian expression plasmids that were constructed using molecular cloning techniques. The plasmids designed to produce the (A) monovalent and (B) bivalent fusion proteins were cloned using the respective endonucleases to desired sections into the pCB-SNAP backbone. Each component of the plasmid plays a role in the cloning, transfection and transient protein expression processes. Plasmid components and relevant functions are described in **Table** 2. Plasmid maps generated with SnapGene.

3.1.2. Molecular cloning

Once the designed ORFs were synthesised, the first step to obtaining the plasmids in **Figure 11** was to isolate the appropriate pCB backbone and scFv inserts. This was achieved using the enzymes SfiI + NotI (monovalent) and SfiI + EcoRI (bivalent) as described in section **2.1.2**. These endonucleases produce "sticky ends" which allow for the subsequent ligation of the backbone and insert. **Figure 12** depicts the fragments after digestion, visualised on an agarose gel. The encircled fragments were excised from the gel and purified according to section **2.1.2.4**. Thereafter, the insert and backbone DNA were ligated at varying ratios of backbone to insert, and the recombinant DNA was transformed into DH5α cells. The transformation efficiencies were calculated accordingly (**Figure 12, B and D**).

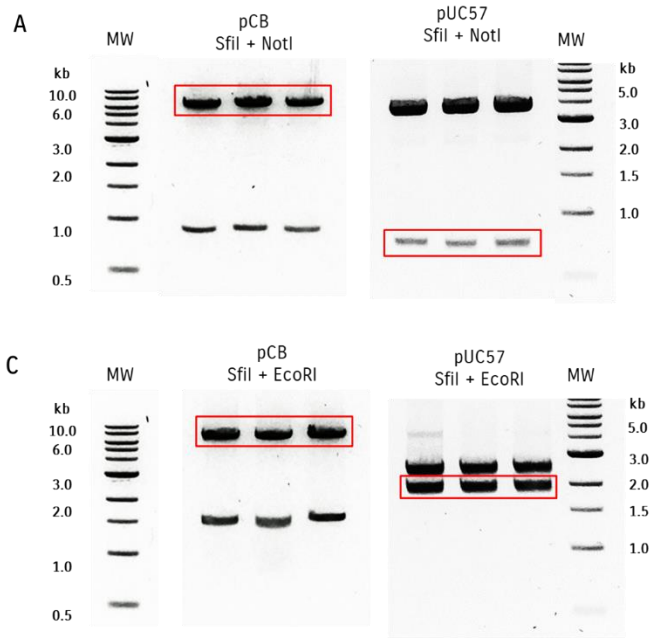

B

Ligation ratio (Backbone : Insert)	Transformation efficiency (cfu/µg)
1 : 0 (vector only)	0
1 : 3 (monovalent)	2.8×10^3
1 : 5 (monovalent)	5.6×10^3

D

Ligation ratio (Backbone : Insert)	Transformation efficiency (cfu/µg)
1 : 0 (vector only)	0
1 : 3 (bivalent)	3.3×10^3
1 : 5 (bivalent)	1.1×10^3

Figure 12. Molecular cloning of mammalian expression plasmids. (A) Agarose gel (1%, w/v) depicting the pCB backbone and αCSPG4 scFv segment isolated using the SfiI and NotI restriction enzymes (endonucleases). These fragments were ligated to produce the monovalent αCSPG4(scFv)-SNAP fusion protein. (B) Transformation efficiency of the recombinant plasmid with different ratios of the backbone and monovalent insert isolated by restriction digestion, agarose gel electrophoresis and extraction. (C) Agarose gel (1%, w/v) depicting the pCB backbone and αCSPG4$(scFv)_2$-SNAP segment isolated using the SfiI and EcoRI restriction enzymes (endonucleases). These fragments were ligated to produce the bivalent αCSPG4$(scFv)_2$-SNAP fusion protein. (B) Transformation efficiency of the recombinant plasmid with different ratios of the backbone and bivalent insert isolated by restriction digestion, agarose gel electrophoresis and extraction.

3.1.3. Verification of recombinant plasmids

A

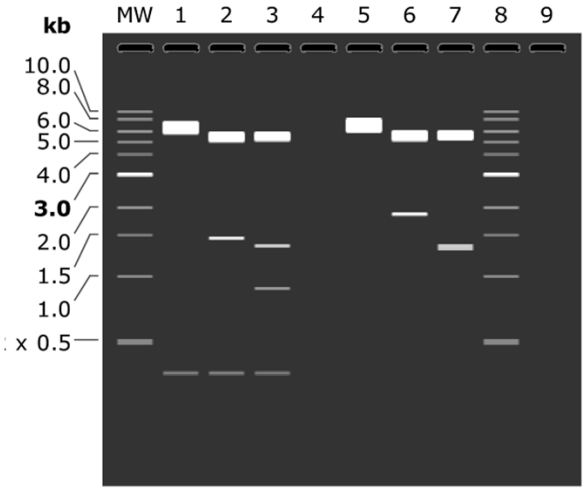

1.2 % agarose

MW: 1 Kb DNA Ladder

1: pCB-AnnexinV-SNAP
HindIII
1. 7528 bp
2. 360 bp
3. 348 bp
4. 360 bp
5. 348 bp

2: pCB-CSPG4-SNAP
HindIII
1. 5868 bp
2. 1453 bp
3. 360 bp
4. 348 bp

3: pCB-CSPG4-SNAP-CSPG4
HindIII
1. 5868 bp
2. 1341 bp
3. 883 bp

5: pCB-AnnexinV-SNAP
BamHI
1. 8236 bp

6: pCB-CSPG4-SNAP
BamHI
1. 6156 bp
2. 1873 bp

7: pCB-CSPG4-SNAP-CSPG4
BamHI
1. 6156 bp
2. 1341 bp
3. 1303 bp

8: 1 Kb DNA Ladder

B

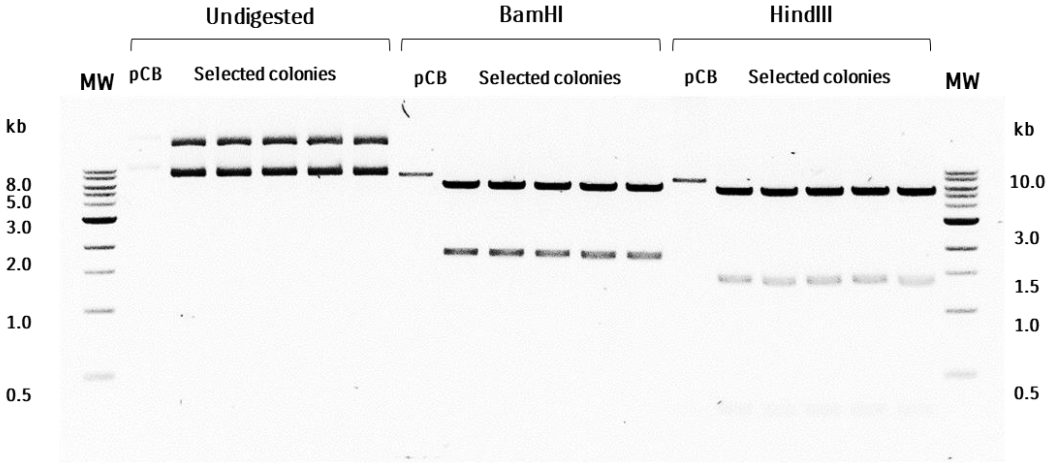

C

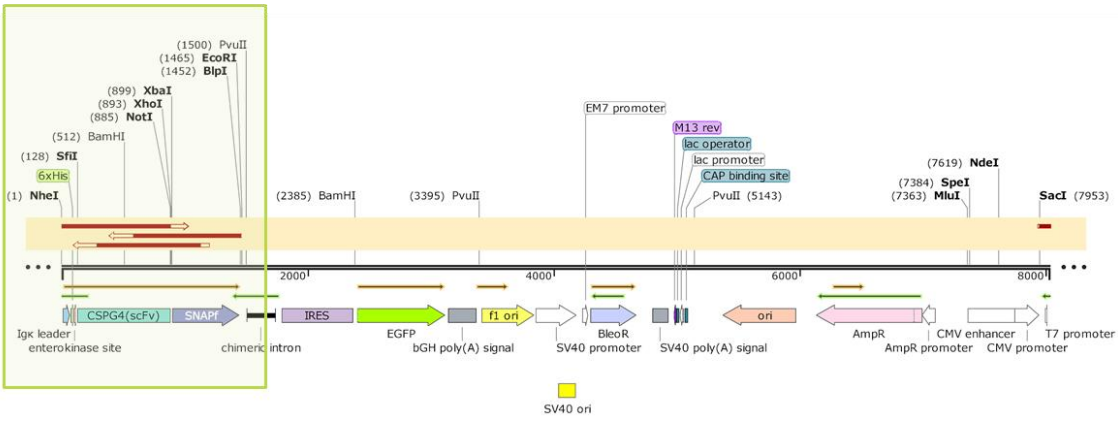

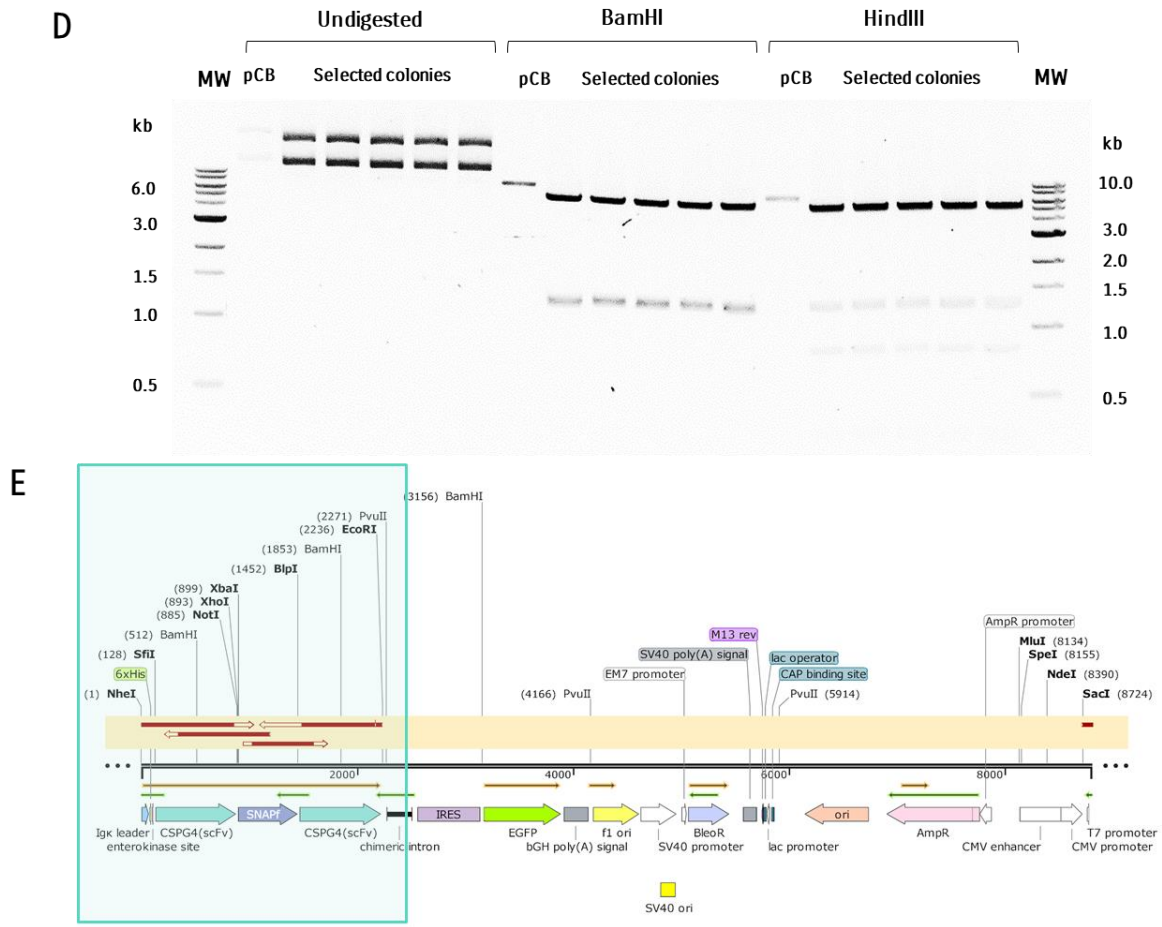

Figure 13. Analysis and validation of recombinant mammalian expression plasmids. (A). In silico restriction digest analysis of the pCB-AnnexinV-SNAP plasmid as well as the recombinant monovalent and bivalent pCB-αCSPG4-SNAP plasmids using the HindIII and BamHI endonucleases. Simulated with SnapGene software. (B) Restriction analysis of monovalent pCB-αCSPG4(scFv)-SNAP recombinant plasmids. Plasmid DNA was isolated from colonies of DH5α colonies transformed with the ligated DNA. (C) Sanger sequence analysis of the successful recombinant monovalent plasmids. Positive plasmids were identified from selected colonies. Red arrows represent the aligned sequences generated using the primers in **Table 5**. (D) Restriction analysis of the bivalent pCB-αCSPG4(scFv)$_2$-SNAP recombinant plasmids isolated from DH5α colonies. (E) Sanger sequence analysis of recombinant bivalent plasmids identified by restriction analysis. Red arrows represent the aligned sequences generated using the primers in **Table 5**.

To screen for positive colonies with the recombinant plasmids, restriction analysis was used (section **2.1.3**). Here we compared the restriction digest pattern of the backbone plasmid (pCB-AnnexinV-SNAPf) to that of the desired recombinant plasmids. The expected digest patterns were simulated with

SnapGene (**Figure 13A**) using the BamHI and HindIII endonucleases. The restriction digestion was then carried out on plasmid DNA from selected individual colonies and visualised using agarose gel electrophoresis (**Figure 13**, B and D). The DNA from these colonies was then subjected to Sanger sequencing (see section **2.1.4**) to ensure that no mutations were present in ORFs (**Figure 13**, C and E).

3.1.4. Transient transfection of HEK293T

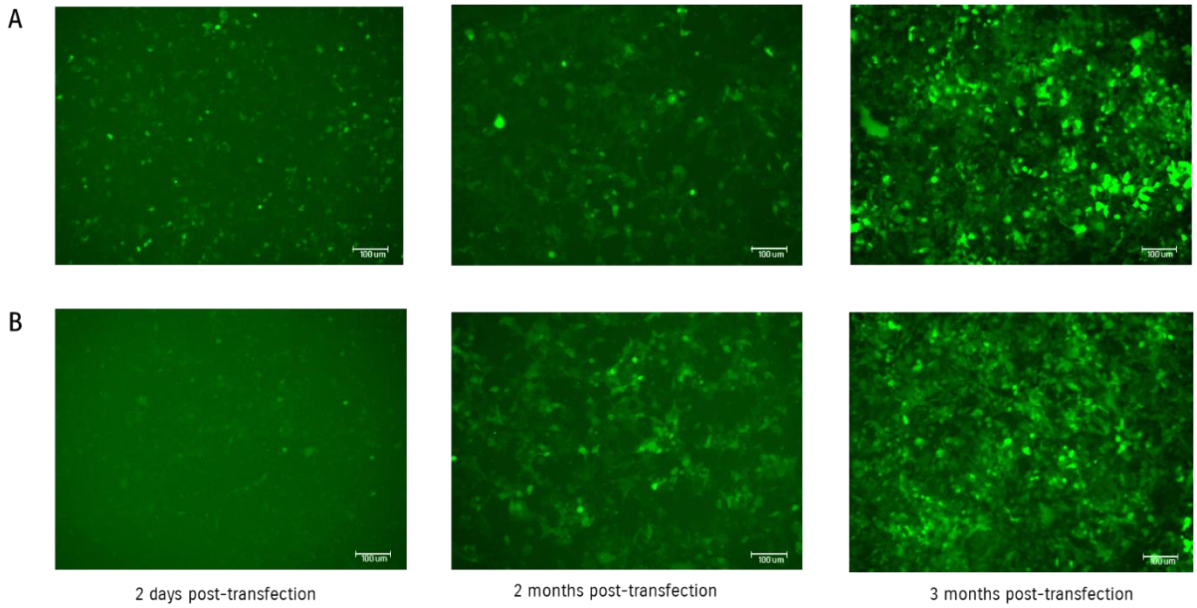

Figure 14. Microscopic analysis of GFP expression in transfected HEK293T cell cultures. Comparison of GFP expression in the cells transfected with the recombinant plasmid encoding the (A) monovalent and (B) bivalent αCSPG4-SNAP fusion proteins. Images were captured two days, two months, and three months after transfection with the recombinant DNA. The enrichment of the GFP signal was achieved using continuous selection for successfully transfected cells with Zeocin. Images were captured with the ZOE fluorescent cell imager. Scale bar = 100 µm.

The recombinant plasmids, verified with Sanger sequencing, were transfected into HEK293T cells, and subjected to selection with Zeocin as described in section **2.2.1** (**Figure 14**). Based on the GFP expression two days after transfection (**Figure 14**, first column), the transfection efficiency was relatively low and estimated to be ~30% for the monovalent construct and ~15% for the bivalent construct. This difference in GFP expression continued regardless of the selection pressure applied. Once the GFP expression was ~80% (3 months after transfection) (**Figure 14**, third column), CFS

containing the secreted FP was collected. At this point, the cell cultures were also expanded for harvesting.

3.2. Characterisation of SNAP-tag fusion proteins

Due to the Ig-kappa leader sequence of the expression vector (**Figure 9**), the FPs that are expressed in the HEK293T cells are secreted into the cell culture medium [147]. To assess the integrity of the FPs, IMAC was used to enrich His-tagged proteins as described in section **2.3.1**.

3.2.1. SDS-PAGE analysis and yield of purified fusion proteins

The chromatograms (**Figures 15A and 16A**) show two distinct peaks which correspond to the gradient elution (0-150 mM imidazole) and the step elution (500 mM imidazole). Based on the chromatogram depicting the elution profiles, the fractions were concentrated into two samples using Amicon centrifugation filters (10 kDa MWCO). These samples were resolved and visualised on SDS polyacrylamide gels (described in section **2.3.2**) along with the flow through from the ÄKTA machine (**Figures 15B and 16B**). Flow through 1 represents the entire volume of cell-free supernatant that passed through the ÄKTA system, excluding His-tagged proteins which remained bound to the column.

Table 13: Calculation of monovalent αCSPG4(scFv)-SNAP fusion protein yield. Comparison between the total amount of protein eluted and the protein of interest: αCSPG4(scFv)-SNAP FP. The absolute amount of purified full-length FP was calculated and used to determine the yield of the transient mammalian expression system and IMAC protein purification process.

Sample	Densitometric concentration (µg/µL)	Total protein concentration (mg/mL)	% FP in sample	Absolute amount (µg)	Yield (mg/L)
MV Fraction A + B	7.40	20.32	36%	2589	2.52
MV Fraction C + D	2.64	8.70	30%	1189	

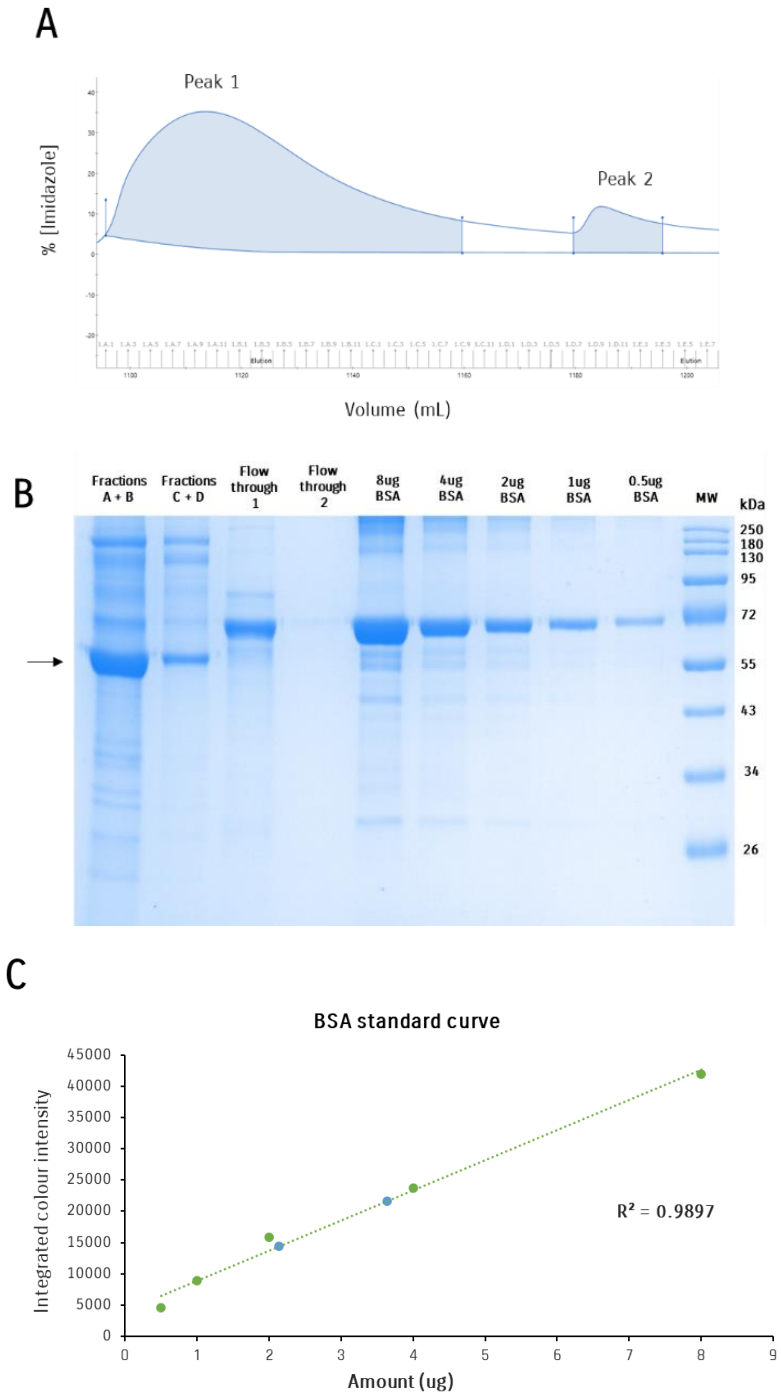

Figure 15. Analysis of the purified monovalent *α*CSPG4(scFv)-SNAP fusion protein. (A) Chromatogram depicting the IMAC elution profile of cell-free supernatant containing the secreted fusion protein. (B) SDS-PAGE analysis of the concentrated eluate containing the monovalent fusion protein (black arrow). The flow through from the IMAC process was also included on the gel to assess whether any fusion protein was not eluted. Two-fold serially diluted BSA was used as a standard to determine the concentration of full-length fusion protein in the eluate. Protein sizes were estimated in alignment with the SuperSignal protein standard. (C) Densitometry analysis using the BSA standard curve (green) to calculate the amount of concentrated full-length monovalent fusion protein (blue).

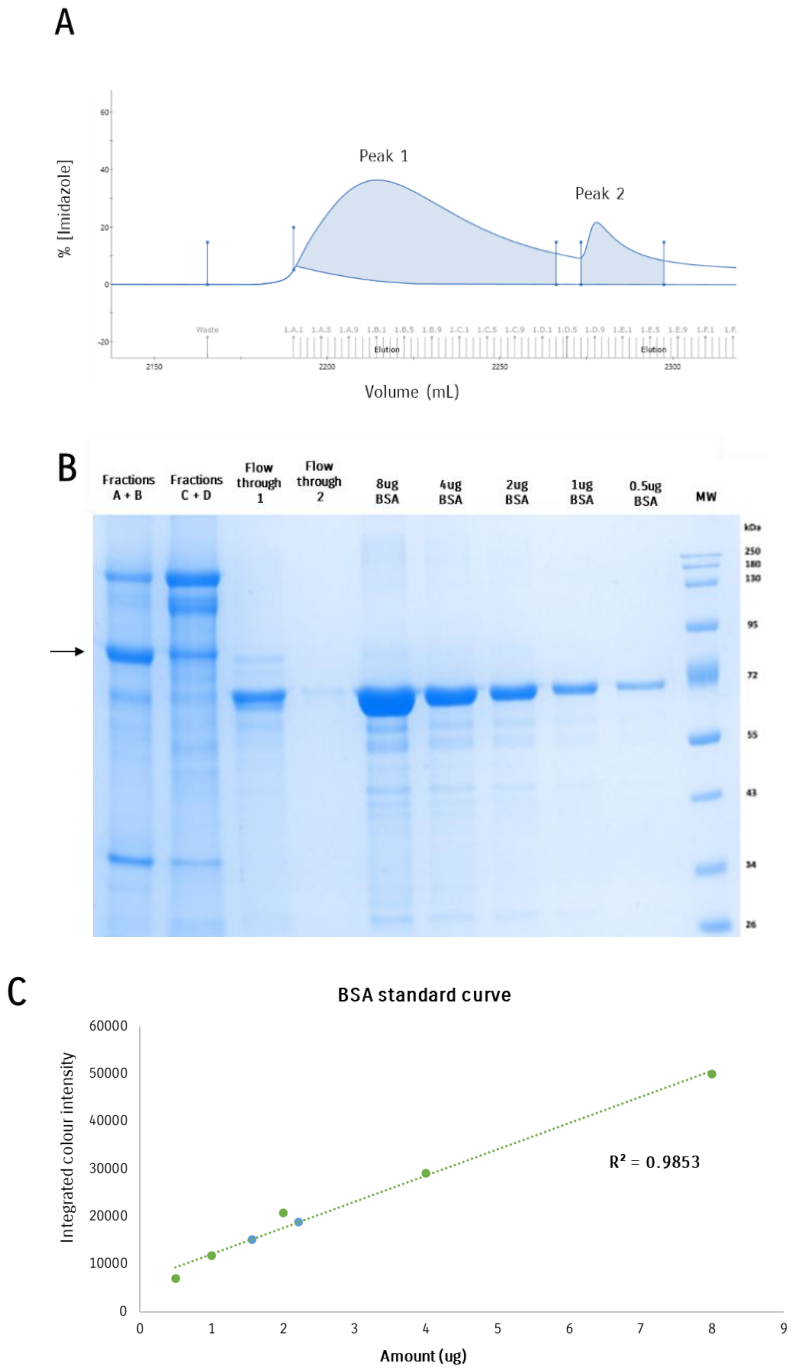

Figure 16. Analysis of the purified bivalent αCSPG4(scFv)$_2$-SNAP fusion protein. (A) Chromatogram depicting the IMAC elution profile of cell-free supernatant containing the secreted bivalent fusion protein. (B) SDS-PAGE analysis of the concentrated eluate containing the bivalent fusion protein (black arrow) under reducing conditions. The flow through from the IMAC process was also included on the gel to assess whether any fusion protein was not eluted. Two-fold serially diluted BSA was used as a standard to determine the concentration of full-length fusion protein in the eluate. Protein sizes were estimated in alignment with the SuperSignal protein standard. (C) Densitometry analysis using the BSA standard curve (green) to calculate the amount of concentrated full-length bivalent fusion protein (blue).

Flow through 2 represents the final wash of the ÄKTA system with an equilibration buffer. The flow-through samples would indicate whether any protein of interest failed to bind to the column and was not eluted in the final fractions. This essentially signifies whether any protein of interest was lost during the IMAC process. From the stained gel images in **Figures 15 and 16**, it appears that some of the full-length protein was lost to flow-through 1, however, flow-through 2 remains clear. The majority of flow through 1 and 2 consists of BSA, which is expected since the cell culture media was supplemented with FBS.

Table 14. Calculation of bivalent αCSPG4(scFv)$_2$-SNAP fusion protein yield. Comparison between the total amount of protein eluted and the protein of interest: αCSPG4(scFv)$_2$-SNAP FP. The absolute amount of purified full-length FP was calculated and used to determine the yield of the transient mammalian expression system and IMAC protein purification process.

Sample	Densitometric concentration (µg/µL)	Total protein concentration (mg/mL)	% FP in sample	Absolute amount (µg)	Yield (mg/L)
BV Fraction A + B	4.88	21.70	22%	1464	1.19
BV Fraction C + D	0.91	4.40	21%	320	

Since the protein samples do not only consist of full-length FPs, evidenced by the presence of additional bands on the stained gel images (**Figures 15B and 16B**), it was necessary to determine the concentrations of full-length protein in the samples. Densitometry analysis was used to achieve this, where BSA standards of known amounts were included in the SDS-PAGE (see section **2.3.2.2**). The intensity of the bands was then determined with ImageJ software and used to construct a standard curve (**Figures 15C and 16C**). From the standard curve, the concentrations and amounts of the full-length FPs were calculated (**Tables 13 and 14**).

The yield of the mammalian expression system was also calculated for these two FPs, where the yield of the bivalent αCSPG4(scFv)$_2$-SNAP FP (1.19 mg/L) was less than half of the yield of the monovalent counterpart (2.52 mg/L) (**Tables 13 and 14**). The percentage of full-length protein in the concentrated

samples is fairly low: ~30% and ~20% for the monovalent and bivalent FPs, respectively. The expression cell cultures, therefore, had to be maintained for months to produce sufficient protein for downstream experiments, with multiple rounds of protein purification. The information represented in **Figures 15 and 16** is consistent with each round of protein purification and quantification (**Table A4**). It should however be noted that the full-length FPs were subject to degradation over time when stored at 4ºC and -20ºC. The rate of degradation was slowed when stored at -20ºC and this was selected as the standard temperature for protein storage before conjugation and downstream experiments.

3.2.2. Immunoblot analysis of concentrated purified protein samples

After determining the yield of the full-length FPs in the concentrated samples, it was important to ensure that the protein was intact and functional at both the N- and C-terminals. Immunoblot analysis using an anti-His antibody that binds to the His tag on the N-terminal of the FPs as described in section **2.3.3** (**Figure 10**) allows for the evaluation thereof. Additional His-tagged proteins that potentially present truncated or degraded FPs are also identified in this manner.

The comparison between the stained SDS polyacrylamide gels and immunoblots (**Figure 17**) indicates that many of the bands present in the concentrated protein samples are His-tagged. The bands that are present below the full-length protein bands in both the monovalent and bivalent FP samples (~34 kDa) may represent truncated, proteolytically cleaved or degraded FP. Faint bands are also present on the immunoblot in the lanes of flow through 1, indicating that some of the His-tagged protein was lost during the IMAC process (**Figure 17**).

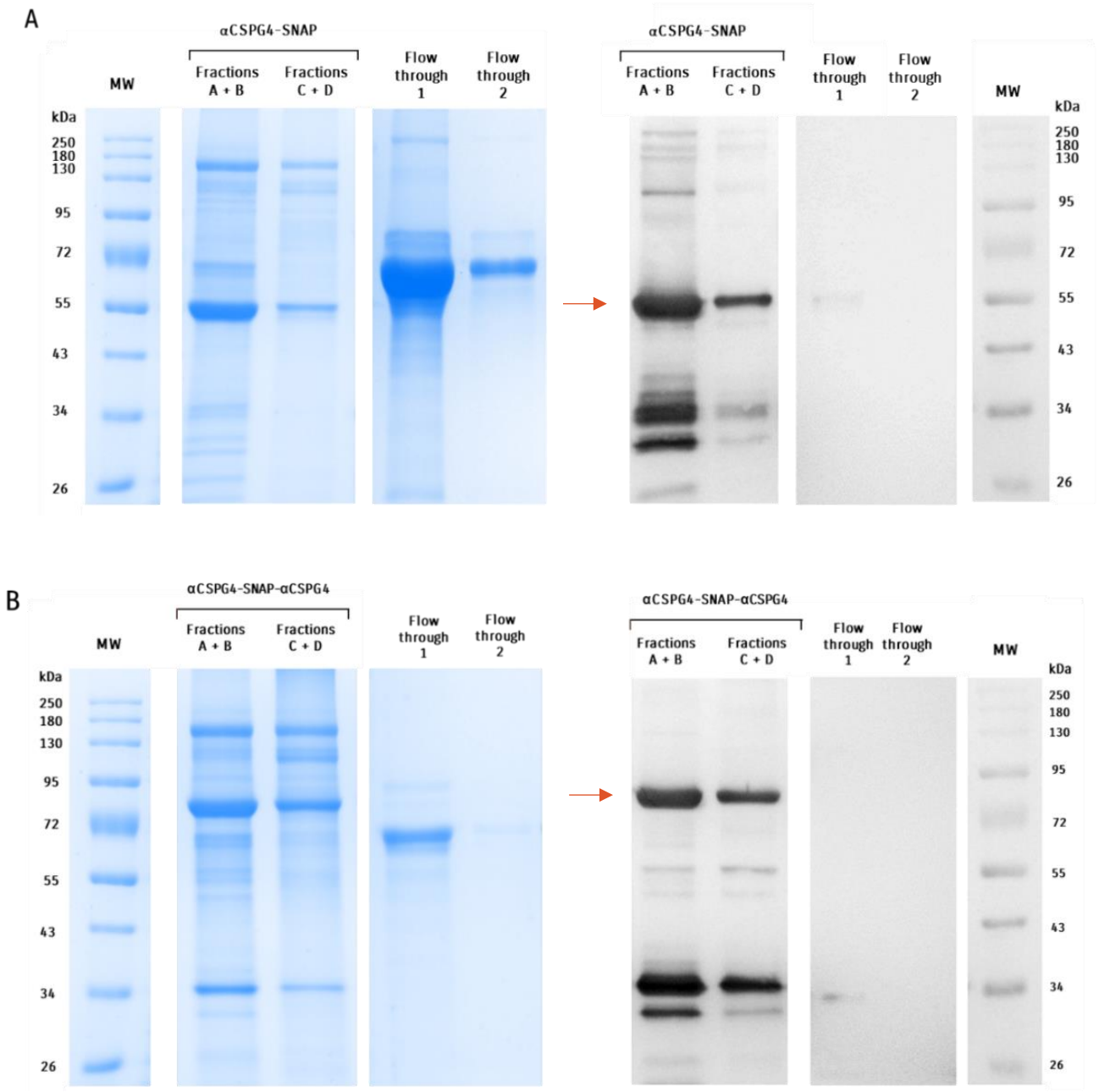

Figure 17. Characterisation of the αCSPG4-SNAP fusion proteins using SDS-PAGE and immunoblot analysis. Protein profile comparison between stained SDS polyacrylamide gel and immunoblot of transferred proteins of (A) monovalent and (B) bivalent αCSPG4-SNAP fusion proteins. The concentrated fractions from the IMAC purification are included as the protein samples as well as the flow through from the process. His-tagged proteins were detected using a rabbit anti-His antibody and the protein sizes were determined by the molecular weight (MW) marker (SuperSignal protein standard). Red arrows indicate the positions of the full-length fusion proteins on the immunoblot.

3.2.3. Conjugation analysis of fusion proteins

Once the integrity of the N-terminal was established, the next step was to assess the integrity and enzymatic functionality of the SNAP-tag, which is situated at the C-terminal of the FPs. To do this, the FPs were conjugated to fluorophores, subjected to SDS-PAGE analysis, and visualised as described in section **2.3.4** (**Figure 18**). Initially, two BG-modified fluorophores, Alexa 488 and 647, were used to determine the ability of SNAP-tag to form a covalent bond with benzyl guanine. Varying concentrations of the fluorophores were used to provide insight into the saturation of the SNAP-tag based on the intensity of the bands representing the conjugated proteins.

For the monovalent FP, the 2:1 and 1:1 ratio of the FP to fluorophore resulted in the highest intensity bands (**Figure 18A**). The bivalent FP, however, seemed to prefer the 1:1 and 1:2 ratio of the FP to a fluorophore (**Figure 18B**). Faint bands were also present below the full-length bivalent protein bands, indicating that there were additional SNAP-tag residues available, presumable the product of degradation or proteolytic cleavage. In all ratio variations of the monovalent FP, unconjugated fluorophore was present, whereas only the 1:1 and 1:2 ratios of the bivalent FP to fluorophore resulted in unconjugated fluorophore, indicating differences in SNAP-tag saturation levels.

To further explore the saturation of the SNAP-tag, dual conjugation experiments were conducted, where the FPs were first conjugated to BG-Alexa 488 at varying concentrations (**Figure 19**). The product of this reaction was then incubated with BG-Alexa 647 and allowed to conjugate (section **2.3.4.1**). Any unconjugated SNAP-tag after the first reaction would form a covalent bond with BG-Alexa 647 instead. The product of the dual conjugation reactions was assessed with SDS-PAGE and visualised.

For both the monovalent and bivalent FPs, the 4:1 and 2:1 ratios of the FP to BG-modified Alexa 488 were insufficient at saturating the SNAP-tag domain, which allowed for additional conjugation to BG-Alexa 647 (**Figure 19**). The 1:1 and 1:2 ratios resulted in successful saturation of the SNAP-tag domain and were more efficient for downstream imaging experiments.

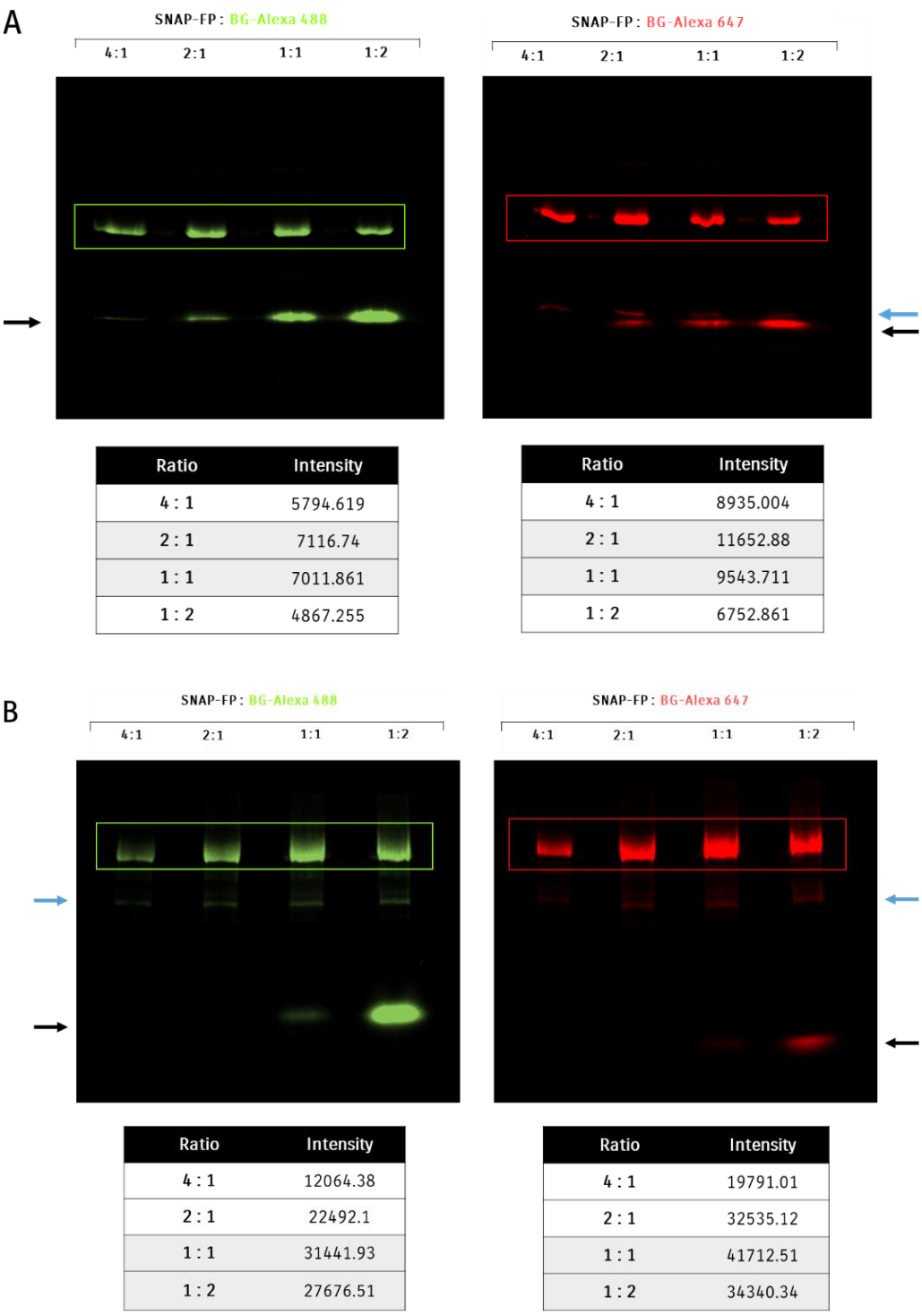

Ratio	Intensity
4 : 1	5794.619
2 : 1	7116.74
1 : 1	7011.861
1 : 2	4867.255

Ratio	Intensity
4 : 1	8935.004
2 : 1	11652.88
1 : 1	9543.711
1 : 2	6752.861

Ratio	Intensity
4 : 1	12064.38
2 : 1	22492.1
1 : 1	31441.93
1 : 2	27676.51

Ratio	Intensity
4 : 1	19791.01
2 : 1	32535.12
1 : 1	41712.51
1 : 2	34340.34

Figure 18. Characterisation of the αCSPG4-SNAP fusion proteins using conjugation analysis and visualised on SDS polyacrylamide gels. The (A) monovalent and (B) bivalent fusion proteins were conjugated to BG-Alexa 488 (green) and BG-Alexa 647 (red) at varying ratios to assess the functionality of SNAP-tag. The intensity of the bands was measured using ImageJ software (listed in tables). Full-length conjugated fusion proteins (enclosed). Unconjugated fluorophore (black arrow). Conjugation of secondary SNAP-tag residue (blue arrow).

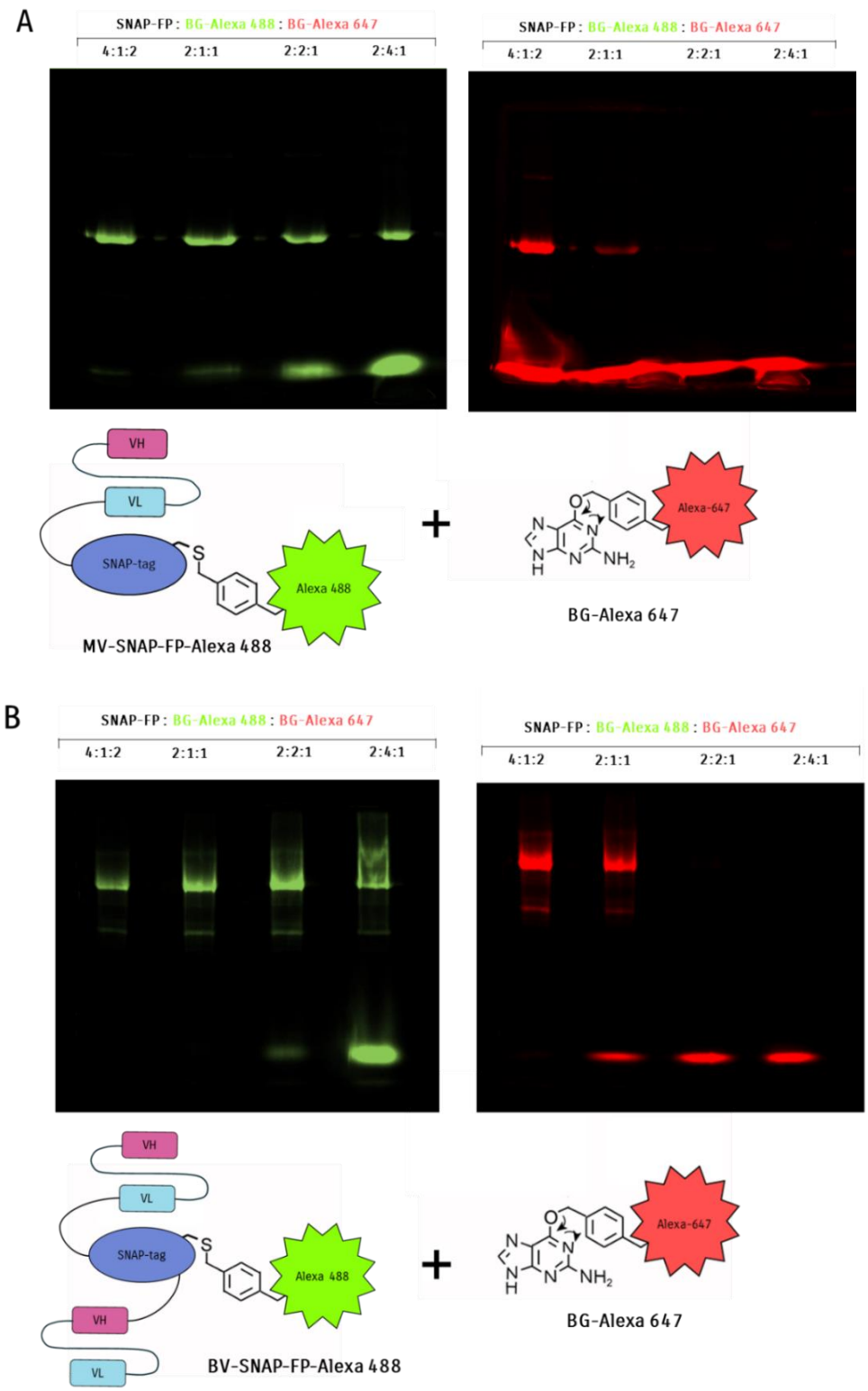

Figure 19. Dual conjugation analysis to determine SNAP-tag saturation at different conjugation ratios. (A) Monovalent and (B) bivalent fusion protein (5 µM) conjugated to BG-Alexa 488 at different ratios and then incubated with BG-Alexa 647 (2.5 µM) to allow for further conjugation. The reaction product was resolved on an SDS polyacrylamide gel under reducing conditions and visualised using appropriate filters for the fluorophores.

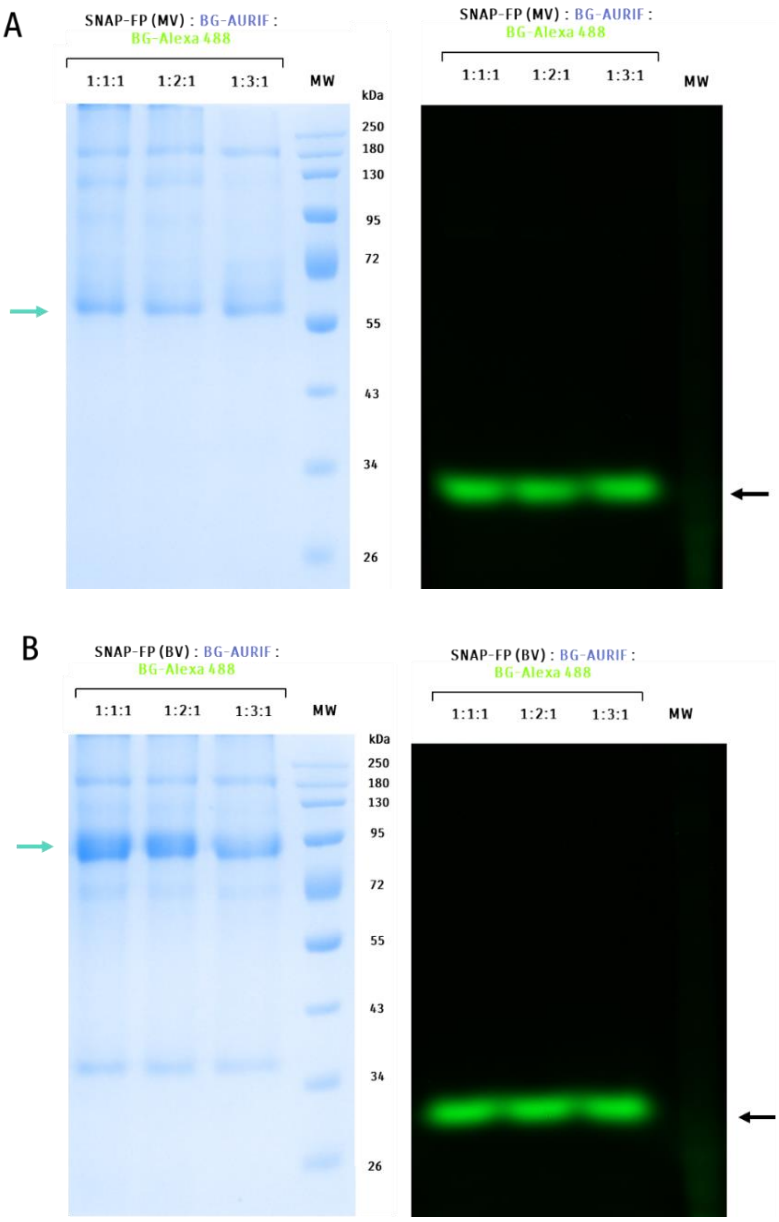

Figure 20. Conjugation analysis of αCSPG4-SNAP fusion proteins with BG-AURIF. The (A) monovalent and (B) bivalent fusion proteins (5 µM) were conjugated to BG-AURIF at different ratios and then incubated with BG-Alexa 488 (5 µM) to allow for further conjugation of any unconjugated SNAP. The reaction products were resolved on SDS polyacrylamide gels under reducing conditions and visualised using the appropriate filter for the Alexa 488 fluorophore. Fusion protein conjugated to AURIF (blue arrow). Unconjugated fluorophore (black arrow).

Similarly, the conjugation efficiency of the mono- and bivalent αCSPG4-SNAP FPs to BG-modified auristatin F (BG-AURIF) was also determined. Dual conjugation analysis was employed, where the FPs were first conjugated to BG-AURIF at varying ratios (section **2.3.4.2**). The product of this initial reaction was then conjugated to a fixed concentration of BG-Alexa 488 and any SNAP-tag domain that remained unconjugated after the first labelling reaction would conjugate to the fluorophore. The products of these reactions were analysed with SDS-PAGE and visualised.

In all varying ratios of the monovalent and bivalent FP to BG-AURIF, the SNAP domain was fully saturated, indicated by the inability of the full-length protein to conjugate to the fluorophore (**Figure 20**). This is apparent since all the BG-Alexa 488 remained unconjugated after the second labelling reaction (**Figure 20**, black arrow).

These experiments demonstrate the profound durability of SNAP-tag in its ability to react with BG-modified substrates even when produced at lower purities. In fact, despite the degradation of full-length FPs, the degradation products containing a SNAP-tag were successfully conjugated to the substrate at detectable levels. This allowed for the identification of these FP derivatives. To be economical with expensive commercial BG-modified fluorescent probes and limited BG-AURIF, a 1:1 ratio was used as the standard for all subsequent conjugation reactions in the downstream experiments.

3.3. Functional evaluation of fusion proteins

3.3.1. Binding, internalisation, and intracellular routing analysis

After successfully producing and verifying the integrity of the αCSPG4-SNAP FPs, functional assays were conducted to evaluate their ability to bind to, infiltrate and induce cytotoxicity in tumour cells. These assays (described in section **2.4.2**) were conducted on CSPG4-positive and -negative TNBC cell lines in triplicate.

The first step to assessing the functionality of the FPs was to demonstrate that the scFv domain can detect and successfully bind the antigen, CSPG4, on the surface of tumour cells. To achieve this, confocal microscopy and live cell imaging techniques were used. Tracking the fluorescent signal from

the Alexa 488-conjugated FPs, allowing for the differentiation between cell surface binding and internalisation. Furthermore, colocalization analysis between the labelled FP and intracellular compartments provided insight into the intracellular routing pattern of the FPs after binding and internalisation.

The imaging analysis indicates that the FPs were able to successfully bind to the antigen expressed on Hs578T (CSPG4-positive) cells and are readily internalised by the tumour cells (**Figure 21**). At similar time points, there is notably more cell surface signal of the monovalent FP (**Figure 21A**) as opposed to the more prominent internal signal for the bivalent counterpart (**Figure 21B**). This is also apparent with the colocalization between the FP signal (green) and the lysosomal compartments (red), indicating that upon uptake, the FPs are shuttled to the lysosomal compartments.

A method for identifying the retrograde transport pathway was also established. In these experiments, the tumour cell lines were incubated with the Alexa-488 labelled FPs followed by the staining of the ER and nuclei. The confocal images indicate that unlike in the case of the lysosomes, no colocalization occurred between the FPs (green) and the ER (red) signal (**Figure 22**). No surface binding or internalised signal of the immunodiagnostic FPs was present in the antigen-negative control cell line (MCF-7).

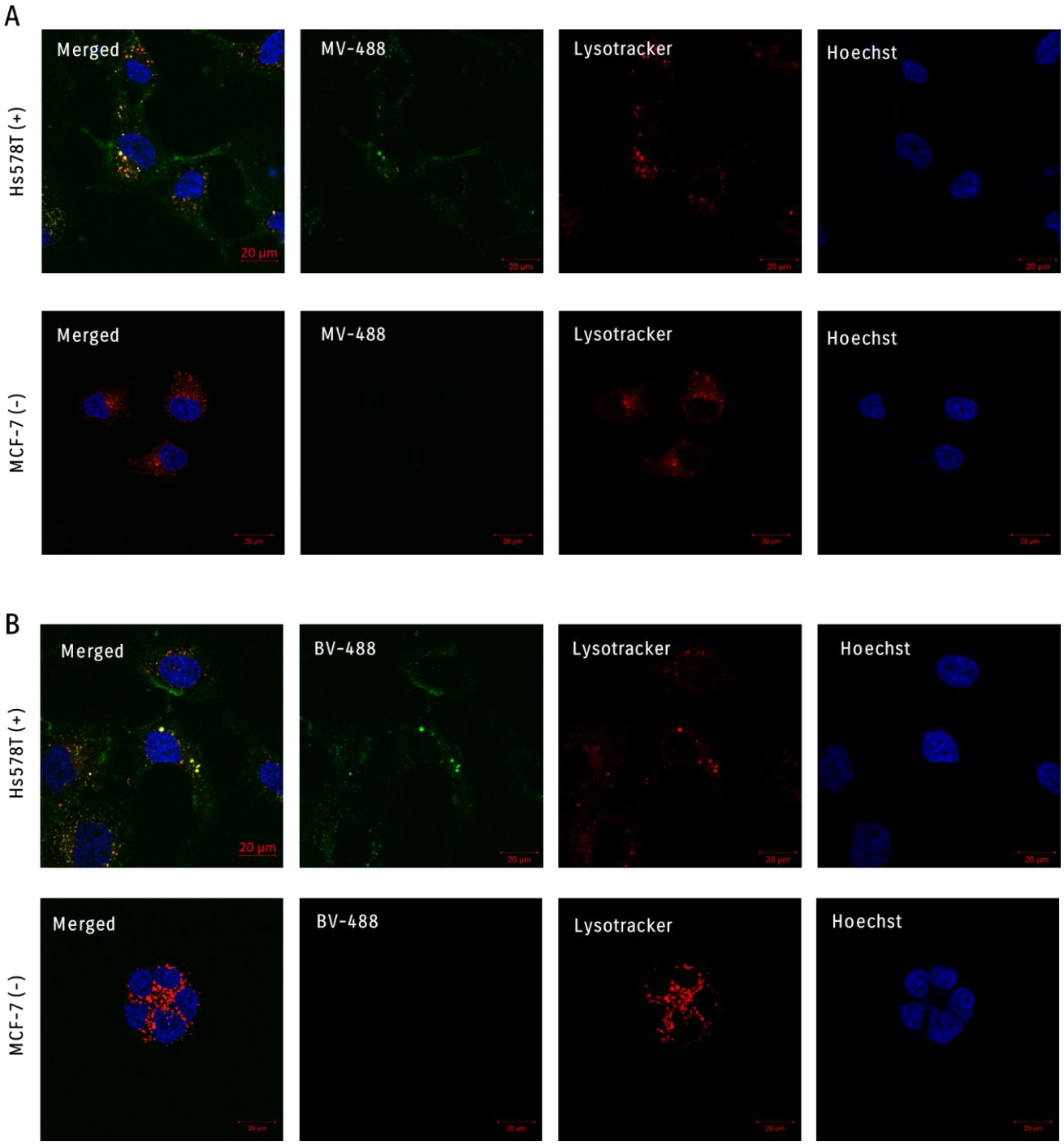

Figure 21. Live-cell imaging to assess binding, internalisation and lysosomal routing of αCSPG4-SNAP fusion proteins conjugated to Alexa 488. Antigen-positive (Hs578T) and antigen-negative (MCF-7) cells were incubated with the (A) monovalent and (B) bivalent αCSPG4-SNAP-488 (green) for 30 min. The lysosomal compartments were stained with LysoTracker (red) and the nuclei with Hoechst (blue). Images were captured with the Zeiss LSM880 (confocal microscope) with Airyscan at 63x magnification. Scale bar = 20 µm.

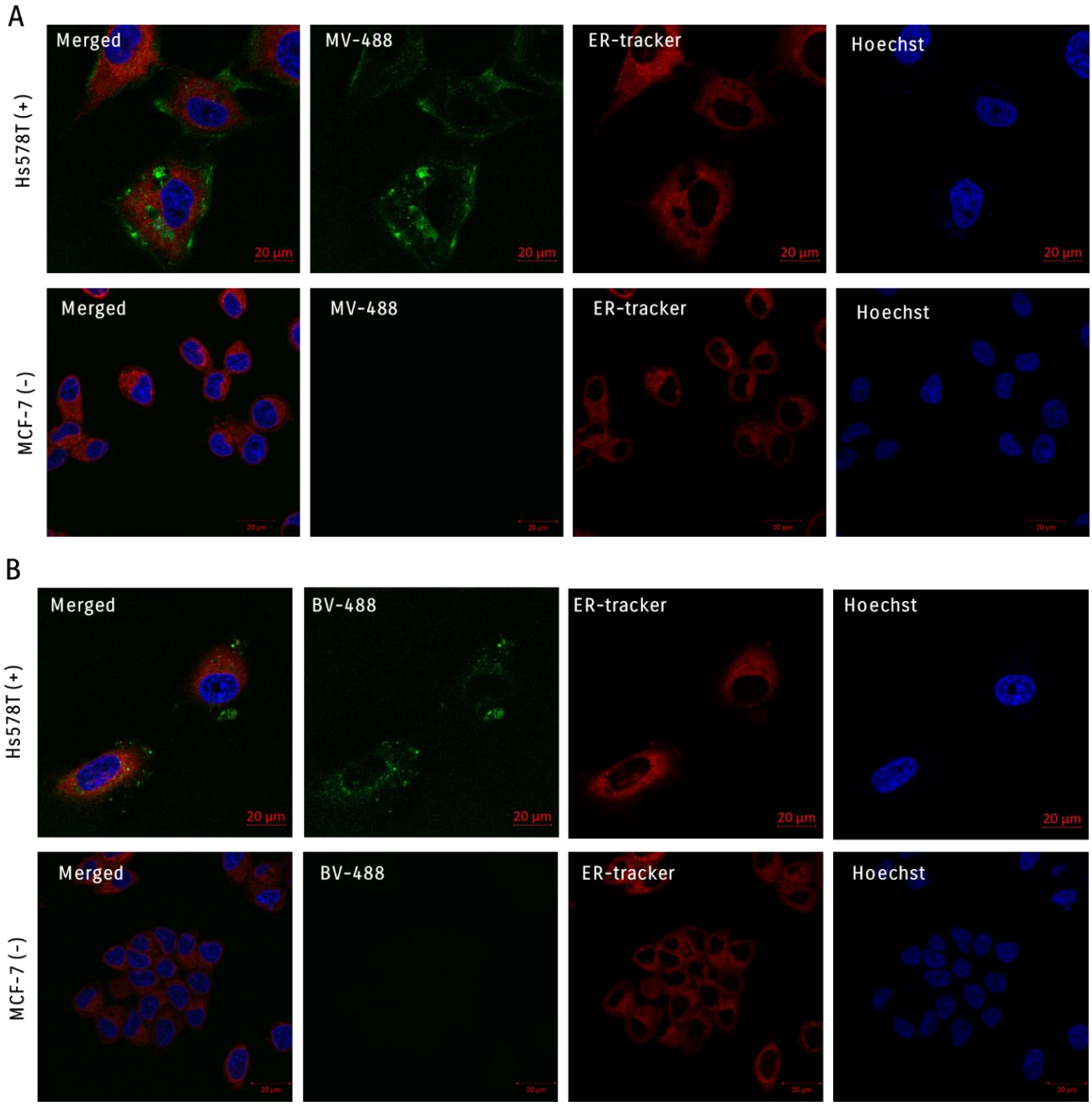

Figure 22. Live-cell imaging to assess binding, internalisation and retrograde routing of αCSPG4-SNAP fusion proteins conjugated to Alexa 488. Antigen-positive (Hs578T) and antigen-negative (MCF-7) cells were incubated with the (A) monovalent and (B) bivalent αCSPG4-SNAP-488 (green) for 30 min. The endoplasmic reticula were stained with ER-Tracker (red) and the nuclei with Hoechst (blue). Images were captured with the Zeiss LSM880 (confocal microscope) with Airyscan at 63x magnification. Scale bar = 20 µm.

3.3.2. Cytotoxic activity of auristatin-F conjugated fusion proteins

Once it was shown that the FPs successfully bind to and are internalised by the antigen-positive tumour cells, their cytotoxic potential was investigated. The immunotherapeutic FPs were generated through conjugation to BG-modified auristatin F. As described in section **2.4.3**, the tumour cell lines were treated with the immunotherapeutic FPs and the XTT cell viability assay was used to determine the cytotoxicity relative to the untreated (100%) and 0% cell viability controls. According to the nature of the colourimetric XTT cell viability assay, a decrease in cell viability is based on the presence of the yellow tetrazolium salt which is detected and measured spectrophotometrically at 450 nm. Using the absorbance readings, the dose-dependent curves were plotted and the IC_{50} values were calculated on GraphPad Prism software. There was a clear concentration-dependent reduction in Hs578T cell viability treated with the immunotherapeutic FPs (**Figure 23**). The IC_{50} value of the bivalent FP was 277 nM whereas the monovalent FP had an IC_{50} value of 409 nM. The response of the antigen-negative cells (MCF-7) was negligible compared to the response of Hs578T.

The cells treated with 1 µM BG-AURIF only had the low cell viabilities indicated by the absorbance readings (data not shown) and the signs of apoptosis in the cells treated with the unconjugated drug (**Figure 24**). The non-specific cytotoxicity and BG-AURIF indicate that it is permeable to cells and could therefore enact the bystander effect. Conversely, the cells treated with 1 µM of the unconjugated FP (monovalent and bivalent) had cell viabilities similar to the PBS controls with comparable absorbance readings (data not shown) and little to no change in the cell morphologies (**Figure 24**).

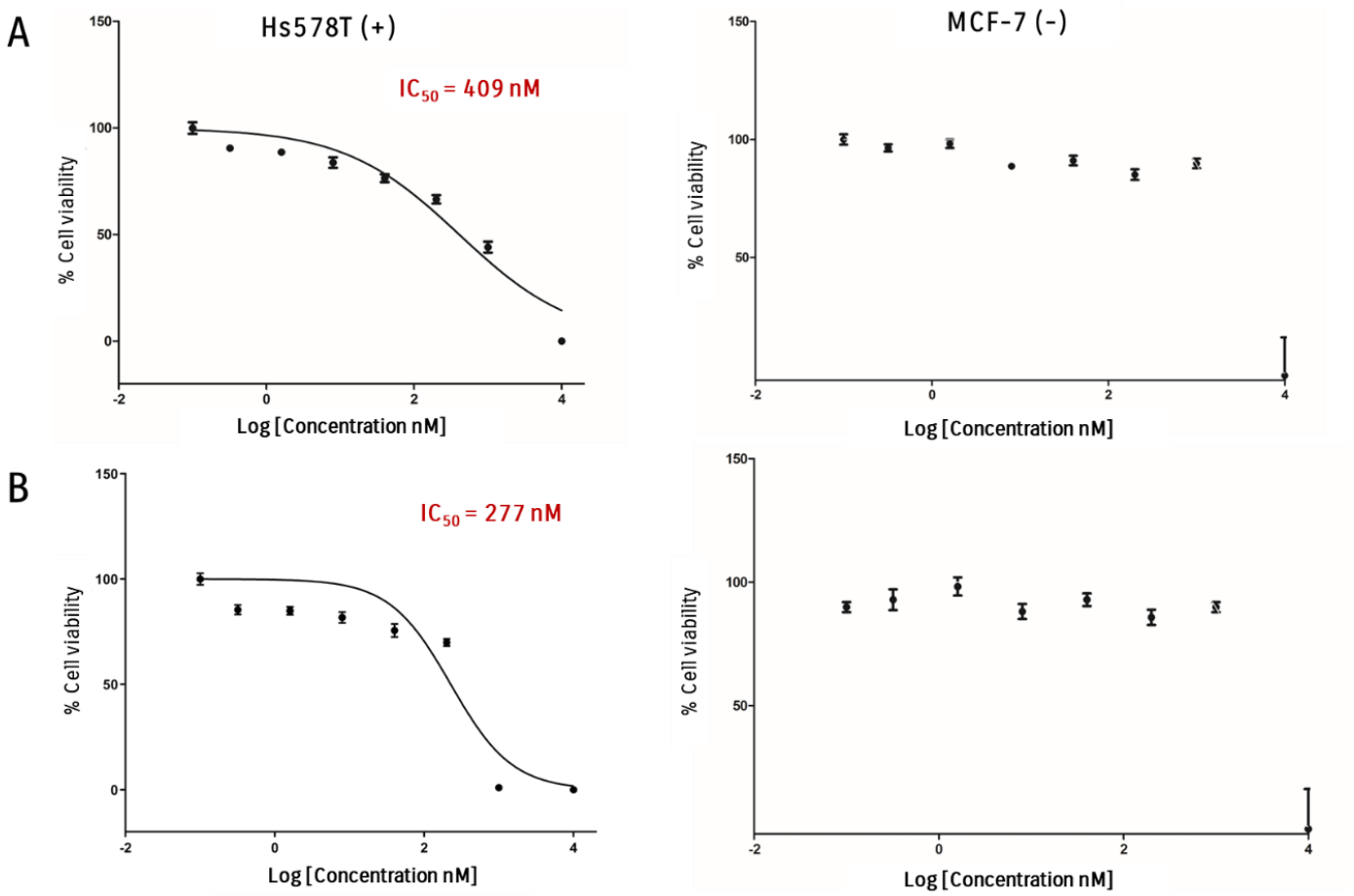

Figure 23. Dose-response curves depicting the cytotoxicity of auristatin F-conjugated αCPSG4-SNAP fusion proteins. The cell viability analysis of antigen-positive (Hs578T) and antigen-negative (MCF-7) cell lines treated with the (A) monovalent and (B) bivalent αCSPG4-SNAP fusion proteins conjugated to auristatin F (5-fold serially diluted concentrations). Cell viability was determined using the XTT-based cell viability assay at 48 hours post-treatment. The IC50 values (indicated in red) relative to the PBS control and Zeocin-treated cells were calculated using GraphPad Prism v5. Data are mean ± standard deviation (SD) of each measurement (presented as a percentage of cell viability), and the measurements were performed in triplicate and the experiment was repeated thrice.

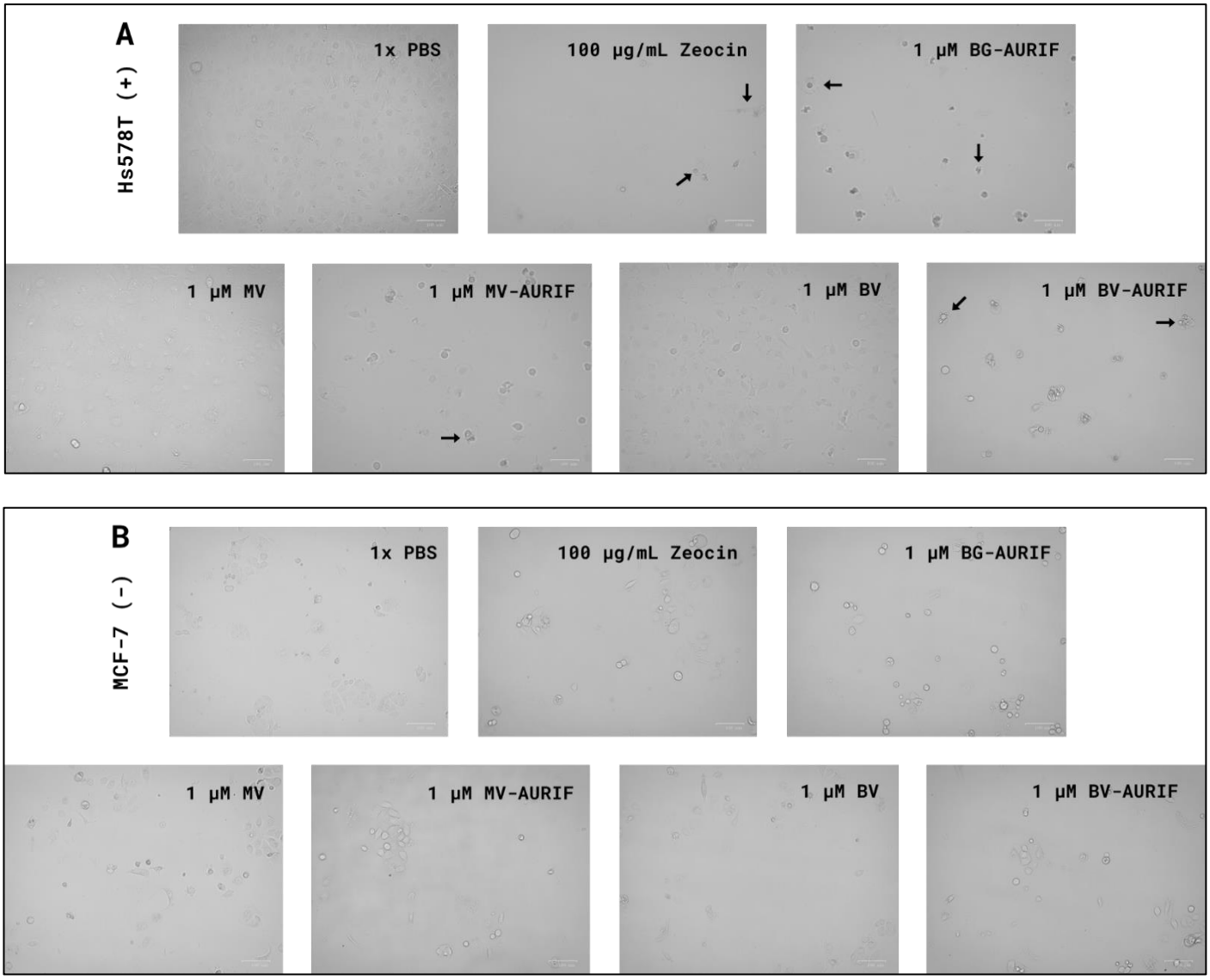

Figure 24. Cytotoxic effect of different molecules on tumour cell lines. (A) Hs578T (antigen-positive) and (B) MCF-7 (antigen-negative) cells were treated with the controls including PBS (negative) and the antibiotic Zeocin (positive) in the cell viability assays. Unconjugated benzyl guanine-modified Auristatin F (BG-AURIF) and unconjugated monovalent (MV) and bivalent (BV) αCSPG4-SNAP fusion proteins were also included to compare the cytotoxic effects of these in comparison with the fusion proteins conjugated to Auristatin F (MV-AURIF and BV-AURIF). Signs of apoptosis (shrinkage, blebbing, apoptotic bodies) are indicated by black arrows. Cells were treated 24 hours post-seeding and images were captured 44 hours later. Images were captured with the ZOE fluorescent cell imager under transmission light. Scale bar = 100 µm.

4. Chapter 4: Discussion

4.1. A precision medicine approach to triple-negative breast cancer

Breast cancer is the most frequently diagnosed female cancer, accounting for the majority of cancer-related deaths in women worldwide [1, 2]. TNBC is classified as one of the most aggressive breast cancer subtypes associated with poor prognosis, increased risk of metastatic recurrence, and decreased survival rates [37]. While the TNBC phenotype is widely reported to represent 15-20% of all breast cancer cases, the incidence rates in African countries are notably higher at approximately 30% [139]. Globally, the TNBC burden is higher on the African continent and among the African diaspora, where greater TNBC-related morbidity and mortality are observed in women with African ancestry [16, 163, 164]. It has also been reported that TNBC is often diagnosed in younger women of premenopausal age, however, the underlying reasons are not yet fully understood [37].

The lack of targeted therapeutic options, largely due to the absence of hormone receptors (ER and PR) and HER2 has led to limited management strategies which further exacerbates the poor prognosis and low survival rates associated with TNBC [26]. Conventional chemotherapy with taxanes and anthracyclines remains the primary treatment strategy, and while successful in the initial stages of treatment, overall disease-free survival is limited due to a higher risk of relapse [36, 165]. Furthermore, chemotherapeutic strategies are significantly less successful in recurring local or distal TNBC tumours [36]. As a result of the molecular diversity associated with TNBC tumours, approaches that employ singular treatment strategies for the management of the disease are unlikely to be successful [32, 47]. It is, therefore, important to evaluate and characterise the heterogeneity of TNBC tumours and apply this information to identifying and predicting a patient's response to targeted and standard therapies. It has become clear that such a personalised approach to TNBC treatment and management has the greatest potential for improving patient prognosis and disease-free survival (**Figure 25**) [166, 167].

For years, the disparity in TNBC prevalence and prognosis in African countries was largely attributed to poor healthcare infrastructure and inadequate screening and diagnostic methods, however, it has become increasingly apparent that there is an ancestral risk factor [168]. A large-scale gene expression analysis study on an African-enriched multinational cohort identified 613 genes associated with African

descent and more than 2000 genes associated with regional African ancestry [139]. Further analysis of these genes revealed that tumour-associated immunological profiles are distinct in patients of African ancestry [139]. This indicates that the ancestral backgrounds of patients will likely influence the molecular diversity of TNBC tumours. Taking this information into consideration to develop novel diagnostic and treatment approaches could significantly improve disease outcomes.

Of the various ongoing studies and clinical trials that are attempting to develop targeted therapies for TNBC, only two have successfully been approved for clinical treatment - the checkpoint inhibition mAb, pembrolizumab and the ADC, Sacituzumab govitecan [49, 52, 169]. While this is promising, due to the heterogeneity of TNBC, it would likely require more than one targeted strategy to successfully treat the disease. This is especially the case in patients of different ancestries since patient ancestry may influence their molecular tumour and tumour-associated immunologic profiles [139]. Essentially, a multi-targeted repository of treatment modalities will likely be required to successfully manage TNBC on a global scale.

The evidence strongly suggests that optimal TNBC management requires a precision medicine approach. Since the BRCA mutation status is currently the only biomarker used to determine personalised breast cancer therapies in clinical settings, it is crucial to identify new prognostic, diagnostic and therapeutic biomarkers across multiple populations [31, 170]. Research aimed at characterising the genomic and proteomic heterogeneity has attempted to achieve this, however, large multinational research efforts will likely be needed to translate this research into clinically validated biomarkers [31, 171–173]. These biomarkers would be used to accurately diagnose and stratify patients based on their predicted disease progression and sensitivity or resistance to potential targeted therapies and standard treatment strategies. This data could then be used to reliably inform clinicians on the best management and treatment strategies for each patient, resulting in improved prognosis and disease-free survival (**Figure 25**).

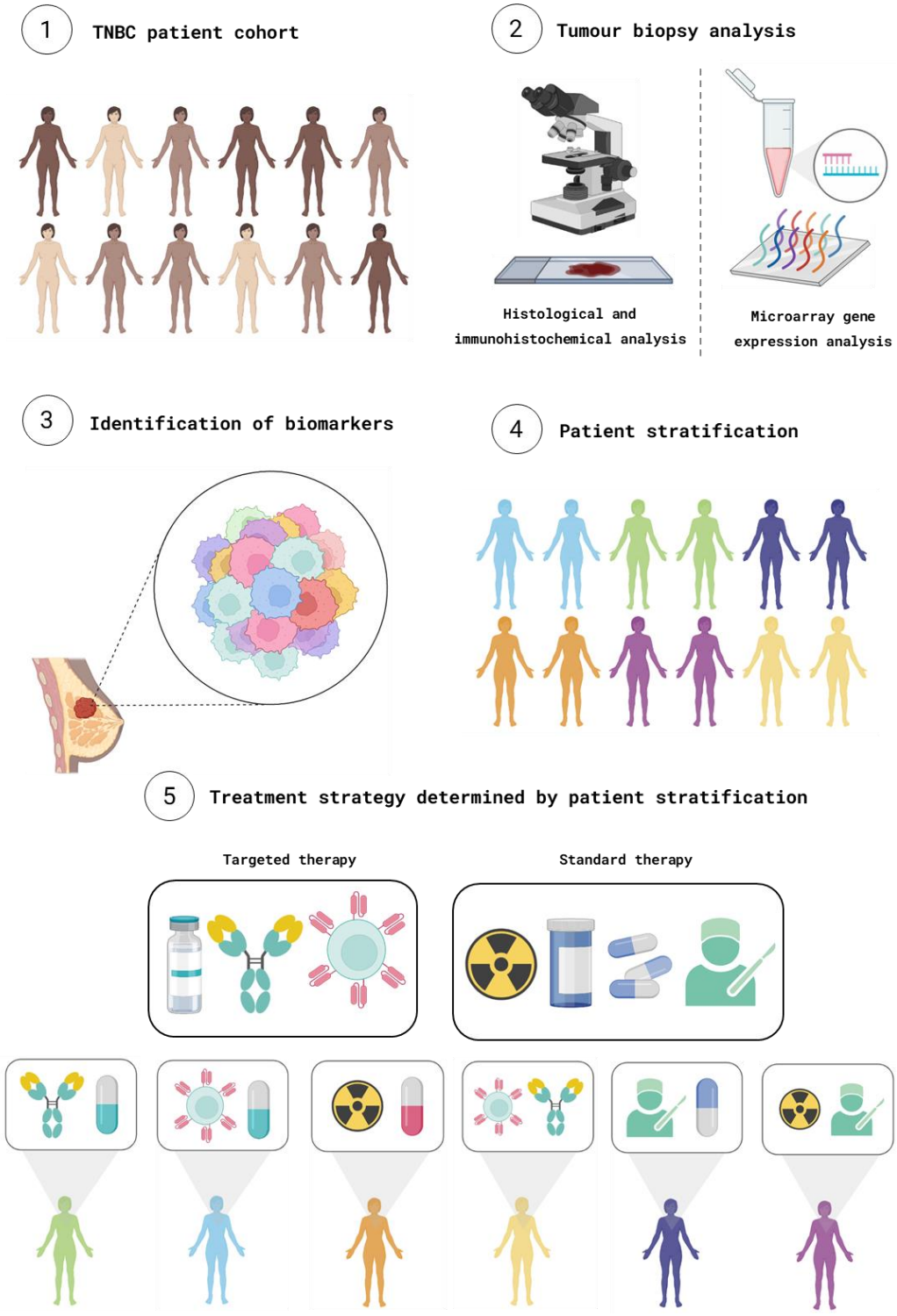

Figure 25. Precision medicine approach to triple-negative breast cancer (TNBC). Tumour biopsies are collected from TNBC patients and subjected to histological, immunohistochemical, and gene expression analysis leading to the categorisation of the tumour and identification of relevant biomarkers (1-3). These biomarkers may be prognostic, therapeutic or predictive of a patient's response to therapy and patients are accordingly stratified based on the presence or absence of biomarkers (4). Personalised treatment strategies can be determined by this stratification - combinations of conventional and contemporary targeted therapies can be employed for optimal treatment response, resulting in improved prognosis and survival (5). Created using BioRender.

4.2. A new generation of immunodiagnostic and immunotherapeutic agents

4.2.1. The design of scFv-SNAP fusion proteins

One of the hallmarks of cancer cells is the ability to resist immune mechanisms responsible for identifying and destroying aberrant cells [4, 174]. Immunotherapy aims to generate an immune response by manipulating components of the host immune system to recognise and destroy cancerous cells [175]. Passive immunotherapy is defined as using immune elements such as antibodies and immune cells that have been generated *ex vivo* to target cancer cells, while active immunotherapy reactivates the host's inherent immune response against cancer cells [46]. This study has employed a passive immunotherapy approach targeting TNBC.

Antibodies, mAbs in particular, are useful therapeutic tools in passive immunotherapy as they can successfully target tumour cells and induce a cytotoxic response [176]. While many mAbs have been successful at improving patient outcomes, tumour cells are renowned for their adaptive capabilities and can, therefore, develop resistance to therapeutic mAbs [177]. Research efforts were, therefore, directed at generating ADCs, which combine the tumour-targeting ability of mAbs with cytotoxic drugs to directly induce cell death. The passive immunotherapy that ADCs offer also addresses the challenges associated with non-targeted therapies. Conventional chemotherapy, the mainstay of TNBC treatment, relies on destroying rapidly dividing cells [178]. It is, therefore, non-specific and highly toxic to healthy dividing cells, leading to systemic toxicity [179]. The side effects associated with this systemic toxicity and the impact on the patient's quality of life can be mitigated with targeted drug delivery systems such as ADCs, where normal healthy cells remain unaffected [94].

To date, only 14 ADCs have been approved for clinical use, all of which contain full-length IgG mAbs linked to drugs that result in microtubule disruption or interfere with DNA replication [104, 105]. The main challenges in generating effective ADCs can be attributed to the inconsistent stoichiometry resulting from the conjugation method, reduced serum stability, and immunogenicity [94, 138, 180]. The conjugation methods typically employed to produce ADCs often result in ADCs with variable drug-to-antibody ratios (DAR) which consequently have varying pharmacokinetic properties and safety

profiles [180]. The ability of these full-length ADCs to penetrate tumour masses can also be relatively poor, presumably due to the large size of the antibody [108].

Some of the shortcomings of full-length mAb-based ADCs may be overcome with scFv-based FPs. scFvs retain the binding specificity of full-length mAbs and are relatively easy and economical to produce in large quantities [181]. Furthermore, the scFv antibody derivative is known for having desirable pharmacokinetic properties as it can easily penetrate tumour masses owing to its small size and is rapidly cleared from circulation due to the absence of an Fc region [112, 181]. While rapid renal clearance is more desirable for diagnostic applications, it can result in low retention and an insufficient serum half-life for therapeutic application. Furthermore, the monovalent nature of the scFv is thought to reduce the avidity, leading to weaker antigen binding which reduces the efficacy [111, 112, 181]. These drawbacks can, however, be addressed with antibody engineering and genetic manipulation to produce multivalent scFv with higher avidities and extended blood circulation times [115, 118].

Increasing the valency of scFvs has been an area of interest in antibody engineering for decades [86, 111, 115, 118]. scFv FPs are relatively easy to generate, given their small size, and engineering bivalent FPs with mono- or bispecific capabilities are of particular interest [84]. Monospecific bivalent scFv FPs result in molecules with favourable pharmacokinetic properties owing to the increase in molecular size and avidity [115]. Various studies have confirmed the increase in tumour penetration and efficacy of bivalent scFvs resulting from an increase in cell surface binding, cellular uptake and bioavailability [86, 88, 112, 117, 182]. Studies have, however, also emphasised that is important to establish a balance between high affinity and retention time since antibodies with very high affinities are susceptible to the binding site barrier phenomenon when targeting solid tumours [110, 125, 129].

Table 15. Clinically approved therapeutic scFv-based antibodies. The antibody formats, antigenic targets, and diseases that the antibodies are approved for are listed. Relevant pharmacokinetic parameters (size, half-life, and route of administration) are included for comparative evaluation.

Name	Target and format	Disease	Year approved	Size and half-life	Administration route
Blinatumomab (Blincyto) [183]	CD19, CD3; Murine bispecific tandem scFv	Acute lymphoblastic leukaemia	2014	55 kDa; 2 hrs	Intravenous
Brolucizumab (BEOVU) [184, 185]	VEGF-A; Humanized scFv	Age-related macular degeneration	2019	26 kDa; 5.6 hrs	Intravitreal
Tebentafusp (KIMMTRAK) [186, 187]	gp100, CD3; Bispecific immunoconjugate (TCR-scFv)	Metastatic uveal melanoma	2022	77 kDa; 7.5 hrs	Intravenous

The benefits of bivalent scFvs are exemplified by several studies that demonstrated the improved cytotoxic activity of bivalent scFv-based immunotoxins as opposed to their monovalent counterparts [82, 119–123]. An immunotoxin is defined as an antibody fragment such as an scFv attached to a bacterial, plant, or human protein toxin [188]. The presence of two receptor-binding domains in bivalent formats results in improved clustering of immunotoxin-receptor complexes and enhanced uptake by target cells [86, 118, 189]. The payload of the toxin to tumour cells is, therefore, higher and accounts for the improved cytotoxic efficacy.

Bispecific scFv FPs are also commonly used to generate BiTEs that display bifunctionality by binding to tumour cells while recruiting cytotoxic T cells to the tumour site [82]. To date, two BiTEs have been approved for clinical use with others currently in the pipeline for approval (**Table 15**) [183, 186]. scFv-based FPs can also be generated with SNAP-tag, where the SNAP-tag molecule is genetically fused to the scFv and produced in various protein expression systems [190, 191]. This results in larger FPs since the SNAP-tag has a molecular weight of ~20 kDa [192]. It has been posited that attaching scFvs to other suitably-sized molecules can increase their stability and retention in circulation [193]. Furthermore, attaching a SNAP-tag molecule introduces great flexibility through the variety of effector molecules

that can be attached to the scFv via the SNAP-tag giving rise to a multitude of immunodiagnostic and immunotherapeutic FPs [92, 190]. Diagnostic probes such as fluorophores and radionuclides can be conjugated to the SNAP-tag and used for the *ex vivo* and *in vivo* detection of tumour-associated antigens via fluorescence imaging or positron emission tomography (PET) [92, 101–103]. Therapeutic probes that can be attached to the scFv via SNAP-tag conjugation include small molecule toxins, cytotoxic drugs, and photosensitisers to induce selective cell killing [92, 190]. Over the last fourteen years, various scFv-SNAP FPs have been successfully produced and validated in preclinical studies [71, 98–101, 103, 194–196]. One study also generated a bivalent scFv-SNAP FP that, like other bivalent scFv-based immunotherapies, displayed improved antigen binding and internalisation by tumour cells while maintaining the site-specific functionality of SNAP-tag [98]. This suggests that multivalent scFv-SNAP FPs can be generated for enhanced targeted delivery of the effector molecule and improved pharmacokinetic properties.

Selecting a suitable target for an ADC is especially important for its therapeutic efficacy. The cell surface receptor, CSPG4, is differentially upregulated in several aggressive cancers, with evidence suggesting its involvement in cellular proliferation, vascular tissue development, and stem cell niche maintenance [62, 67, 69]. CSPG4 expression in normal tissue is limited to foetal developmental stages and expression in adult tissue is relatively low [62]. Studies have demonstrated the role of CSPG4 in cancer initiation as it is found in early-stage malignant cells and cancer stem cells [60, 197]. CSPG4 is, therefore, an attractive immunotherapeutic target and has been validated by various preclinical studies [60, 63, 65, 71, 72, 103]. In TNBC, this biomarker is of particular interest since its preferential expression was reported in the majority of primary TNBC lesions, in TNBC cell lines as well as tumour cells in the pleural effusions of TNBC patients [60]. As such, antibody-based therapeutics targeting CSPG4 in TNBC have been attempted and this cell surface proteoglycan, therefore, represents a validated TNBC target [63, 71, 103].

4.2.2. Production of monovalent and bivalent fusion proteins

Most scFv-SNAP FPs are monovalent and may lose avidity and the ability to sufficiently form clustering of receptor-antibody homodimers for clathrin-mediated endocytosis – resulting in reduced

efficacy and delivery of the payload (**Figure 6**) [85, 112, 115, 181]. This study, therefore, sought to identify valency-dependent differences between mono- and bivalent αCSPG4-SNAP FPs. The binding and uptake of the FPs in a CSPG4-positive TNBC cell line and the ability of the FPs to induce cell death through the delivery of a cytotoxic payload were assessed.

A similar monovalent αCSPG4(scFv)-SNAP FP was previously generated and validated *in vitro* (TNBC cell lines) and *ex vivo* (breast cancer biopsies) [71, 198]. This study builds upon this work by generating a novel bivalent αCSPG4(scFv)$_2$-SNAP FP and comparing the kinetics of tumour cell binding and uptake and how differences in this capacity affect their therapeutic efficacy. Since previous research demonstrated the successful generation of a bivalent scFv-SNAP FP, and various bivalent immunotoxins have been generated using similar methods, we were confident that the bivalent design would have two functional scFv domains without interfering with the SNAP-tag conjugation site [98, 119–123].

Using *in silico* plasmid design and the resulting amino acid sequences, the isoelectric points (pI) and molecular weights of the resultant FPs were estimated (**Figure 10**). The pI is important to consider when preparing the buffers for protein purification and storage since the proteins should remain soluble and stable for downstream experiments which can be affected by the pH of the solution [199]. The estimated molecular weights allow for the identification of the proteins on SDS polyacrylamide gels and immunoblots and differentiation between any contaminants or degraded proteins. ORFs encoding the monovalent and bivalent αCSPG4-SNAP FPs were successfully cloned into the pCB expression vector and validated using restriction analysis and bi-directional Sanger sequencing (**Figure 13**). The plasmid carrying the ORF for the bivalent FP was ~700 bp larger than the monovalent plasmid due to the addition of an scFv sequence. The transformation efficiencies of FP-encoding plasmids into DH5α cells were relatively low for these commercial-grade competent cells, which may be due to lower plasmid purity, the larger size of the plasmid, suboptimal growth conditions, loss of competency due to insufficient storage conditions or incomplete cold chains during transport [200, 201]. Regardless of the low transformation efficiency, positive plasmids were identified from colonies (**Figure 13**). Once the plasmid sequences were validated, the plasmid DNA from the colonies with 100% sequence identity to

the reference sequences was isolated and transfected into the HEK293T cells for transient expression of the FPs.

The transfection efficiencies were also relatively low and the cell cultures, therefore, required extended conditioning and selection with Zeocin before attaining an estimated GFP-positive status of 80% (**Figure 14**). This was the highest GFP expression that could be achieved, even when the confluency of the cell culture was close to 100%. Consequently, occasional Zeocin treatment was used to maintain a relatively high GFP-positive state. During the first three months, insufficient amounts of the FPs were expressed and secreted, thus CFS could only be collected once a suitable GFP-positive status was confirmed. Notably, the transfection efficiency was lower for the bivalent FP, which may be attributed to the difference in plasmid size, since smaller plasmids are taken up into the host cells more rapidly and able to escape degradation by endogenous nucleases once internalised [202]. This could be resolved by optimising the transfection protocol by optimising the concentrations of DNA, transfection reagent and the number of cells transfected or by attempting multiple successive transfections [203, 204]. In fact, members of the MB&I have since improved the transfection protocol (section **2.2.1**) and achieved transfection efficiencies between 60-70% (Ursula-Clair Andon-Koung-Edzidzi, PhD), which is in line with reports from the literature [205].

4.2.3. Fusion protein yield, stability, and functionality

The CFS from the expression cell cultures was subjected to IMAC for the enrichment of the FPs, enabled by the polyhistidine tag genetically fused to the N-terminal of the peptide sequence (**Figure 10**) [148]. While the FPs were successfully detected at their designated molecular weights, the IMAC protocol was insufficient for achieving high purity and yield of the FPs. This is apparent in the SDS-PAGE analysis, which detected multiple additional proteins in the IMAC-enriched samples (**Figures 15B and 16B**). Due to the presence of contaminating proteins in the enriched samples, full-length FP concentration could not be accurately quantified using standard spectrophotometry measurements. Therefore, in order to determine the purity and yield of the FPs, densitometric measurements were employed (**Figures 15 and 16**) to more accurately determine the concentrations of full-length mono- and bivalent αCSPG4-SNAP FPs (**Tables 13 and 14**). This information was important for the

conjugation experiments since the SNAP-tag reacts with BG-modified substrates with a 1:1 stoichiometry [91]. The purity and yield of the FPs (MV ~35% and BV ~20%) (**Tables 13 and 14**) were considerably lower compared to reports from several studies that successfully produced scFv-SNAP FPs. The lower yield of the bivalent FP (**Tables 13 and 14**) may be attributed to the differences in transfection efficiency or the larger size of the protein. The previous studies, in addition to the protocol by Hussain *et al.*, reported yields between 10-15 mg/L of cell culture supernatant subjected to IMAC purification with high purities (>90%) [90–92, 99, 103, 194, 206]. The reason for this may be twofold: (i) the initial low transfection efficiencies and (ii) suboptimal cell culture conditions since there were limitations to rapidly increasing the cell culture capacity and collecting sufficient volumes of CFS for purification. The CFS was, therefore, collected over several months and stored at 4ºC prior to IMAC purification, which may have promoted proteolytic cleavage and degradation of the full-length FPs. This is apparent when comparing the yield and purity from smaller purification soon after the supernatant was collected with larger purification volumes with longer storage times (data not shown). Due to the various challenges and setbacks, the timeline for developing scFv-SNAP FPs outlined by Hussain *et al.* was considerably delayed, emphasising the need to optimised protein expression and purification protocols and increased production cell culture capacity using high-density cell cultivation processes [92].

In the short term, the low purity owing to the degradation of the full-length recombinant proteins may be addressed by utilising protease inhibitors in the collected CFS to prevent the proteolytic degradation of the full-length FPs [207]. Furthermore, size exclusion chromatography (SEC) and ion-exchange chromatography (IEC) techniques have been employed by members of the MB&I to increase the purity by removing contaminating proteins from the sample (**Figures 15 and 16**) [208]. To increase the yield, alternative protein expression systems that would allow improvements to the yield by scaling up the cell culture capacity while producing recombinant FPs with accurate post-translation folding have also been explored in the group. These include using expression systems such as *E. coli*, yeast cells, and transgenic plants as expression systems, which allow for cost-effective, fast and scalable protein production [209]. Due to the various challenges and setbacks, the timeline for developing scFv-SNAP

FPs outlined by Hussain *et al.* was considerably delayed, emphasising the need to optimised protein expression and purification protocols and increased production cell culture capacity using high-density cell cultivation processes [92].

The additional proteins detected in the samples may signify proteins from the cell culture medium that carried endogenous histidine residues or metal-binding motifs and consequently bound to the IMAC column, resulting in their co-elution with the His-tagged FPs [210]. Alternatively, some of these contaminating bands may represent partially degraded, truncated or proteolytically cleaved FPs with functional N-terminals. The presence of FP derivatives with functional scFv and SNAP-tag domains may have implications for the downstream imaging and cytotoxicity experiments. The immunoblot analysis using an anti-His antibody detected proteins containing histidine residues around 30 kDa in size which may correspond with an intact scFv protein that had been cleaved from the SNAP-tag protein (**Figure 17**). Consequently, a corresponding SNAP-tag (~20 kDa) molecule or scFv-SNAP FP (~50 kDa) should be present in the monovalent and bivalent samples, respectively. This was confirmed using conjugation analysis, where the protein samples were conjugated to BG-Alexa 488, resolved using SDS-PAGE and visualised (**Figure 18**). In the bivalent sample (**Figure 18B)**, there is a faint band present around the 55 kDa point, indicating the conjugation of a small concentration of monovalent αCSPG4(scFv)-SNAP to the fluorophore. This protein fragment is also present in the immunoblot indicating that the cleavage occurred proximal to the C-terminal (the scFv closest to the C-terminal was cleaved) since the His-tag is located at the N-terminal (**Figures 10 and 17B**). This is more difficult to visualise in the monovalent sample (**Figure 18A)** since the fluorophore-conjugated SNAP-tag molecule (~20 kDa) may be masked by the presence of the unconjugated fluorophore. However, in samples conjugated to BG-Alexa 647, there are faint bands present above the unconjugated fluorophore (**Figure 18A)**, indicating that there is an active SNAP-tag molecule in the sample. This could impact the binding and cytotoxicity experiments and emphasises the need for the implementation of SEC or IEC as a secondary protein purification step. It was also noted that after several freeze-thaw cycles or extended storage of the IMAC-purified samples at 4ºC, the degradation of full-length FPs would be more pronounced (data not shown). This implies that the IMAC-purified samples are unstable and susceptible

to degradation, therefore, compatible solutes such as ectoine should be considered to improve the stability and optimise the storage conditions [211].

Using conjugation analysis, where the FPs were conjugated to fluorophores and AURIF at varying concentration ratios, it was determined that a 1:1 ratio of these SNAP-based FPs (mono- and bivalent) to BG-modified substrate sufficiently saturated the SNAP-tag molecule (**Figures 17 and 20**). While it is recommended to use 1.5 or 2-fold molar excess of BG-modified substrate for efficient SNAP-tag conjugation, these results indicate that where these scFv-SNAP FPs are concerned, an equimolar ratio was efficient and economical [92]. This may be due to the instability and low purity of the FPs illustrated by the presence of degraded protein fragments in the samples, further emphasising the need for improved protein purification protocols. In fact, in addition to the increased transfection efficiencies, MB&I members have also improved the protein purification protocols by successfully combining IMAC enrichment with IEC and/or SEC which resulted in FP yields of 10 mg/L (Amanda Shangase, MSc). Nonetheless, in this study, the 1:1 ratio of scFv-SNAP FP to BG-substrate was implemented for all subsequent conjugation reactions used for downstream experiments.

4.3. Mechanism of action: CSPG4-targeting SNAP fusion proteins

To generate effective ADCs, various factors need to be considered. These include the specificity and affinity of the antibody, the internalisation and processing of the ADC as well as the release of the cytotoxic drug [93, 114]. It is, therefore, important to understand and optimise these parameters when considering the application of the ADC.

4.3.1. Binding, internalisation, and intracellular routing

To determine the mechanism of action of the recombinant scFv-SNAP FPs, confocal imaging with fluorophore-conjugated FP was employed. Using live-cell imaging, the specific tumour cell-surface binding and the fate of the αCSPG4-SNAP FPs once internalised by the target cells were actively visualised and captured. The effects of monovalent and bivalent binding and uptake were also evaluated by visually determining cell surface and intracellular fluorophore signal levels.

After 30 min, the monovalent FP (conjugated to Alexa 488) displayed more cell surface binding compared to the internalised signal (**Figure 21**). This may either be due to the recycling of the receptor-FP complex back to the cell membrane (**Figure 6**) or may indicate the delayed uptake of the FP. Previous studies using monovalent scFv-based FPs performed internalisation assays with longer incubation times (60 min and 2 hours), which resulted in more internalised signal as opposed to cell surface binding [71, 103]. Time-dependent internalisation assays may, therefore, be incorporated into future experiments. Alternatively, to distinguish between internalised signal and receptor recycling, a study describes a releasable SNAP-tag probe by incorporating a cleavable disulphide bond between the BG moiety and the fluorescent probe [212]. This allows for the removal of extracellular fluorophores using a cell-impermeable reducing agent and may also be considered in the future. For the bivalent FP, a greater fluorescent signal was visually located within the cell based on the colocalization between the FPs and the lysosomes. This implies that the velocity of uptake of the bivalent FP is faster than that of the monovalent FP which is likely due to the formation of receptor-FP homodimers [111, 132]. The result of this is hypothesised to cause an increased clustering of receptors and consequently, amplified signalling for more robust clathrin-mediated endocytosis [111, 116, 132]

This phenomenon is also apparent when considering the colocalization between bivalent FP and lysosomes. As depicted in **Figure 21**, the yellow signal indicating the overlap between the fluorophore-labelled FP (green) and the lysosomes (red) is more enhanced in **Figure 21B** (bivalent FP) as opposed to **Figure 21A** (monovalent FP). It is, however, noteworthy that there is clear colocalization between the αCSPG4-SNAP FPs and the lysosomes indicating that both are subjected to lysosomal degradation after receptor-mediated endocytosis [180]. This is important for targeted drug delivery which requires the cleavage of the conjugated drug in the lysosomes and subsequent release into the cytosol to exert its cytotoxic effect (**Figure 6**) [114].

Contrastingly, no colocalization occurs between the FPs and the endoplasmic reticulum, suggesting that they are not subjected to retrograde transport (**Figure 7**). This is a desirable outcome since these recombinant proteins are intended to act as ADCs, which require the release of the cytotoxin from the antibody once internalised into the cell [94]. The surest way to achieve this is through the cleavage of

the linker attaching the toxin to the antibody via lysosomal degradation [94, 213]. If the ADC were, alternatively, subjected to retrograde transport, the toxin is unlikely to be released from the antibody, thereby remaining inactive [94, 131]. It is, however, important to note that colocalization with the tGN using a suitable Golgi tracker should also be considered since this is the first hallmark of the retrograde route (**Figure 22**) [133]. In this study, access to different organelle trackers was limited, however, future studies should incorporate this aspect for accuracy. Furthermore, future research may benefit from prolonged binding and internalisation studies (1, 3, 24 hours) to determine the duration that conjugated fluorescent signal is active and detectable within the cells and whether routing patterns change with time.

This study is the first of its kind to demonstrate the intracellular routing of scFv-SNAP FPs and establish a method to distinguish between lysosomal and retrograde transport. In corroboration with the literature, valency-dependent differences in antigen binding and uptake were also illustrated, which bodes well for the therapeutic application of scFv-SNAP FPs [86, 88, 98, 115, 117–123]. Although the presence of proteolytic degradation products with potential competitive binding activities has been demonstrated, the fluorophore-labelled proteins successfully confirmed antigen-specific binding and intracellular routing in TNBC cells.

4.3.2. Antigen-mediated cytotoxicity

The capacity of αCSPG4-SNAP FPs to effectively be used for targeted drug delivery was assessed and valency-dependent differences in AURIF-mediated cytotoxicity were determined. The FPs were conjugated to the microtubule inhibitor drug, AURIF, which had been modified to contain an inert poly(ethylene glycol) (PEG) spacer (PEG_3-NH_2) by Prof. Roger Hunter's research group (Department of Chemistry, University of Cape Town). The PEG spacer was incorporated to improve hydrophobicity and facilitate conjugation by distancing the AURIF molecule from the SNAP-tag [214]. Excess BG-AURIF was removed through buffer exchange since it is known to be toxic to cells in a non-specific manner [100].

The positive binding and internalisation demonstrated by the fluorophore-conjugated FPs were reflected in the cell viability assays. Dose-dependent cytotoxicity was demonstrated by both FPs and, notably, the bivalent FP induced a more potent cytotoxic effect on the antigen-positive cells, indicated by the lower IC_{50} value (**Figure 23**). This, in combination with the imaging results, provides evidence of improved binding and uptake of bivalent scFv-based immunotherapies compared to the monovalent counterparts [86, 98, 115, 119]. These results confirm the hypothesis that bivalent antibody-based therapies induce improved cytotoxic potency owing to the enhanced binding affinity.

Upon comparing these IC_{50} values (MV = 409 nM; BV = 277 nM) to that of a previous study using scFv-SNAP FPs conjugated to AURIF (0.6-12 nM), it is clear the FPs produced in this study are less effective at inducing cytotoxicity [100]. However, the lower purity of the FPs in addition to differences in the target antigen and cell lines used should be considered. Although the presence of the degraded recombinant protein products may introduce competitive binding, this study documented suitable dose-dependent cytotoxicity in antigen-positive cells. This confirms the general capabilities of these as recombinant ADCs. These experiments should ideally be repeated with high-purity FPs (using additional purification techniques such as SEC or IEC) to more accurately determine the cytotoxic effect mediated by antigen-specific binding and uptake.

Notably, the unconjugated FPs had no cytotoxic effect on the antigen-positive cells, indicating that the cytotoxicity is mediated by the AURIF. Conversely, the unconjugated BG-AURIF displayed potent cytotoxicity on the cells in a non-specific manner, illustrated by the cell shrinkage, membrane blebbing and presence of apoptotic bodies which are classic signs of apoptosis (**Figure 24**) [100, 215]. This suggests that the unconjugated BG-AURIF is cell-permeable and could result in a bystander effect. The scFv-SNAP FPs conjugated to BG-AURIF could, therefore, induce a bystander effect on neighbouring cells in the tumour environment, thereby improving the efficacy of the drug [216, 217]. This may also decrease the need for high concentrations of the administered therapy [218].

Whether the enhanced cytotoxic effect of the bivalent FP owing to the increased avidity translates from this *in vitro* system into *in vivo* application remains to be determined. Various studies have reported that

high-affinity mAbs fail to sufficiently diffuse into and penetrate solid tumour masses citing the binding site barrier as one of the underlying causes [110, 125, 129]. This phenomenon can be assessed to some extent using spheroid tumour cell models until *in vivo* tumour xenograft models can be established [219]. Compared to the monomeric scFv format (~28 kDa), the FPs have higher molecular weights – with the monovalent ~55 kDa and the bivalent ~80 kDa. This may translate into more desirable pharmacokinetic properties such as longer blood retention times for prolonged effects while maintaining the improved diffusion and penetration into the tumour mass [220, 221]. In comparison with the scFv-based immunotherapies that have been approved (**Table 15**), the sizes of the FPs indicate that they may have similar pharmacokinetic properties. Furthermore, compared to the sizes of the bivalent immunotoxins from previous studies (~97 kDa), the FPs (~55 kDa and ~80 kDa) may hold up in terms of balancing tumour penetration and renal clearance [119–121]. Another *in vivo* study reported that the best anti-tumour efficacy was induced by antibody-based molecules approximately 45-69 kDa in size which corresponded with serum half-lives under 24 hours [222]. This evidence bodes well for the potential pharmacokinetic properties of the αCSPG4-SNAP FPs.

4.4. Application of αCSPG4-SNAP fusion proteins

The mono- and bivalent FPs were able to positively identify CSPG4 on the surfaces of tumour cells and mediate CSPG4-specific binding and endocytosis. This indicates that these FPs are capable of targeted delivery of SNAP-conjugated substrates once internalised into the cells, and the substrate can be cleaved in the lysosome [213].

The imaging data suggest that the monovalent FP is suited for *in vivo* diagnostic purposes owing to its smaller size and likely rapid renal clearance, in addition to its less rapid internalisation and lysosomal degradation [112, 181, 223]. Studies have shown that similar recombinant SNAP-tag FPs can be conjugated to fluorophores and radiotracers for fluorescent and PET imaging in mouse models [89, 102]. This can be used as an immunodiagnostic tool, where the conjugated substrate is an imaging probe for *ex vivo* and *in vivo* detection of antigen-positive tumour cells [101, 102, 192]. *Ex vivo* detection using monovalent αCSPG4(scFv)-SNAP conjugated to a fluorophore was displayed in breast cancer

biopsies by Amoury *et al.* and Mungra *et al.* [71, 198]. Similar *in vivo* diagnostic detection can be achieved using fluorophore or radionuclide labels attached to scFv-SNAP FPs for fluorescent or PET imaging, respectively [101, 102, 206, 224]. Using these, tumours can accurately be detected based on cell-surface biomarkers, whereby the patients are stratified, and treatment options are predicted (**Figure 25**). Alternatively, the evidence suggests that the bivalent FP would be better suited for therapeutic purposes. A larger size resulting from further antibody and Fc engineering strategies would likely translate into a longer serum half-life and increased avidity resulting in potent tumour elimination potential [88]. Additionally, the enhanced avidity and cytotoxic potency on the bivalent FP indicate that it would be able to induce CSPG4-mediated cytotoxicity in antigen-positive tumour cells.

This study, therefore, provides further support for using monovalent scFv-SNAP FPs for immunodiagnostic functions and bivalent scFv-SNAP FPs in immunotherapeutic applications. Furthermore, this study has established a method for studying intracellular routing and confirming valency-dependent differences in the binding and internalisation of scFv-SNAP FPs. The versatility of SNAP-tag technology combined with the specificity of scFv antibody derivatives in identifying and selectively targeting tumour-associated antigens is promising for the future of immunodiagnostics and immunotherapeutics.

5. Conclusions and future prospects

Understanding, characterising, and managing TNBC has proven to be challenging given its inherent complexity and heterogeneity. The evidence suggests that the intertumoral and intratumoral diversity associated with TNBC is substantial, especially among patients from different ancestral and demographic backgrounds [28, 43, 163]. Therefore, the need for a multi-targeted precision medicine approach has become increasingly apparent. Such an approach should involve the screening and assessment of tumours for prognostic and therapeutic biomarkers that can accurately inform clinicians on the treatment strategy that patients would be most responsive to (**Figure 25**) [167, 225].

Novel immunotherapies in combination with standard therapeutic strategies have shown great potential for improving the quality of life and survival of cancer patients [48, 226]. However, in the case of

TNBC, these immunotherapies are often implemented as a last resort when conventional therapies have failed. This is exemplified by the ADC, Sacituzumab govitecan, which has only been approved for TNBC patients with unresectable and locally advanced or metastatic tumours and who received prior systemic therapies for metastatic disease [54]. Even pembrolizumab, which has been validated in multiple cancers and is more widely available, is only approved for TNBC patients with recurring, advanced and metastatic tumours that cannot be surgically removed [49, 227]. These therapies are, therefore, not accessible to newly diagnosed TNBC patients and they are likely not screened for their sensitivity to either. Personalised medicine approaches are thus not currently available to all TNBC patients, even though all patients could benefit from them since they may improve patient outcomes and decrease the risk of relapse [48, 166, 167]. As such, there is still an unmet need for novel prognostic and therapeutic targets to effectively manage TNBC across patients with different tumour profiles.

Currently, multiple therapeutic targets are being explored for TNBC, including PD-L1, Trop-2, epidermal growth factor receptor (EGFR), vascular endothelial growth factor (VEGF), and epithelial cell adhesion molecule (EpCAM) [47, 228]. Additionally, promising prognostic and therapeutic targets are being discovered with high-throughput gene expression and proteomic analysis [171–173]. This data can be used to develop diagnostic, prognostic and therapeutic biomarkers in the tumour microenvironment that can be translated into clinical treatment strategies. The tumour microenvironment is defined as the proliferating cancerous cells, non-cancerous cells (stroma), signalling molecules and extracellular matrix elements that are present within the tumour [229]. Interactions between components of the tumour microenvironment are known to dictate tumour morphology, proliferation, and invasiveness [230]. The ability to target multiple antigens in the tumour microenvironment that play a role in tumorigenesis and metastasis, in combination with standard therapy may be incredibly effective in turning the tide against this highly aggressive disease [167, 226, 231].

While this study targeted one tumour-associated antigen (CSPG4), multiple scFv-based immunotherapies targeting TNBC-associated biomarkers have been developed at the MB&I (publications in development). As mentioned previously, various elements of the recombinant protein

production pipeline are consistently established and optimised by members of the MB&I. While the purity, yield, and stability of the FPs produced in this study were not comparable with reports from the literature, it is not an accurate reflection of the current capabilities of the MB&I. Future studies will, therefore, benefit from the improvements to the protein production pipeline, where the results will be tantamount to the current standards reported in the literature. It should, however, be emphasised that despite the low purity, yield, and stability of the recombinant proteins produced in this study, these proteins were successfully conjugated to BG-modified fluorophores and auristatin F, where a 1:1 ratio of FP to BG-substrate was determined to be efficient (section **2.3.4**). Furthermore, these conjugated FPs demonstrated their targeted functionality through antigen-specific binding activity, intracellular routing analysis, and dose-dependent cytotoxicity on a CSPG4-positive TNBC cell line (section **3.3**). Members of the MB&I have produced scFv-SNAP FPs targeting various TAAs and regardless of poor yields, purities, and stabilities, have successfully demonstrated *in vivo* and *ex vivo* binding on tumour cell lines and patient biopsies, respectively (publications in development). This highlights the robust nature of SNAP-tag in this unique antibody format which allows for conjugation and validation despite preliminary protein purification conditions owing to the high-efficiency autocatalytic reaction [92, 190].

The findings of this study confirmed that restoring the bivalent state of natural antibodies and mAbs results in improved binding, uptake and cytotoxic potency owing to the increase in functional affinity (avidity) in an *in vitro* model [85, 86, 115, 121, 122, 182]. Furthermore, the increase in molecular weight may confer desirable pharmacokinetic properties that monovalent scFvs lose due to small size and rapid renal clearance [117, 140, 193]. This confirms the findings of previous studies and is promising for the future designs of scFv-based immunotherapeutic strategies. Using the methodology of this study, bispecific scFv-based immunotherapies could also be developed, which holds great therapeutic potential, illustrated by the BiTES that have been approved for clinical application (**Table 15**). While the bivalent FP demonstrate greater cytotoxic potential, the findings also suggest that monovalent scFv-SNAP FPs may be more suited for immunodiagnostic applications since the smaller size is desirable when using fluorophores or radionuclides in an *in vivo* context to detect tumour masses and monitor patient responses to treatment [88, 102, 223, 224, 232].

This study was the first of its kind to explore the intracellular routing pathway that scFv-SNAP FPs undergo once endocytosed by tumour cells. For the effective delivery of the conjugated drug, the FPs should be routed to the lysosomal compartment, where the drug is released through proteolytic cleavage [104, 180]. It is, therefore, important to confirm the lysosomal degradation of the FPs post-endocytosis during the functional evaluation and optimisation stages. Furthermore, since different receptors (antigens) may inherently be prone to receptor recycling mechanisms or the presence of an active Fc region could induce recycling, novel ADCs should employ similar intracellular routing studies to confirm the lysosomal degradation after internalisation [176, 180, 213]. Alternatively, immunotoxins that are composed of protein toxins would benefit from retrograde transport to prevent their lysosomal degradation and mediate their release into the cytosol. Using similar methods employed in this study, the retrograde pathway can be detected by labelling organelles such as the Golgi and the endoplasmic reticulum (**Figure 7**) [133, 136]. This study, therefore, established a methodology for identifying the intracellular routing pathways after receptor-mediated endocytosis. This methodology will be used to distinguish the lysosomal degradation of ADC formats such as scFv-SNAP FPs from the retrograde transport of immunotoxins at the MB&I.

In conclusion, the findings of this study may have implications for the future designs of scFv-based immunodiagnostics and immunotherapeutics. As previously emphasised, there is an increasing need for the development of precision medicine strategies to effectively manage TNBC. Consequently, to account for the diversity of the disease, an arsenal of diagnostic and therapeutic methodologies will be required. We propose using multiplex fluorescence imaging with monovalent fluorophore-conjugated scFv-SNAP FPs to identify prognostic and therapeutic biomarkers on patient tumour biopsies (**Figure 26**). This information can be translated into immunotherapeutic strategies with bivalent scFv-SNAP FPs for targeted drug delivery that effectively induces tumour cell death. These novel targeted immunotherapies should be used in combination with conventional therapies to improve TNBC patient prognosis and long-term survival. This work serves as a preliminary framework for producing versatile, efficient, and economically viable immunodiagnostic and immunotherapeutic tools using SNAP-tag technology combined with high-affinity scFvs as depicted in **Figure 26**.

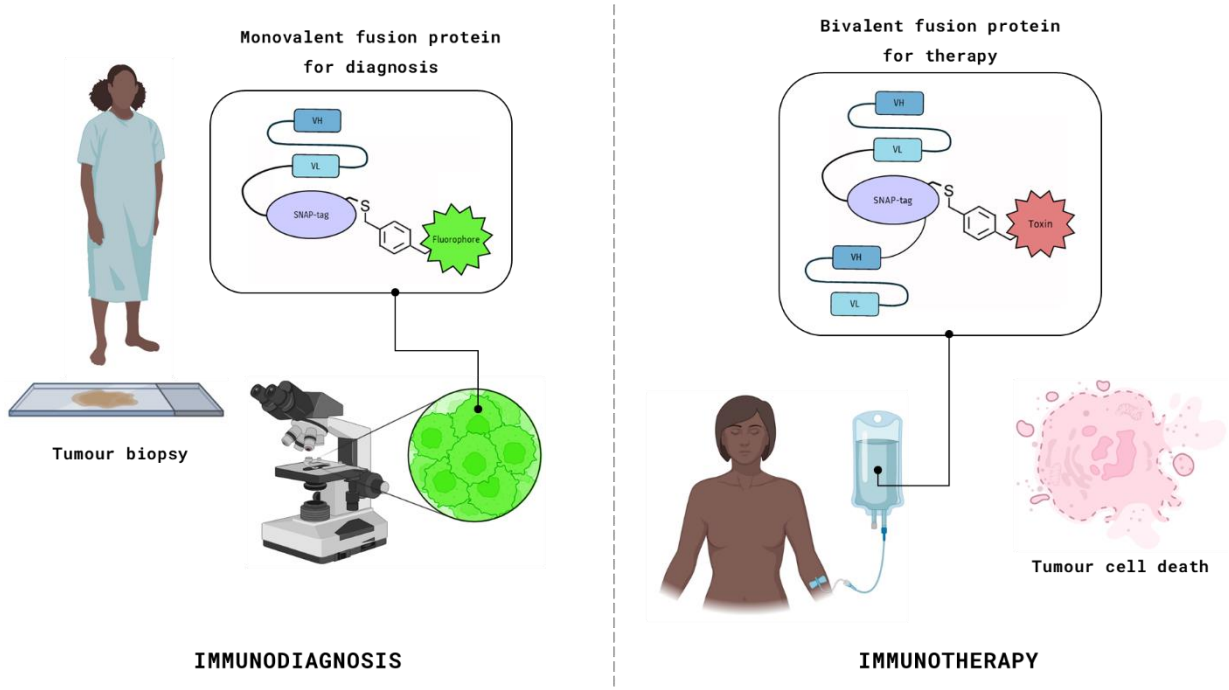

Figure 26. Potential application of mono- and bivalent scFv-SNAP fusion proteins in precision medicine. Cell surface biomarkers or tumour-associated antigens would be identified on patient tumour biopsies by a monovalent scFv-SNAP fusion protein conjugated to a diagnostic label such as a fluorophore. Once the antigen is identified, a bivalent variant of the same fusion protein conjugated to a cytotoxic molecule can be administered to the patient, resulting in antigen-mediated tumour elimination. The monovalent and bivalent scFv-SNAP fusion proteins can be applied in immunodiagnostic and immunotherapeutic strategies, respectively. The diagnosis can, therefore, directly inform the treatment.

6. References

1. Sung H, Ferlay J, Siegel RL, et al (2021) Global Cancer Statistics 2020: GLOBOCAN Estimates of Incidence and Mortality Worldwide for 36 Cancers in 185 Countries. CA Cancer J Clin 71:209–249. https://doi.org/10.3322/CAAC.21660

2. Arnold M, Morgan E, Rumgay H, et al (2022) Current and future burden of breast cancer: Global statistics for 2020 and 2040. Breast 66:15–23. https://doi.org/10.1016/j.breast.2022.08.010

3. Paulsson AK, Sherertz T, Park CC (2018) Breast cancer facts and figures 2017-2018. Handb Evidence-Based Radiat Oncol 343–399. https://doi.org/10.1007/978-3-319-62642-0_17

4. Hanahan D, Weinberg RA (2011) Hallmarks of cancer: The next generation. Cell 144:646–674. https://doi.org/10.1016/j.cell.2011.02.013

5. Hanahan D (2022) Hallmarks of Cancer: New Dimensions. Cancer Discov 12:31–46. https://doi.org/10.1158/2159-8290.CD-21-1059

6. Libson S, Lippman M (2014) A review of clinical aspects of breast cancer. Int Rev Psychiatry 26:4–15. https://doi.org/10.3109/09540261.2013.852971

7. Beral V, Bull D, Doll R, et al (2001) Familial breast cancer: collaborative reanalysis of individual data from 52 epidemiological studies including 58,209 women with breast cancer and 101,986 women without the disease. Lancet (London, England) 358:1389–1399. https://doi.org/10.1016/S0140-6736(01)06524-2

8. Torre LA, Islami F, Siegel RL, et al (2017) Global Cancer in Women: Burden and Trends. Cancer Epidemiol Biomarkers Prev 26:444–457. https://doi.org/10.1158/1055-9965.EPI-16-0858

9. Ma H, Bernstein L, Ross RK, Ursin G (2006) Hormone-related risk factors for breast cancer in women under age 50 years by estrogen and progesterone receptor status: results from a case-control and a case-case comparison. Breast Cancer Res 8:. https://doi.org/10.1186/BCR1514

10. Shah TA, Guraya SS (2017) Breast cancer screening programs: Review of merits, demerits, and

recent recommendations practised across the world. J Microsc Ultrastruct 5:59. https://doi.org/10.1016/J.JMAU.2016.10.002

11. Singletary SE, Greene FL (2003) Revision of breast cancer staging: the 6th edition of the TNM Classification. Semin Surg Oncol 21:53–59. https://doi.org/10.1002/SSU.10021

12. Malhotra GK, Zhao X, Band H, Band V (2010) Histological, molecular and functional subtypes of breast cancers. Cancer Biol Ther 10:955. https://doi.org/10.4161/CBT.10.10.13879

13. Zaha DC (2014) Significance of immunohistochemistry in breast cancer. World J Clin Oncol 5:382. https://doi.org/10.5306/wjco.v5.i3.382

14. Gabriele L, Moretti F, Pierotti MA, et al (2006) The use of microarray technologies in clinical oncology. J Transl Med 4:8. https://doi.org/10.1186/1479-5876-4-8

15. Dai X, Li T, Bai Z, et al (2015) Breast cancer intrinsic subtype classification, clinical use and future trends. Am J Cancer Res 5:2929

16. Pearce ST, Jordan VC (2004) The biological role of estrogen receptors α and β in cancer. Crit Rev Oncol Hematol 50:3–22. https://doi.org/10.1016/j.critrevonc.2003.09.003

17. Yu F, Bender W (2001) The mechanism of tamoxifen in breast cancer prevention. Breast Cancer Res 3:A74. https://doi.org/10.1186/BCR404

18. Yip CH, Rhodes A (2014) Estrogen and progesterone receptors in breast cancer. Future Oncol 10:2293–2301. https://doi.org/10.2217/FON.14.110

19. Gutierrez C, Schiff R (2011) HER 2: Biology, Detection, and Clinical Implications. Arch Pathol Lab Med 135:55. https://doi.org/10.1043/2010-0454-RAR.1

20. Loibl S, Gianni L (2017) HER2-positive breast cancer. Lancet 389:2415–2429. https://doi.org/10.1016/S0140-6736(16)32417-5

21. Vu T, Claret FX (2012) Trastuzumab: Updated Mechanisms of Action and Resistance in Breast Cancer. Front Oncol 2:. https://doi.org/10.3389/FONC.2012.00062

22. Zhang A, Wang X, Fan C, Mao X (2021) The Role of Ki67 in Evaluating Neoadjuvant Endocrine Therapy of Hormone Receptor-Positive Breast Cancer. Front Endocrinol (Lausanne) 12:1426. https://doi.org/10.3389/fendo.2021.687244

23. Hashmi AA, Hashmi KA, Irfan M, et al (2019) Ki67 index in intrinsic breast cancer subtypes and its association with prognostic parameters. BMC Res Notes 12:. https://doi.org/10.1186/S13104-019-4653-X

24. Brown M, Cress RD, Caggiano V, et al (2007) Descriptive analysis of estrogen receptor (ER)-negative, progesterone receptor (PR)-negative, and HER2-negative invasive breast cancer, the so-called triple-negative phenotype. Cancer 109:1721–1728. https://doi.org/10.1002/cncr.22618

25. Bianchini G, Balko JM, Mayer IA, et al (2016) Triple-negative breast cancer: Challenges and opportunities of a heterogeneous disease. Nat Rev Clin Oncol 13:674–690. https://doi.org/10.1038/nrclinonc.2016.66

26. Kumar P, Aggarwal R (2016) An overview of triple-negative breast cancer. Arch Gynecol Obstet 293:247–269. https://doi.org/10.1007/s00404-015-3859-y

27. Gonzalez-Angulo AM, Timms KM, Liu S, et al (2011) Incidence and outcome of BRCA mutations in unselected patients with triple receptor-negative breast cancer. Clin Cancer Res 17:1082–1089. https://doi.org/10.1158/1078-0432.CCR-10-2560

28. Carey LA, Perou CM, Livasy CA, et al (2006) Race, Breast Cancer Subtypes, and Survival in the Carolina Breast Cancer Study. JAMA 295:2492–2502. https://doi.org/10.1001/JAMA.295.21.2492

29. Gorodetska I, Kozeretska I, Dubrovska A (2019) BRCA Genes: The Role in Genome Stability, Cancer Stemness and Therapy Resistance. J Cancer 10:2109. https://doi.org/10.7150/JCA.30410

30. Cleator S, Heller W, Coombes RC (2007) Triple-negative breast cancer: therapeutic options. Lancet Oncol 8:235–244. https://doi.org/10.1016/S1470-2045(07)70074-8

31. Sporikova Z, Koudelakova V, Trojanec R, Hajduch M (2018) Genetic Markers in Triple-Negative Breast Cancer. Clin Breast Cancer 18:e841–e850. https://doi.org/10.1016/j.clbc.2018.07.023

32. Lehmann BD, Bauer JA, Chen X, et al (2011) Identification of human triple-negative breast cancer subtypes and preclinical models for selection of targeted therapies. J Clin Invest 121:2750. https://doi.org/10.1172/JCI45014

33. Rapiti E, Pinaud K, Chappuis PO, et al (2017) Opportunities for improving triple-negative breast cancer outcomes: results of a population-based study. Cancer Med 6:526–536. https://doi.org/10.1002/cam4.998

34. Foulkes WD, Smith IE, Reis-Filho JS (2010) Triple-negative breast cancer. N Engl J Med. https://doi.org/10.1007/978-3-319-41761-5_6

35. Zaparoli Zucoloto A, Swely E, Monteiro Sanches A, et al (2015) Challenges in the treatment of triple-negative breast cancer: chemoresistance and identification of molecular targets. Appl Cancer Res 35:72–78

36. Carey LA, Dees EC, Sawyer L, et al (2007) The triple negative paradox: Primary tumor chemosensitivity of breast cancer subtypes. Clin Cancer Res 13:2329–2334. https://doi.org/10.1158/1078-0432.CCR-06-1109

37. Anders CK, Carey LA (2009) Biology, Metastatic Patterns, and Treatment of Patients with Triple-Negative Breast Cancer. Clin Breast Cancer 9:S73. https://doi.org/10.3816/CBC.2009.S.008

38. Ginsburg O, Yip CH, Brooks A, et al (2020) Breast Cancer Early Detection: A Phased Approach to Implementation. Cancer 126:2379–2393. https://doi.org/10.1002/cncr.32887

39. Eberlein TJ (2007) Race, Breast Cancer Subtypes, and Survival in the Carolina Breast Cancer Study. Yearb Surg 2007:304–305. https://doi.org/10.1016/S0090-3671(08)70227-1

40. Liedtke C, Mazouni C, Hess KR, et al (2008) Response to neoadjuvant therapy and long-term

survival in patients with triple-negative breast cancer. J Clin Oncol. https://doi.org/10.1200/JCO.2007.14.4147

41. Dent R, Trudeau M, Pritchard KI, et al (2007) Triple-Negative Breast Cancer: Clinical Features and Patterns of Recurrence. Clin Cancer Res 13:4429–4434. https://doi.org/10.1158/1078-0432.CCR-06-3045

42. Sharma R, Aashima, Nanda M, et al (2022) Mapping Cancer in Africa: A Comprehensive and Comparable Characterization of 34 Cancer Types Using Estimates From GLOBOCAN 2020. Front Public Heal 10:1–14. https://doi.org/10.3389/fpubh.2022.839835

43. Kruger W, Apffelstaedt J (2014) Young breast cancer patients in the developing world: incidence, choice of surgical treatment and genetic factors. South African Fam Pract. https://doi.org/10.1080/20786204.2007.10873634

44. Dua I, Tan AR (2017) Immunotherapy for Triple-Negative Breast Cancer: A Focus on Immune Checkpoint Inhibitors. Am J Hematol Oncol 13:20–27

45. Katz H, Alsharedi M (2018) Immunotherapy in triple-negative breast cancer. Med Oncol 35:1–9. https://doi.org/10.1007/s12032-017-1071-6

46. Wang X, Qi Y, Kong X, et al (2019) Immunological therapy: A novel thriving area for triple-negative breast cancer treatment. Cancer Lett 442:409–428. https://doi.org/10.1016/j.canlet.2018.10.042

47. Sukumar J, Gast K, Quiroga D, et al (2021) Triple-negative breast cancer: promising prognostic biomarkers currently in development. Expert Rev Anticancer Ther 21:135. https://doi.org/10.1080/14737140.2021.1840984

48. Qiu D, Zhang G, Yan X, et al (2022) Prospects of Immunotherapy for Triple-Negative Breast Cancer. Front Oncol 11:5386. https://doi.org/10.3389/fonc.2021.797092

49. Cortes J, Rugo HS, Cescon DW, et al (2022) Pembrolizumab plus Chemotherapy in Advanced Triple-Negative Breast Cancer. N Engl J Med 387:217–226.

https://doi.org/10.1056/NEJMoa2202809

50. Kang SP, Gergich K, Lubiniecki GM, et al (2017) Pembrolizumab KEYNOTE-001: An adaptive study leading to accelerated approval for two indications and a companion diagnostic. Ann Oncol 28:1388–1398. https://doi.org/10.1093/annonc/mdx076

51. Mckertish C, Kayser V (2021) Advances and Limitations of Antibody Drug Conjugates for Cancer. Biomedicines 9:872. https://doi.org/10.3390/biomedicines9080872

52. Bardia A, Hurvitz SA, Tolaney SM, et al (2021) Sacituzumab Govitecan in Metastatic Triple-Negative Breast Cancer. N Engl J Med 384:1529–1541. https://doi.org/10.1056/nejmoa2028485

53. Zaman S, Jadid H, Denson AC, Gray JE (2019) Targeting Trop-2 in solid tumors: future prospects. Onco Targets Ther 12:1781. https://doi.org/10.2147/OTT.S162447

54. Carey LA, Loirat D, Punie K, et al (2022) Sacituzumab govitecan as second-line treatment for metastatic triple-negative breast cancer—phase 3 ASCENT study subanalysis. NPJ Breast Cancer 8:. https://doi.org/10.1038/S41523-022-00439-5

55. Song E, Mechref Y (2015) Defining glycoprotein cancer biomarkers by MS in conjunction with glycoprotein enrichment. Biomark Med 9:835–844. https://doi.org/10.2217/bmm.15.55

56. Criscitiello C (2012) Tumor-associated antigens in breast cancer. Breast Care 7:262–266. https://doi.org/10.1159/000342164

57. Firer MA, Gellerman G (2012) Targeted drug delivery for cancer therapy: The other side of antibodies. J Hematol Oncol 5:1. https://doi.org/10.1186/1756-8722-5-70

58. Yuan P, Zhang H, Cai C, et al (2014) Chondroitin sulfate proteoglycan 4 functions as the cellular receptor for Clostridium difficile toxin B. Nat Publ Gr 25:157–168. https://doi.org/10.1038/cr.2014.169

59. Verma RS, Bonavida B (2015) Resistance to Immunotoxins in Cancer Therapy. Springer International Publishing, Cham

60. Wang X, Osada T, Wang Y, et al (2010) CSPG4 protein as a new target for the antibody-based immunotherapy of triple-negative breast cancer. J Natl Cancer Inst 102:1496–1512. https://doi.org/10.1093/jnci/djq343

61. Kozanoglu I, Boga C, Ozdogu H, et al (2009) Human bone marrow mesenchymal cells express NG2: Possible increase in discriminative ability of flow cytometry during mesenchymal stromal cell identification. Cytotherapy 11:527–533. https://doi.org/10.1080/14653240902923153

62. Price MA, Colvin Wanshura LE, Yang J, et al (2011) CSPG4, a potential therapeutic target, facilitates malignant progression of melanoma. Pigment Cell Melanoma Res 24:1148–1157. https://doi.org/10.1111/j.1755-148X.2011.00929.x

63. Eng MS, Kaur J, Prasmickaite L, et al (2018) Enhanced targeting of triple-negative breast carcinoma and malignant melanoma by photochemical internalization of CSPG4-targeting immunotoxins. Photochem Photobiol Sci 17:539–551. https://doi.org/10.1039/C7PP00358G

64. Zhang H, Wu Z, Hu D, et al (2022) Immunotherapeutic Targeting of NG2/CSPG4 in Solid Organ Cancers. Vaccines 10:. https://doi.org/10.3390/vaccines10071023

65. Hoffmann RM, Crescioli S, Mele S, et al (2020) A Novel Antibody-Drug Conjugate (ADC) Delivering a DNA Mono-Alkylating Payload to Chondroitin Sulfate Proteoglycan (CSPG4)-Expressing Melanoma. Cancers 2020, Vol 12, Page 1029 12:1029. https://doi.org/10.3390/CANCERS12041029

66. Campoli MR, Chang C-C, Kageshita T, et al (2004) Human High Molecular Weight-Melanoma-Associated Antigen (HMW-MAA): A Melanoma Cell Surface Chondroitin Sulfate Proteoglycan (MSCP) with Biological and Clinical Significance. Crit Rev Immunol 24:267–296. https://doi.org/10.1615/CritRevImmunol.v24.i4.40

67. Ilieva KM, Cheung A, Mele S, et al (2018) Chondroitin Sulfate Proteoglycan 4 and Its Potential As an Antibody Immunotherapy Target across Different Tumor Types. Front Immunol 8:1911. https://doi.org/10.3389/fimmu.2017.01911

68. Guo Y, Pan W, Liu S, et al (2020) ERK/MAPK signalling pathway and tumorigenesis (Review). Exp Ther Med 19:1997–2007. https://doi.org/10.3892/ETM.2020.8454

69. Wang X, Wang Y, Yu L, et al (2010) CSPG4 in Cancer: Multiple Roles. Curr Mol Med 10:419–429. https://doi.org/10.2174/156652410791316977

70. Wilson BS, Imai K, Natali PG, Ferrone S (1981) Distribution and molecular characterization of a cell-surface and a cytoplasmic antigen detectable in human melanoma cells with monoclonal antibodies. Int J Cancer 28:293–300. https://doi.org/10.1002/ijc.2910280307

71. Amoury M, Bauerschlag D, Zeppernick F, et al (2016) Photoimmunotheranostic agents for triple-negative breast cancer diagnosis and therapy that can be activated on demand. Oncotarget 7:54925–54936. https://doi.org/10.18632/oncotarget.10705

72. Brehm H, Niesen J, Mladenov R, et al (2014) A CSPG4-specific immunotoxin kills rhabdomyosarcoma cells and binds to primary tumor tissues. Cancer Lett 352:228–235. https://doi.org/10.1016/j.canlet.2014.07.006

73. Murphy K, Janeway C, Travers P, Walport M (2012) Janeway's Immunobiology, Garland Science, Eighth Edi. Garland Science, Taylor & Francis Group, LLC, New York, NY, USA

74. Köhler G, Milstein C (1975) Continuous cultures of fused cells secreting antibody of predefined specificity. Nat 1975 2565517 256:495–497. https://doi.org/10.1038/256495a0

75. Adams GP, Weiner LM (2005) Monoclonal antibody therapy of cancer. Nat Biotechnol 23:1147–1157. https://doi.org/10.1038/NBT1137

76. Saxena A, Wu D (2016) Advances in therapeutic Fc engineering - modulation of IgG-associated effector functions and serum half-life. Front Immunol 7:. https://doi.org/10.3389/fimmu.2016.00580

77. Mullard A (2021) FDA approves 100th monoclonal antibody product. Nat Rev Drug Discov 20:491–495. https://doi.org/10.1038/d41573-021-00079-7

78. Wang SS, Yan Y, Ho K (2021) US FDA-approved therapeutic antibodies with high-concentration formulation: summaries and perspectives. Antib Ther 4:262. https://doi.org/10.1093/ABT/TBAB027

79. Charles A Janeway J, Travers P, Walport M, Shlomchik MJ (2001) The structure of a typical antibody molecule. In: Immunobiology: The Immune System in Health and Disease. 5th edition. Garland Science

80. Nimmerjahn F, Gordan S, Lux A (2015) FcgR dependent mechanisms of cytotoxic, agonistic, and neutralizing antibody activities. Trends Immunol 36:325–336. https://doi.org/10.1016/j.it.2015.04.005

81. Arlotta KJ, Owen SC (2019) Antibody and antibody derivatives as cancer therapeutics. Wiley Interdiscip Rev Nanomedicine Nanobiotechnology 11:e1556. https://doi.org/10.1002/WNAN.1556

82. Jin S, Sun Y, Liang X, et al (2022) Emerging new therapeutic antibody derivatives for cancer treatment. Signal Transduct Target Ther 2022 71 7:1–28. https://doi.org/10.1038/s41392-021-00868-x

83. Yokota T, Milenic DE, Whitlow M, Schlom J (1992) Rapid Tumor Penetration of a Single-Chain Fv and Comparison with Other Immunoglobulin Forms. Cancer Res 52:3402–3408

84. Ahmad ZA, Yeap SK, Ali AM, et al (2012) scFv Antibody: Principles and Clinical Application. Clin Dev Immunol 2012:15. https://doi.org/10.1155/2012/980250

85. Adams GP, Tai MS, McCartney JE, et al (2006) Avidity-mediated enhancement of in vivo tumor targeting by single-chain Fv dimers. Clin Cancer Res 12:1599–1605. https://doi.org/10.1158/1078-0432.CCR-05-2217

86. Hudson PJ, Kortt AA (1999) High avidity scFv multimers; diabodies and triabodies. J Immunol Methods 231:177–189. https://doi.org/10.1016/S0022-1759(99)00157-X

87. Beckman RA, Weiner LM, Davis HM (2007) Antibody constructs in cancer therapy. Cancer

109:170–179. https://doi.org/10.1002/cncr.22402

88. Kontermann RE (2009) Strategies to extend plasma half-lives of recombinant antibodies. BioDrugs 23:93–109. https://doi.org/10.2165/00063030-200923020-00003

89. Amoury M, Kolberg K, Pham AT, et al (2016) Granzyme B-based cytolytic fusion protein targeting EpCAM specifically kills triple negative breast cancer cells in vitro and inhibits tumor growth in a subcutaneous mouse tumor model. Cancer Lett 372:201–209. https://doi.org/10.1016/j.canlet.2016.01.027

90. Niesen J, Sack M, Seidel M, et al (2016) SNAP-Tag Technology: A Useful Tool to Determine Affinity Constants and Other Functional Parameters of Novel Antibody Fragments. Bioconjug Chem 27:1931–1941. https://doi.org/10.1021/acs.bioconjchem.6b00315

91. Hussain AF, Kampmeier F, Von Felbert V, et al (2011) SNAP-tag technology mediates site specific conjugation of antibody fragments with a photosensitizer and improves target specific phototoxicity in tumor cells. Bioconjug Chem 22:2487–2495. https://doi.org/10.1021/bc200304k

92. Hussain AF, Heppenstall PA, Kampmeier F, et al (2019) One-step site-specific antibody fragment auto-conjugation using SNAP-tag technology. Nat Protoc 14:3101–3125. https://doi.org/10.1038/s41596-019-0214-y

93. Kamath A V., Iyer S (2015) Preclinical Pharmacokinetic Considerations for the Development of Antibody Drug Conjugates. Pharm Res 32:3470–3479. https://doi.org/10.1007/s11095-014-1584-z

94. Tsuchikama K, An Z (2018) Antibody-drug conjugates: recent advances in conjugation and linker chemistries. Protein Cell 9:33–46. https://doi.org/10.1007/s13238-016-0323-0

95. Gauzy-Lazo L, Sassoon I, Brun MP (2020) Advances in Antibody–Drug Conjugate Design: Current Clinical Landscape and Future Innovations. SLAS Discov 25:843–868. https://doi.org/10.1177/2472555220912955

96. Gautier A, Juillerat A, Heinis C, et al (2008) An Engineered Protein Tag for Multiprotein Labeling in Living Cells. Chem Biol 15:128–136. https://doi.org/10.1016/j.chembiol.2008.01.007

97. Sun X, Zhang A, Baker B, et al (2011) Development of SNAP-Tag Fluorogenic Probes for Wash- Free Fluorescence Imaging. 2217–2226. https://doi.org/10.1002/cbic.201100173

98. Amoury M, Blume T, Brehm H, et al (2013) SNAP-tag based Agents for Preclinical In Vitro Imaging in Malignant Diseases. Curr Pharm Des 19:

99. Woitok M, Klose D, Niesen J, et al (2016) The efficient elimination of solid tumor cells by EGFR-specific and HER2-specific scFv-SNAP fusion proteins conjugated to benzylguanine-modified auristatin F. Cancer Lett 381:323–330. https://doi.org/10.1016/j.canlet.2016.08.003

100. Woitok M, Klose D, Di Fiore S, et al (2017) Comparison of a mouse and a novel human scFv-SNAP-auristatin F drug conjugate with potent activity against EGFR-overexpressing human solid tumor cells. Onco Targets Ther 10:3313. https://doi.org/10.2147/OTT.S140492

101. Pardo A, Stöcker M, Kampmeier F, et al (2012) In vivo imaging of immunotoxin treatment using Katushka-transfected A-431 cells in a murine xenograft tumour model. Cancer Immunol Immunother 61:1617–1626. https://doi.org/10.1007/s00262-012-1219-3

102. Li X, Yang X, Li Z, et al (2022) Development of a Radiotracer for PET Imaging of the SNAP Tag. ACS Omega 7:7550–7555. https://doi.org/10.1021/acsomega.1c05856

103. Amoury M, Mladenov R, Nachreiner T, et al (2016) A novel approach for targeted elimination of CSPG4-positive triple-negative breast cancer cells using a MAP tau-based fusion protein. Int J Cancer 139:916–927. https://doi.org/10.1002/IJC.30119

104. Fu Z, Li S, Han S, et al (2022) Antibody drug conjugate: the “biological missile” for targeted cancer therapy. Signal Transduct Target Ther 2022 71 7:1–25. https://doi.org/10.1038/s41392-022-00947-7

105. Matulonis UA, Lorusso D, Oaknin A, et al (2023) Efficacy and Safety of Mirvetuximab

Soravtansine in Patients With Platinum-Resistant Ovarian Cancer With High Folate Receptor Alpha Expression: Results From the SORAYA Study. J Clin Oncol JCO2201900. https://doi.org/10.1200/JCO.22.01900

106. Nagayama A, Vidula N, Ellisen L, Bardia A (2020) Novel antibody–drug conjugates for triple negative breast cancer. Ther Adv Med Oncol 12:. https://doi.org/10.1177/1758835920915980

107. Nelson AL, Reichert JM (2009) Development trends for therapeutic antibody fragments. Nat Biotechnol 2009 274 27:331–337. https://doi.org/10.1038/nbt0409-331

108. Xenaki KT, Oliveira S, van Bergen en Henegouwen PMP (2017) Antibody or antibody fragments: Implications for molecular imaging and targeted therapy of solid tumors. Front Immunol 8:1287. https://doi.org/10.3389/fimmu.2017.01287

109. Schweizer D, Serno T, Goepferich A (2014) Controlled release of therapeutic antibody formats. Eur J Pharm Biopharm 88:291–309. https://doi.org/10.1016/j.ejpb.2014.08.001

110. Mumper RJ, Parrott MC, Glatt DM, et al (2016) The Interplay of Antigen Affinity, Internalization, and Pharmacokinetics on CD44-Positive Tumor Targeting of Monoclonal Antibodies. Mol Pharm 13:1894–1903. https://doi.org/10.1021/acs.molpharmaceut.6b00063

111. Labrijn AF, Aalberse RC, Schuurman J (2008) When binding is enough: nonactivating antibody formats. Curr Opin Immunol 20:479–485. https://doi.org/10.1016/j.coi.2008.05.010

112. Rudnick SI, Adams GP (2009) Affinity and Avidity in Antibody-Based Tumor Targeting. Cancer Biother Radiopharm 24:155. https://doi.org/10.1089/CBR.2009.0627

113. Kaksonen M, Roux A (2018) Mechanisms of clathrin-mediated endocytosis. Nat Rev Mol Cell Biol 19:313–326. https://doi.org/10.1038/nrm.2017.132

114. Chalouni C, Doll S (2018) Fate of Antibody-Drug Conjugates in Cancer Cells. J Exp Clin Cancer Res 37:1–12. https://doi.org/10.1186/s13046-017-0667-1

115. Holliger P, Prospero T, Winter G (1993) “Diabodies”: Small bivalent and bispecific antibody

fragments. Proc Natl Acad Sci U S A 90:6444–6448. https://doi.org/10.1073/pnas.90.14.6444

116. Li JY, Perry SR, Muniz-Medina V, et al (2016) A Biparatopic HER2-Targeting Antibody-Drug Conjugate Induces Tumor Regression in Primary Models Refractory to or Ineligible for HER2-Targeted Therapy. Cancer Cell 29:117–129. https://doi.org/10.1016/j.ccell.2015.12.008

117. Zhou Y, Goenaga A-L, Harms BD, et al (2012) Impact of Intrinsic Affinity on Functional Binding and Biological Activity of EGFR Antibodies. Mol Cancer Ther 11:1467–1476. https://doi.org/10.1158/1535-7163.MCT-11-1038

118. Adams GP, Schier R, Marshall K, et al (1998) Increased affinity leads to improved selective tumor delivery of single- chain Fv antibodies. Cancer Res 58:485–490

119. Ribbert T, Thepen T, Tur MK, et al (2010) Recombinant, ETA′-based CD64 immunotoxins: Improved efficacy by increased valency, both in vitro and in vivo in a chronic cutaneous inflammation model in human CD64 transgenic mice. Br J Dermatol 163:279–286. https://doi.org/10.1111/j.1365-2133.2010.09824.x

120. Bera TK, Onda M, Brinkmann U, Pastan I (1998) A bivalent disulfide-stabilized Fv with improved antigen binding to erbB2. J Mol Biol 281:475–483. https://doi.org/10.1006/jmbi.1998.1948

121. Meng J, Liu Y, Gao S, et al (2016) A bivalent recombinant immunotoxin with high potency against tumors with EGFR and EGFRvIII expression. http://dx.doi.org/101080/1538404720151095403 16:1764–1774. https://doi.org/10.1080/15384047.2015.1095403

122. Zhang F, Shan L, Liu Y, et al (2013) An Anti-PSMA Bivalent Immunotoxin Exhibits Specificity and Efficacy for Prostate Cancer Imaging and Therapy. Adv Healthc Mater 2:736–744. https://doi.org/10.1002/ADHM.201200254

123. Thompson J, Stavrou S, Weetall M, et al (2001) Improved binding of a bivalent single-chain immunotoxin results in increased efficacy for in vivo T-cell depletion. Protein Eng 14:1035–

1041. https://doi.org/10.1093/PROTEIN/14.12.1035

124. Wolff EA, Schreiber GJ, Cosand WL, Raff H V (1993) Monoclonal antibody homodimers: enhanced antitumor activity in nude mice. Cancer Res 53:2560–5

125. Rudnick SI, Lou J, Shaller CC, et al (2011) Influence of affinity and antigen internalization on the uptake and penetration of anti-HER2 Antibodies in Solid Tumors. Cancer Res 71:2250–2259. https://doi.org/10.1158/0008-5472.CAN-10-2277

126. Chen KC, Kim J, Li X, Lee B (2008) Modeling Recombinant Immunotoxin Efficacies in Solid Tumors. 36:486–512. https://doi.org/10.1007/s10439-007-9425-4

127. Fujimori K, Covell DG, Fletcher JE, Weinstein JN (1990) A Modeling Analysis of Monoclonal Antibody Percolation Through Tumors: A Binding-Site Barrier. J Nucl Med 31:1191–1198

128. Mager DE, Jusko WJ (2001) General Pharmacokinetic Model for Drugs Exhibiting Target-Mediated Drug Disposition. 28:507–532. https://doi.org/10.1023/a:1014414520282

129. Muchekehu R, Liu D, Horn M, et al (2014) The Effect of Molecular Weight, PK, and Valency on Tumor Biodistribution and Efficacy of Antibody-Based Drugs. Transl Oncol 6:562-IN6. https://doi.org/10.1593/tlo.13409

130. Takei K, Haucke V (2001) Clathrin-mediated endocytosis: Membrane factors pull the trigger. Trends Cell Biol 11:385–391. https://doi.org/10.1016/S0962-8924(01)02082-7

131. Cullen PJ, Steinberg F (2018) To degrade or not to degrade: mechanisms and significance of endocytic recycling. Nat Rev Mol Cell Biol 19:679–696. https://doi.org/10.1038/s41580-018-0053-7

132. Ciechanover A, Schwartz AL, Lodish HL (1985) Sorting and Recycling of Cell Surface Receptors and Endocytosed Ligands. In: Mechanisms of Receptor Regulation. Springer US, Boston, MA, pp 225–253

133. Johannes L, Popoff V (2008) Tracing the Retrograde Route in Protein Trafficking. Cell

135:1175–1187. https://doi.org/10.1016/j.cell.2008.12.009

134. Spangler JB, Neil JR, Abramovitch S, et al (2010) Combination antibody treatment down-regulates epidermal growth factor receptor by inhibiting endosomal recycling. Proc Natl Acad Sci 107:13252–13257. https://doi.org/10.1073/pnas.0913476107

135. Friedman LM, Rinon A, Schechter B, et al (2005) Synergistic down-regulation of receptor tyrosine kinases by combinations of mAbs: Implications for cancer immunotherapy. Proc Natl Acad Sci 102:1915–1920. https://doi.org/10.1073/pnas.0409610102

136. Kreitman RJ (2006) Immunotoxins for Targeted Cancer Therapy. AAPS J 8:532–551. https://doi.org/10.1208/aapsj080363

137. Polakis P (2016) Antibody Drug Conjugates for Cancer Therapy. Pharmacol Rev 68:3–19. https://doi.org/10.1124/PR.114.009373

138. Alley SC, Okeley NM, Senter PD (2010) Antibody–drug conjugates: targeted drug delivery for cancer. Curr Opin Chem Biol 14:529–537. https://doi.org/10.1016/J.CBPA.2010.06.170

139. Martini R, Delpe P, Chu TR, et al (2022) African Ancestry–Associated Gene Expression Profiles in Triple-Negative Breast Cancer Underlie Altered Tumor Biology and Clinical Outcome in Women of African Descent. Cancer Discov 12:2530–2551. https://doi.org/10.1158/2159-8290.CD-22-0138

140. Safdari Y, Ahmadzadeh V, Khalili M, et al (2016) Use of Single-Chain Antibody Derivatives for Targeted Drug Delivery. Mol Med 22:258. https://doi.org/10.2119/MOLMED.2016.00043

141. Bumol TF, Reisfeld RA (1982) Unique glycoprotein-proteoglycan complex defined by monoclonal antibody on human melanoma cells. Proc Natl Acad Sci U S A 79:1245. https://doi.org/10.1073/PNAS.79.4.1245

142. Morgan AC, Galloway DR, Reisfeld RA (1981) Production and characterization of monoclonal antibody to a melanoma specific glycoprotein. Hybridoma 1:27–36. https://doi.org/10.1089/HYB.1.1981.1.27

143. Schwenkert M, Birkholz K, Schwemmlein M, et al (2008) The single-chain immunotoxin MCSP-ETA', targeting melanoma-associated chondroitin sulfate proteoglycan, is a potent inducer of apoptosis in cultured human melanoma cells. Melanoma Res 18:73. https://doi.org/10.1097/CMR.0B013E3282F7C8F9

144. Walker JM, Gasteiger E, Hoogland C, et al (2005) Protein Identification and Analysis Tools on the ExPASy Server. Proteomics Protoc Handb 571–607. https://doi.org/10.1385/1-59259-890-0:571

145. Smith RL, Traul DL, Schaack J, et al (2000) Characterization of promoter function and cell-type-specific expression from viral vectors in the nervous system. J Virol 74:11254–11261. https://doi.org/10.1128/JVI.74.23.11254-11261.2000

146. Tabor S (2001) Expression using the T7 RNA polymerase/promoter system. Curr Protoc Mol Biol Chapter 16: https://doi.org/10.1002/0471142727.MB1602S11

147. Haryadi R, Ho S, Kok YJ, et al (2015) Optimization of Heavy Chain and Light Chain Signal Peptides for High Level Expression of Therapeutic Antibodies in CHO Cells. PLoS One 10:e0116878. https://doi.org/10.1371/journal.pone.0116878

148. Bornhorst JA, Falke JJ (2000) Purification of Proteins Using Polyhistidine Affinity Tags. Methods Enzymol 326:254. https://doi.org/10.1016/S0076-6879(00)26058-8

149. Zhao X, Li G, Liang S (2013) Several Affinity Tags Commonly Used in Chromatographic Purification. J Anal Methods Chem 2013:. https://doi.org/10.1155/2013/581093

150. Reutelingsperger CP, van Heerde WL (1997) Annexin V, the regulator of phosphatidylserine-catalyzed inflammation and coagulation during apoptosis. Cell Mol Life Sci 53:527–532. https://doi.org/10.1007/s000180050067

151. Sun X, Zhang A, Baker B, et al (2011) Development of SNAP-Tag Fluorogenic Probes for Wash-Free Fluorescence Imaging. Chembiochem 12:2217. https://doi.org/10.1002/CBIC.201100173

152. Hermening S, Kügler S, Bähr M, Isenmann S (2004) Increased protein expression from adenoviral shuttle plasmids and vectors by insertion of a small chimeric intron sequence. J Virol Methods 122:73–77. https://doi.org/10.1016/J.JVIROMET.2004.08.005

153. Makrides SC (1999) Components of vectors for gene transfer and expression in mammalian cells. Protein Expr Purif 17:183–202. https://doi.org/10.1006/PREP.1999.1137

154. Pfarr DS, Rieser LA, Woychik RP, et al (1986) Differential effects of polyadenylation regions on gene expression in mammalian cells. DNA 5:115–122. https://doi.org/10.1089/DNA.1986.5.115

155. Clark DP, Pazdernik NJ, McGehee MR (2019) Molecular biology, Third. Elsevier

156. Wildeman AG (1988) Regulation of SV40 early gene expression. Biochem Cell Biol 66:567–577. https://doi.org/10.1139/O88-067

157. Jaishankar J, Srivastava P (2020) Strong synthetic stationary phase promoter-based gene expression system for Escherichia coli. Plasmid 109:102491. https://doi.org/10.1016/J.PLASMID.2020.102491

158. Guo C, Fordjour FK, Tsai SJ, et al (2021) Choice of selectable marker affects recombinant protein expression in cells and exosomes. J Biol Chem 297:. https://doi.org/10.1016/J.JBC.2021.100838

159. Wang X, Du Q, Zhang W, et al (2022) Enhanced Transgene Expression by Optimization of Poly A in Transfected CHO Cells. Front Bioeng Biotechnol 10:40. https://doi.org/10.3389/fbioe.2022.722722

160. Czarniecki D, Noel RJ, Reznikoff WS (1997) The -45 region of the Escherichia coli lac promoter: CAP-dependent and CAP-independent transcription. J Bacteriol 179:423–429. https://doi.org/10.1128/JB.179.2.423-429.1997

161. Busby S, Ebright RH (1999) Transcription activation by catabolite activator protein (CAP). J Mol Biol 293:199–213. https://doi.org/10.1006/JMBI.1999.3161

162. Sutcliffe JG (1978) Nucleotide Sequence of the Ampicillin Resistance Gene of Escherichia coli Plasmid pBR322. Proc Natl Acad Sci U S A 75:3737–3741

163. Newman LA, Kaljee LM (2017) Health Disparities and Triple-Negative Breast Cancer in African American Women. JAMA Surg 152:485. https://doi.org/10.1001/jamasurg.2017.0005

164. Newman LA, Jenkins B, Chen Y, et al (2019) Hereditary Susceptibility for Triple Negative Breast Cancer Associated With Western Sub-Saharan African Ancestry. Ann Surg 270:484–492. https://doi.org/10.1097/SLA.0000000000003459

165. Collignon J, Lousberg L, Schroeder H, Jerusalem G (2016) Triple-negative breast cancer: treatment challenges and solutions. Breast cancer (Dove Med Press 8:93–107. https://doi.org/10.2147/BCTT.S69488

166. García-Aranda M, Redondo M (2019) Immunotherapy: A challenge of breast cancer treatment. Cancers (Basel) 11:. https://doi.org/10.3390/cancers11121822

167. Sicklick JK, Kato S, Okamura R, et al (2019) Molecular profiling of cancer patients enables personalized combination therapy: the I-PREDICT study. Nat Med 25:744–750. https://doi.org/10.1038/s41591-019-0407-5

168. Hercules SM, Alnajar M, Chen C, et al (2022) Triple-negative breast cancer prevalence in Africa: a systematic review and meta-analysis. BMJ Open 12:e055735. https://doi.org/10.1136/BMJOPEN-2021-055735

169. Li Y, Zhan Z, Yin X, et al (2021) Targeted Therapeutic Strategies for Triple-Negative Breast Cancer. Front Oncol 11:. https://doi.org/10.3389/FONC.2021.731535

170. Brewster AM, Chavez-MacGregor M, Brown P (2014) Epidemiology, biology, and treatment of triple-negative breast cancer in women of African ancestry. Lancet Oncol 15:e625. https://doi.org/10.1016/S1470-2045(14)70364-X

171. Phillips L, Gill AJ, Baxter RC (2019) Novel Prognostic Markers in Triple-Negative Breast Cancer Discovered by MALDI-Mass Spectrometry Imaging. Front Oncol 9:379.

https://doi.org/10.3389/fonc.2019.00379

172. Lawrence RT, Perez EM, Hernández D, et al (2015) The proteomic landscape of triple-negative breast cancer. Cell Rep 11:630. https://doi.org/10.1016/J.CELREP.2015.03.050

173. Gromova I, Espinoza JA, Grauslund M, et al (2021) Functional proteomic profiling of triple-negative breast cancer. Cells 10:. https://doi.org/10.3390/CELLS10102768/S1

174. Farkona S, Diamandis EP, Blasutig IM (2016) Cancer immunotherapy: The beginning of the end of cancer? BMC Med 14:1–18. https://doi.org/10.1186/s12916-016-0623-5

175. Naran K, Nundalall T, Chetty S, Barth S (2018) Principles of Immunotherapy: Implications for Treatment Strategies in Cancer and Infectious Diseases. Front Microbiol 9:1–23. https://doi.org/10.3389/fmicb.2018.03158

176. Hendriks D, Choi G, de Bruyn M, et al (2017) Antibody-Based Cancer Therapy: Successful Agents and Novel Approaches, 1st ed. Elsevier Inc.

177. Sharma P, Hu-Lieskovan S, Wargo JA, Ribas A (2017) Primary, Adaptive, and Acquired Resistance to Cancer Immunotherapy. Cell 168:707–723. https://doi.org/10.1016/j.cell.2017.01.017

178. Tilsed CM, Fisher SA, Nowak AK, et al (2022) Cancer chemotherapy: insights into cellular and tumor microenvironmental mechanisms of action. Front Oncol 12:3761. https://doi.org/10.3389/fonc.2022.960317

179. Zeien J, Qiu W, Triay M, et al (2022) Clinical implications of chemotherapeutic agent organ toxicity on perioperative care. Biomed Pharmacother 146:112503. https://doi.org/10.1016/J.BIOPHA.2021.112503

180. Perez HL, Cardarelli PM, Deshpande S, et al (2014) Antibody-drug conjugates: current status and future directions. Drug Discov Today 19:869–881. https://doi.org/10.1016/J.DRUDIS.2013.11.004

181. Monnier PP, Vigouroux RJ, Tassew NG (2013) In Vivo Applications of Single Chain Fv (Variable Domain) (scFv) Fragments. Antibodies 2013, Vol 2, Pages 193-208 2:193–208. https://doi.org/10.3390/ANTIB2020193

182. Petrov K, Dion M, Hoffmann L, et al (2004) Bivalent Fv antibody fragments obtained by substituting the constant domains of a fab fragment with heterotetrameric molybdopterin synthase. J Mol Biol 341:1039–1048. https://doi.org/10.1016/j.jmb.2004.06.075

183. Burt R, Warcel D, Fielding AK (2019) Blinatumomab, a bispecific B-cell and T-cell engaging antibody, in the treatment of B-cell malignancies. Hum Vaccin Immunother 15:594. https://doi.org/10.1080/21645515.2018.1540828

184. Nimz EL, Land CWV, Yáñez JA, Chastain JE (2016) Intraocular and systemic pharmacokinetics of brolucizumab (RTH258) in nonhuman primates. Invest Ophthalmol Vis Sci 57:4996–4996

185. Yannuzzi NA, Freund KB (2019) Brolucizumab: evidence to date in the treatment of neovascular age-related macular degeneration. Clin Ophthalmol 13:1323. https://doi.org/10.2147/OPTH.S184706

186. Hwa G, Carlson D, Starr JR (2022) Tebentafusp-tebn: A Novel Bispecific T-Cell Engager for Metastatic Uveal Melanoma. J Adv Pract Oncol 13:717. https://doi.org/10.6004/JADPRO.2022.13.7.8

187. Montazeri K, Pattanayak V, Sullivan RJ (2023) Tebentafusp in the Treatment of Metastatic Uveal Melanoma: Patient Selection and Special Considerations. Drug Des Devel Ther 17:333–339. https://doi.org/10.2147/DDDT.S368954

188. Kellner C, Peipp M (2013) Engineered Antibody Derivatives in Preclinical and Clinical Development. In: Molecular and Cellular Mechanisms of Antibody Activity. Springer New York, New York, NY, pp 251–284

189. Goel A, Colcher D, Baranowska-Kortylewiez J, et al (2000) Genetically engineered tetravalent single-chain Fv of the pancarcinoma monoclonal antibody CC49: Improved biodistribution and

potential for therapeutic application. Cancer Res 60:6964–6971

190. Hussain A, Amoury M, Barth S (2013) SNAP-Tag Technology: A Powerful Tool for Site Specific Conjugation of Therapeutic and Imaging Agents. Curr Pharm Des 19:5437–5442. https://doi.org/10.2174/1381612811319300014

191. Hinner MJ, Johnsson K (2010) How to obtain labeled proteins and what to do with them. Curr Opin Biotechnol 21:766–776. https://doi.org/10.1016/j.copbio.2010.09.011

192. Barth S (2013) Editorial (The SNAP-tag Technology – A Versatile Tool with many Applications). Curr Pharm Des 19:5404–5405. https://doi.org/10.2174/1381612811319300009

193. Kiseleva RY, Glassman PG, LeForte KM, et al (2020) Bivalent engagement of endothelial surface antigens is critical to prolonged surface targeting and protein delivery in vivo. FASEB J 34:11577–11593. https://doi.org/10.1096/FJ.201902515RR

194. Kessler C, Pardo A, Tur MK, et al (2017) Novel PSCA targeting scFv-fusion proteins for diagnosis and immunotherapy of prostate cancer. J Cancer Res Clin Oncol 143:2025–2038. https://doi.org/10.1007/s00432-017-2472-9

195. Ibach J, Subramaniam V, Corrêa IR, et al (2014) Evaluation of Fluorophores to Label SNAP-Tag Fused Proteins for Multicolor Single-Molecule Tracking Microscopy in Live Cells. Biophys J 107:803–814. https://doi.org/10.1016/j.bpj.2014.06.040

196. Kampmeier F, Ribbert M, Nachreiner T, et al (2009) Site-Specific, Covalent Labeling of Recombinant Antibody Fragments via Fusion to an Engineered Version of 6-O-Alkylguanine DNA Alkyltransferase. Bioconjug Chem 20:1010–1015. https://doi.org/10.1021/BC9000257

197. Rolih V, Barutello G, Iussich S, et al (2017) CSPG4: a prototype oncoantigen for translational immunotherapy studies. J Transl Med 2017 151 15:1–14. https://doi.org/10.1186/S12967-017-1250-4

198. Mungra N, Biteghe FAN, Malindi Z, et al (2023) CSPG4 as a target for the specific killing of triple-negative breast cancer cells by a recombinant SNAP-tag-based antibody-auristatin F drug

conjugate. J Cancer Res Clin Oncol 149:12203–12225. https://doi.org/10.1007/s00432-023-05031-3

199. Zhang C-Y, Wu Z-Q, Yin D-C, et al (2013) A strategy for selecting the pH of protein solutions to enhance crystallization. Acta Crystallogr Sect F Struct Biol Cryst Commun 69:821–826. https://doi.org/10.1107/S1744309113013651

200. Hanahan D (1983) Studies on transformation of Escherichia coli with plasmids. J Mol Biol 166:557–580. https://doi.org/10.1016/S0022-2836(83)80284-8

201. Liu J, Chang W, Pan L, et al (2018) An Improved Method of Preparing High Efficiency Transformation Escherichia coli with Both Plasmids and Larger DNA Fragments. Indian J Microbiol 58:448. https://doi.org/10.1007/S12088-018-0743-Z

202. Lukacs GL, Haggie P, Seksek O, et al (2000) Size-dependent DNA mobility in cytoplasm and nucleus. J Biol Chem 275:1625–1629. https://doi.org/10.1074/JBC.275.3.1625

203. De Los Milagros Bassani Molinas M, Beer C, Hesse F, et al (2014) Optimizing the transient transfection process of HEK-293 suspension cells for protein production by nucleotide ratio monitoring. Cytotechnology 66:493. https://doi.org/10.1007/S10616-013-9601-3

204. Swiech K, Kamen A, Ansorge S, et al (2011) Transient transfection of serum-free suspension HEK 293 cell culture for efficient production of human rFVIII. BMC Biotechnol 11:114. https://doi.org/10.1186/1472-6750-11-114

205. Thomas P, Smart TG (2005) HEK293 cell line: A vehicle for the expression of recombinant proteins. J Pharmacol Toxicol Methods 51:187–200. https://doi.org/10.1016/J.VASCN.2004.08.014

206. Kampmeier F, Niesen J, Koers A, et al (2010) Rapid optical imaging of EGF receptor expression with a single-chain antibody SNAP-tag fusion protein. Eur J Nucl Med Mol Imaging 37:1926–1934. https://doi.org/10.1007/s00259-010-1482-5

207. Ryan BJ, Henehan GT (2017) Avoiding Proteolysis During Protein Purification. Methods Mol

Biol 1485:53–69. https://doi.org/10.1007/978-1-4939-6412-3_4

208. Hong P, Koza S, Bouvier ESP (2012) Size-Exclusion Chromatography for the Analysis of Protein Biotherapeutics and their Aggregates. J Liq Chromatogr Relat Technol 35:2923. https://doi.org/10.1080/10826076.2012.743724

209. Tripathi NK, Shrivastava A (2019) Recent Developments in Bioprocessing of Recombinant Proteins: Expression Hosts and Process Development. Front Bioeng Biotechnol 7:420. https://doi.org/10.3389/fbioe.2019.00420

210. Spriestersbach A, Kubicek J, Schäfer F, et al (2015) Purification of His-Tagged Proteins. Methods Enzymol 559:1–15. https://doi.org/10.1016/BS.MIE.2014.11.003

211. Lippert K, Galinski E (1992) Enzyme stabilization be ectoine-type compatible solutes: protection against heating, freezing and drying. Appl Microbiol Biotechnol 37:61–65. https://doi.org/10.1007/BF00174204

212. Cole NB, Donaldson JG (2012) Releasable SNAP-tag Probesfor Studying Endocytosisand Recycling. ACS Chem Biol 7:464. https://doi.org/10.1021/CB2004252

213. Durbin KR, Phipps C, Liao X (2018) Mechanistic Modeling of Antibody–Drug Conjugate Internalization at the Cellular Level Reveals Inefficient Processing Steps. Mol Cancer Ther 17:1341–1351. https://doi.org/10.1158/1535-7163.mct-17-0672

214. Xue Y, O'Mara ML, Surawski PPT, et al (2011) Effect of poly(ethylene glycol) (PEG) spacers on the conformational properties of small peptides: a molecular dynamics study. Langmuir 27:296–303. https://doi.org/10.1021/LA103800H

215. Saraste A, Pulkki K (2000) Morphologic and biochemical hallmarks of apoptosis. Cardiovasc Res 45:528–537. https://doi.org/10.1016/S0008-6363(99)00384-3

216. Staudacher AH, Brown MP (2017) Antibody drug conjugates and bystander killing: is antigen-dependent internalisation required? Br J Cancer 2017 11712 117:1736–1742. https://doi.org/10.1038/bjc.2017.367

217. Giugliano F, Corti C, Tarantino P, et al (2022) Bystander effect of antibody-drug conjugates: fact or fiction? Curr Oncol Rep 24:809–817. https://doi.org/10.1007/S11912-022-01266-4

218. Singh AP, Sharma S, Shah DK (2016) Quantitative Characterization of In Vitro Bystander Effect of Antibody-Drug Conjugates. J Pharmacokinet Pharmacodyn 43:567. https://doi.org/10.1007/S10928-016-9495-8

219. Zanoni M, Piccinini F, Arienti C, et al (2016) 3D tumor spheroid models for in vitro therapeutic screening: a systematic approach to enhance the biological relevance of data obtained. Sci Reports 2016 61 6:1–11. https://doi.org/10.1038/srep19103

220. Ryman JT, Meibohm B (2017) Pharmacokinetics of Monoclonal Antibodies. CPT Pharmacometrics Syst Pharmacol 6:576. https://doi.org/10.1002/PSP4.12224

221. Ovacik M, Lin K (2018) Tutorial on Monoclonal Antibody Pharmacokinetics and Its Considerations in Early Development. Clin Transl Sci 11:540. https://doi.org/10.1111/CTS.12567

222. Brandl F, Busslinger S, Zangemeister-Wittke U, Plückthun A (2020) Optimizing the anti-tumor efficacy of protein-drug conjugates by engineering the molecular size and half-life. J Control Release 327:186–197. https://doi.org/10.1016/J.JCONREL.2020.08.004

223. Olafsen T, Wu AM (2010) Antibody Vectors for Imaging. Semin Nucl Med 40:167–181. https://doi.org/10.1053/j.semnuclmed.2009.12.005

224. Depke DA, Konken CP, Rösner L, et al (2021) A novel 18 F-labeled clickable substrate for targeted imaging of SNAP-tag expressing cells by PET in vivo. Chem Commun 57:9850–9853. https://doi.org/10.1039/D1CC03871K

225. Yin L, Duan J-J, Bian X-W, Yu S (2020) Triple-negative breast cancer molecular subtyping and treatment progress. Breast Cancer Res 22:61. https://doi.org/10.1186/s13058-020-01296-5

226. Li Y, Zhang H, Merkher Y, et al (2022) Recent advances in therapeutic strategies for triple-negative breast cancer. J Hematol Oncol 15:1–30. https://doi.org/10.1186/s13045-022-01341-0

227. Khoja L, Butler MO, Kang SP, et al (2015) Pembrolizumab. J Immunother Cancer 3:. https://doi.org/10.1186/S40425-015-0078-9

228. da Silva JL, Cardoso Nunes NC, Izetti P, et al (2020) Triple negative breast cancer: A thorough review of biomarkers. Crit Rev Oncol Hematol 145:102855. https://doi.org/10.1016/J.CRITREVONC.2019.102855

229. Hanahan D, Coussens LM (2012) Accessories to the Crime: Functions of Cells Recruited to the Tumor Microenvironment. Cancer Cell 21:309–322. https://doi.org/10.1016/J.CCR.2012.02.022

230. Mittal S, Brown NJ, Holen I (2018) The breast tumor microenvironment: role in cancer development, progression and response to therapy. Expert Rev Mol Diagn 18:227–243. https://doi.org/10.1080/14737159.2018.1439382

231. Papaioannou NE, Beniata O V, Vitsos P, et al (2016) Harnessing the immune system to improve cancer therapy. Ann Transl Med 4:. https://doi.org/10.21037/atm.2016.04.01

232. Day JJ, Marquez B V., Beck HE, et al (2010) Chemically Modified Antibodies as Diagnostic Imaging Agents. Curr Opin Chem Biol 14:803. https://doi.org/10.1016/J.CBPA.2010.09.015

7. Appendix

Buffer solutions and media were prepared according to laboratory protocols using deionised or ultrapure (type I) water, as appropriate. NaOH or HCl solutions were used to adjust the pH of buffer solutions. Where necessary, sterile filtration (0.45 µm filter) or autoclaving for 20 min at 120°C was used to sterilise the solutions. Buffers for IMAC protein purification were filtered and de-gassed using a 0.45 µm polyvinylidene difluoride (PVDF) membrane. In cases where the medium was supplemented with antibiotics, the following final concentrations were used: 100 µg/mL ampicillin, 100 U/mL penicillin, 100 µg/mL streptomycin, and 100 µg/mL zeocin. The complete medium was further supplemented with 10% FBS. All cells were cultured under standard tissue culture conditions: 37°C with 5% CO_2 and 95% humidity.

Table A1. Summary of buffers and media used for experiments in this study, including their compositions.

Buffers and media	**Composition**
1x SDS-PAGE Running Buffer pH 8.3	25 mM Glycine 192 mM Tris 0.1% SDS
10% Polyacrylamide gel (Resolving gel)	10% Acrylamide/Bis-acrylamide 375 mM Tris-Cl, pH 8.8 0.1% SDS 0.1% Ammonium persulphate 0.1% TEMED
4% Polyacrylamide gel (Stacking gel)	4% Acrylamide/Bis-acrylamide 190 mM Tris-Cl, pH 6.8 0.1% SDS 0.1% Ammonium persulphate 0.1% TEMED
4x Incubation Buffer (IMAC pH 8.0	200 mM NaCl 1.2 M Na_2HPO_4 40 mM Imidazole
Equilibration Buffer (IMAC) pH 8.0	300 mM NaCl 50 mM Na_2HPO_4

Elution Buffer (IMAC) pH 8.0	300 mM NaCl 50 mM Na_2HPO_4 500 mM Imidazole
Alkaline Lysis Solution I (Plasmid purification) pH 8.0	50 mM Glucose 25 mM Tris-HCl 10mM EDTA
Alkaline Lysis Solution II (Plasmid purification)	1% SDS 200 mM NaOH
Alkaline Lysis Solution III (Plasmid purification)	3 M Potassium acetate 11.5% (v/v) Acetic acid
1x Tris-acetate-EDTA (TAE) buffer (Agarose gel electrophoresis)	40 mM Tris 20 mM Glacial acetic acid 1 mM EDTA
1x Phosphate-Buffered Saline (PBS) pH 7.4	137 mM NaCl 8.8 mM Na_2HPO_4 2.7 mM KCl 1.75 mM KH_2PO_4
1x Tris-Buffered Saline (TBS) – Tween (Immunoblot)	20 mM Tris 150 mM NaCl 0.1% (v/v) Tween 20
1x Transfer buffer (Immunoblot)	25 mM Tris 192 mM Glycine 20% Methanol
Luria-Bertani (LB) broth	1.0% (w/v) Casein peptone 0.5% (w/v) Yeast extract 1.0% (w/v) NaCl
Luria-Bertani (LB) agar	1.0% (w/v) Casein peptone 0.5% (w/v) Yeast extract 1.0% (w/v) NaCl 1.2% (w/v) Agar

Table A2. The cell lines that were obtained and used in this study. The supplier and catalogue information, along with the medium they were cultured in is provided.

Cell lines	Origin	Media	Species	Description/type
DH5α	New England BioLabs (C2987)	Luria Bertani broth and agar	*E. coli*	*fhuA2 Δ(argF-lacZ)U169 phoA glnV44 Φ80 Δ(lacZ)M15 gyrA96 recA1 relA1 endA1 thi-1 hsdR17*
HEK293T	ATCC (CRL-3216)	RPMI-1640	Human	Human embryonic kidney cells
Hs578T	ATCC (HTB-126)	DMEM	Human	Triple-negative breast cancer
MCF-7	ATCC (HTB-22)	RPMI-1640	Human	Breast carcinoma

Table A3. The antibiotics and serum used to supplement media and the final concentrations that were used throughout the experiments in this study.

Supplement	Medium	Concentration
Ampicillin	Luria Bertani broth and agar	100 µg/mL
Penicillin	Roswell Park Memorial Institute (RPMI) 1640 and Dulbecco's Modified Eagle Medium (DMEM)	100 U/mL
Streptomycin	RPMI-1640 and DMEM	100 µg/mL
Foetal Bovine Serum (Gamma irradiated; heat inactivated)	RPMI-1640 and DMEM	10%
Zeocin	RPMI-1640 and DMEM	100 µg/mL

Table A4. Recorded yield and purity of various immobilised metal affinity chromatography (IMAC) purification events. Data was recorded over approximately two years. Yield and purity were quantified using densitometric measurements as described in section **2.3.2.2.**

Fusion protein	Purification date	Yield (mg/L)	Purity (%)
Monovalent αCSPG4(scFv)-SNAP	20.10.2020	2.14	33
	27.10.2020	3.03	36
	24.03.2021	1.78	14
	21.07.2021	2.51	33
	29.09.2021	1.85	37
	Average	**2.26**	**31**
Bivalent αCSPG4(scFv)$_2$-SNAP	26.02.2020	1.22	14
	27.10.2020	1.02	17
	16.03.2021	1.47	24
	30.03.2021	2.13	15
	29.04.2021	1.02	10
	29.07.2021	1.19	22
	30.10.2021	1.34	16
	Average	**1.34**	**17**